GROUNDWATER MANAGEMENT INSTITUTE

PEGASYS
CHANGING LIVES CHANGING WORLDS

L2K2 Consultants

SADC-GMI – Groundwater Drought Risk Interventions (GMI-GDRI)

Revised Groundwater Drought Risk Map

July 2020

This report emanates from the project Assessment of Groundwater Resources Development Priority Intervention Areas in the SADC Region commissioned by the Southern African Development Community Groundwater Management Institute (SADC-GMI) and executed by Pegasys.

SADC GROUNDWATER MANAGEMENT INSTITUTE (SADC-GMI)
Dean Street, University of the Free State
205 Nelson Mandela Drive, Bloemfontein, 9300
South Africa
E-mail info@sadc-gmi.org Website www.sadc-gmi.org
Project team:

Traci Reddy (Project Manager), Pegasys
Kevin Pietersen (Team Leader), L2K2 Consultants
Chiedza Musekiwa (Hydrogeologist), Council for Geoscience
Verno Jonker (Hydrologist), Zutari
Maryna Storie (Remote Sensing and Geographic Information Systems Expert)
Deepti Maharaj (Project Coordinator), Pegasys
Zaheed Gaffoor, L2K2 Consultants
Luc Chevallier, L2K2 Consultants
Anya Eilers, Zutari
Erika Braune, Zutari

© SADC-GMI, 2020

Boxes, Tables, Figures, Maps, Photos and Illustrations as specified

This report is accessible online through SADC-GMI website: www.sadc-gmi.org
Citation: SADC-GMI, (2020). *Revised Groundwater Drought Risk Map.* SADC GMI report: Bloemfontein, South Africa.

The designation of geographical entities, use of any name in this publication, and the presentation of the material do not imply the expression of any opinion whatsoever on the part of SADC-GMI or Pegasys concerning the legal status of any country or territory, or area of its authority, or concerning the delimitation of its frontiers or boundaries

TABLE OF CONTENTS

LIST OF FIGURES

LIST OF TABLES

LIST OF BOXES

LIST OF ACRONYMS

Acronym	Definition
CHIRPS	Climate Hazards Group InfraRed Precipitation with Station
CV	Coefficient of Variation
DRC	Democratic Republic of the Congo
ET	Evapotranspiration
FAO	Food and Agriculture Organization
GDR	Groundwater Drought Risk
GDRI	Groundwater Drought Risk Intervention
GGDI	GRACE Groundwater Drought Index
GIS	Geographic Information System
GLDAS	Global Land Data Assimilation System
GRACE	Gravity Recovery and Climate Experiment
GRiMMS	Groundwater Drought Risk Mapping and Management System
IGRAC	International Groundwater Resources Assessment Centre
NASA	National Aeronautics and Space Administration
NDVI	Normalized Difference Vegetation Index

Acronym	Definition
SADC-GMI	Southern African Development Community Groundwater Management Institute
SADC GMI-GDRI	Assessment of Groundwater Resources Development Priority Intervention Areas in the SADC Region
SADC	Southern African Development Community
SPEI	Standardized Precipitation Evapotranspiration Index
SPI	Standard Precipitation Index
TBA	Transboundary Aquifer
TWSA	Terrestrial Water Storage Anomaly
WMO	World Meteorological Organisation

1. INTRODUCTION

1.1. Background

The Southern African Development Community Groundwater Management Institute (SADC-GMI) is implementing the project: *Assessment of Groundwater Resources Development Priority Intervention Areas in the SADC Region (SADC GMI-GDRI)* which seeks to bring the role of groundwater in securing water supply during periods of droughts to the forefront and provide for proactive planning, recommendations and management of groundwater and surface water systems.

The project is identifying areas that are prone to drought in the SADC region by revising the current Groundwater Drought Risk (GDR) map (SADC 2011, Villholth *et al* 2013) of the region and to move towards practical assessment of the water resources which can be quickly mobilised to support sustainable water supply investments in underserved areas (also referred to as population vulnerability hotspots) in the region.

The overall objective of the study is to assess the groundwater resources and identify areas that are prone to groundwater drought in the SADC region. The task is to make use of the existing geospatial, hydrological and hydrogeological datasets and deliver a revised GDR map of the SADC region. The study will also perform practical assessment of the ground-water resources which can be quickly mobilised to support sustainable domestic water supply investments in areas with high groundwater drought risk and have limited access to safe domestic water supply - based on population vulnerability hotspots. The study will further identify the most adequate and cost-effective infrastructure interventions in the areas in most need.

1.1. Purpose of this Report

This report presents the revised GDR map. Similar to deriving the SADC (2011) map, the GDR Mapping and Management System (GRiMMS) is derived, updated and depicts GDR map on the basis of relative indicators, using a composite mapping analysis technique in a traditional geographic information system (GIS) environment. Separate thematic layers showing different factors influencing GDR (through indicators given for the entire SADC region at a certain resolution) are superimposed and mathematically combined through a simple linear algorithm and an associated weighting scheme for the relative importance of the various factors to derive a spatially distributed measure of GDR across the SADC region (Villholth *et al* 2013). The revised GDR map incorporates updated datasets until 2019 at a resolution of 5 kilometres (km) (the meteorological parameters are at this resolution) and incorporates a groundwater storage

sensitivity module driven from Gravity Recovery and Climate Experiment (GRACE) satellite datasets.

2. GRIMMS METHOD

The original GRiMMS algorithm is shown in Figure 2-1 and comprises four modules:

1. Climate sensitivity
2. Hydrogeological drought proneness
3. Human groundwater drought vulnerability
4. Groundwater threats

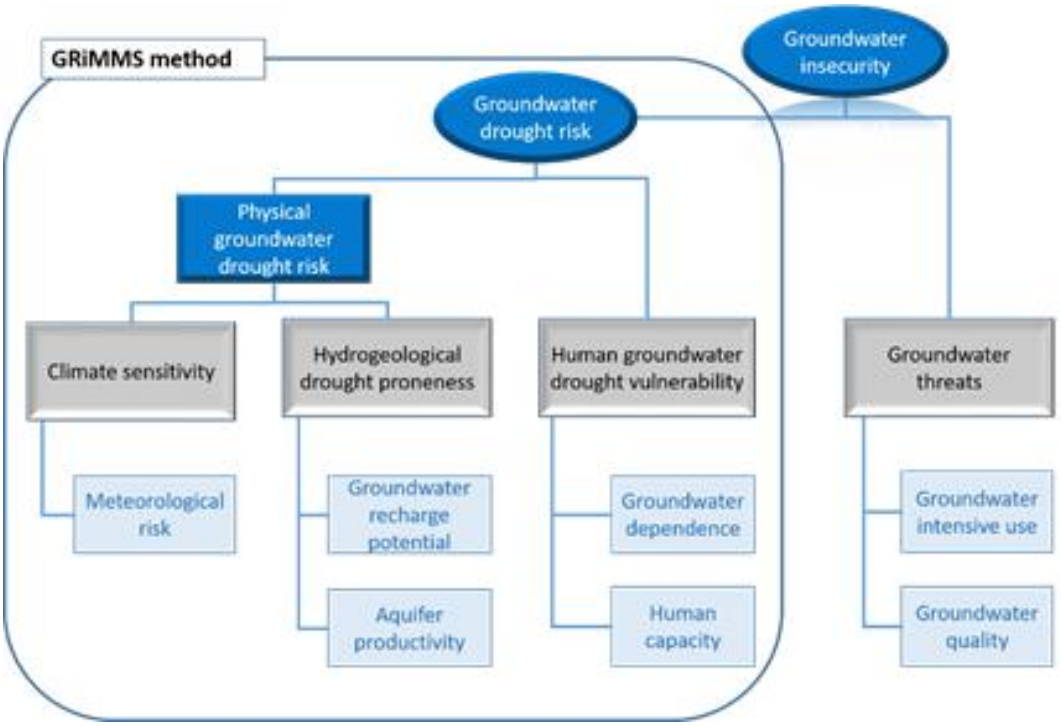

Figure 2-1: Schematic diagram of the governing thematic layers entering the composite mapping analysis and resulting aggregated layers in the original GRiMMS (Villholth et al 2013)

The original GRiMMS algorithm was modified to include the groundwater storage sensitivity derived from GRACE satellite data. The revised algorithm is shown in Figure 2-2 and associated datasets in Table 2-1.

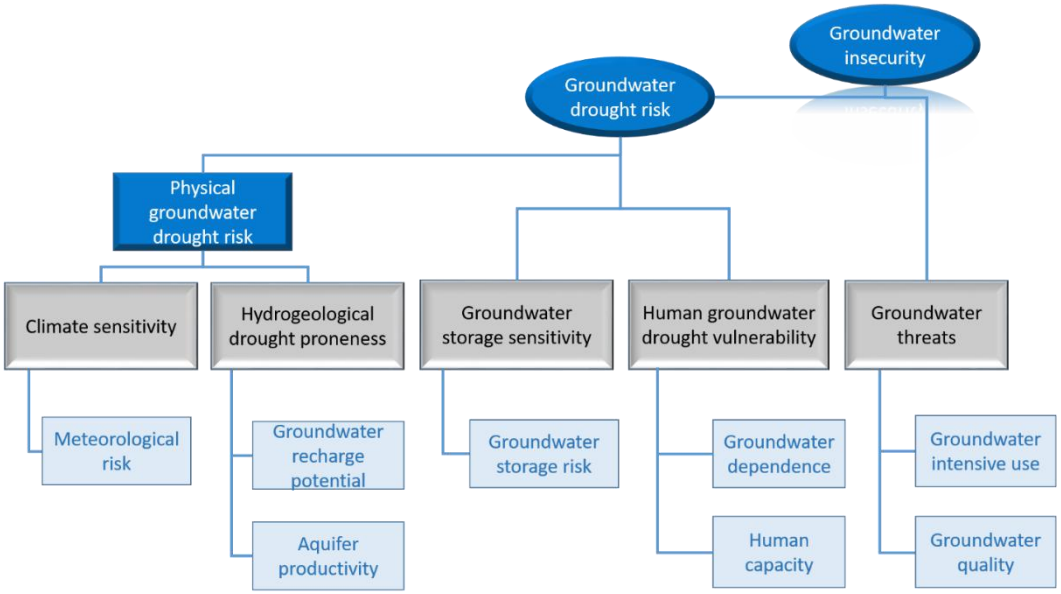

Figure 2-2: **Updated GRiMMS algorithm to incorporate the groundwater storage sensitivity derived from GRACE satellite data**

Table 2-1: **The list of GRiMMS sub-modules and datasets**

Meteorological drought risk			
1	Rainfall amount	Rainfall time-series	Climate Hazards Group InfraRed Precipitation with Station (CHIRPS) version 2 daily data (1981-2019) (~5km resolution)
2	Coefficient of variation (CV)	Rainfall time-series	Worldclim monthly data (1960-2019) (~21 km resolution)
3	Number of consecutive dry days in one calendar year	Rainfall time-series	CHIRPS version 2 daily data (1981-2019) (~5km resolution)
4	Number of consecutive dry days in more than one calendar year	Rainfall time-series	CHIRPS version 2 daily data (1981-2019) (~5km resolution)
Aquifer productivity			
5	Aquifer type	SADC geohydrology map	1:2.5 million scale vector map
Groundwater recharge potential			
6	Slope	Derived from 90m STRM	90m resolution data
7	Normalised Difference Vegetation Index	MODIS NDVI	~1 km resolution (2003-2019)
8	Rainfall	Mean annual rainfall	~5 km resolution raster (1981-2019)
Groundwater storage risk			
9	Percentage negative GRACE Groundwater Drought Index (GGDI)	Derived from GRACE data	~5 km resolution raster
10	Mean negative GGDI	Derived from GRACE data	~5 km resolution raster
11	Trend GGDI	Derived from GRACE data	~5 km resolution raster
Groundwater dependence			
12	Livestock density	Animals per km^2	~10 km resolution raster
13	Irrigation density	Irrigation density	% per unit area irrigated by groundwater (~10km raster)
14	Population density	People per km^2	~1 km resolution raster (2015)
15	Distance to surface water	Euclidean distance to rivers	Vector data from SADC-GMI GIP

3. GIS COMPOSITE MAPPING METHOD

The outline of the method used in a GIS software is as follows:

- The vector data are converted to raster format at a suitable resolution
- The raster layers are left in their native resolution, e.g. slope at 90m, rainfall datasets at ~5km, livestock density at ~10km
- All the datasets are classified into selected ranges and assigned values from 1 to 5, with 1 indicating very low groundwater drought risk and 5 indicating very high groundwater drought risk
- The raster layers are then multiplied by the assigned weights and added together to make the final map constituting each submodule or module

3.1. Meteorological drought risk

The World Meteorological Organization (WMO) published a list of extreme weather indices that have to be assessed in climate monitoring and prediction. WMO recommends analysis over at least a 30-year period as that indicates the "average weather" and typical behaviour. WMO (2015) defines meteorological drought as "atmospheric conditions resulting in the absence or reduction of precipitation over a period of time". Drought typically begins as a dry spell—a period of abnormally dry weather; however, the conditions are less severe than those of the actual drought. In this study, the datasets in

Table 3-1 are combined into one index that constitutes meteorological drought risk. These are based on the WMO defined set of core descriptive indices of climate extremes:

Rainfall amount- this is used to map dry areas with areas receiving average daily rainfall lower than 1 millimetre per day (mm/day) over the time-series being classified as dry (

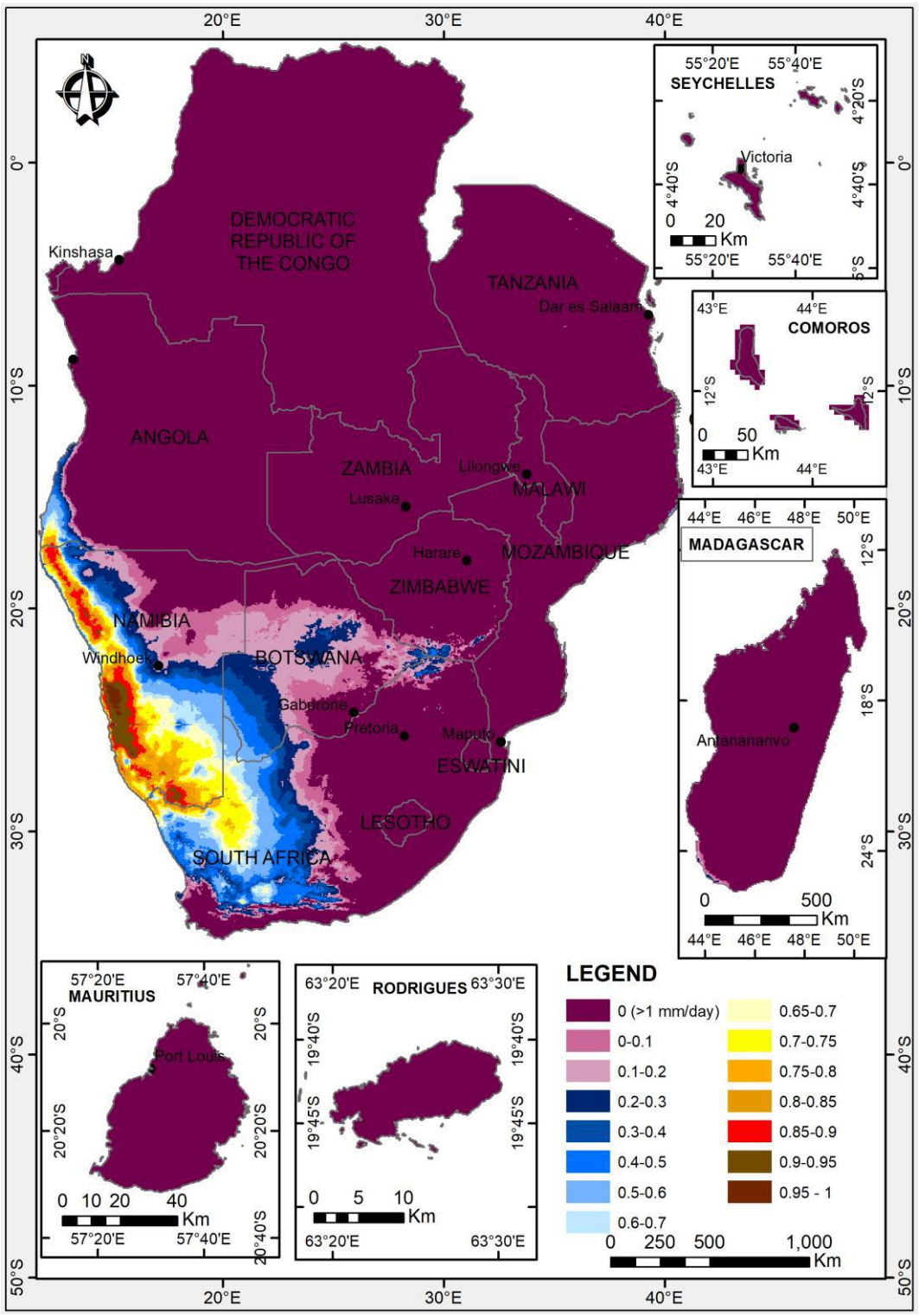

- Figure 3-1)

Rainfall variability - coefficient of variation of rainfall; which is calculated by dividing the standard deviation of monthly rainfall by the mean monthly rainfall, the higher the coefficient of variation (CV), the more variable the year-to-year (i.e. inter-annual) rainfall

of a locality is the higher the drought risk (

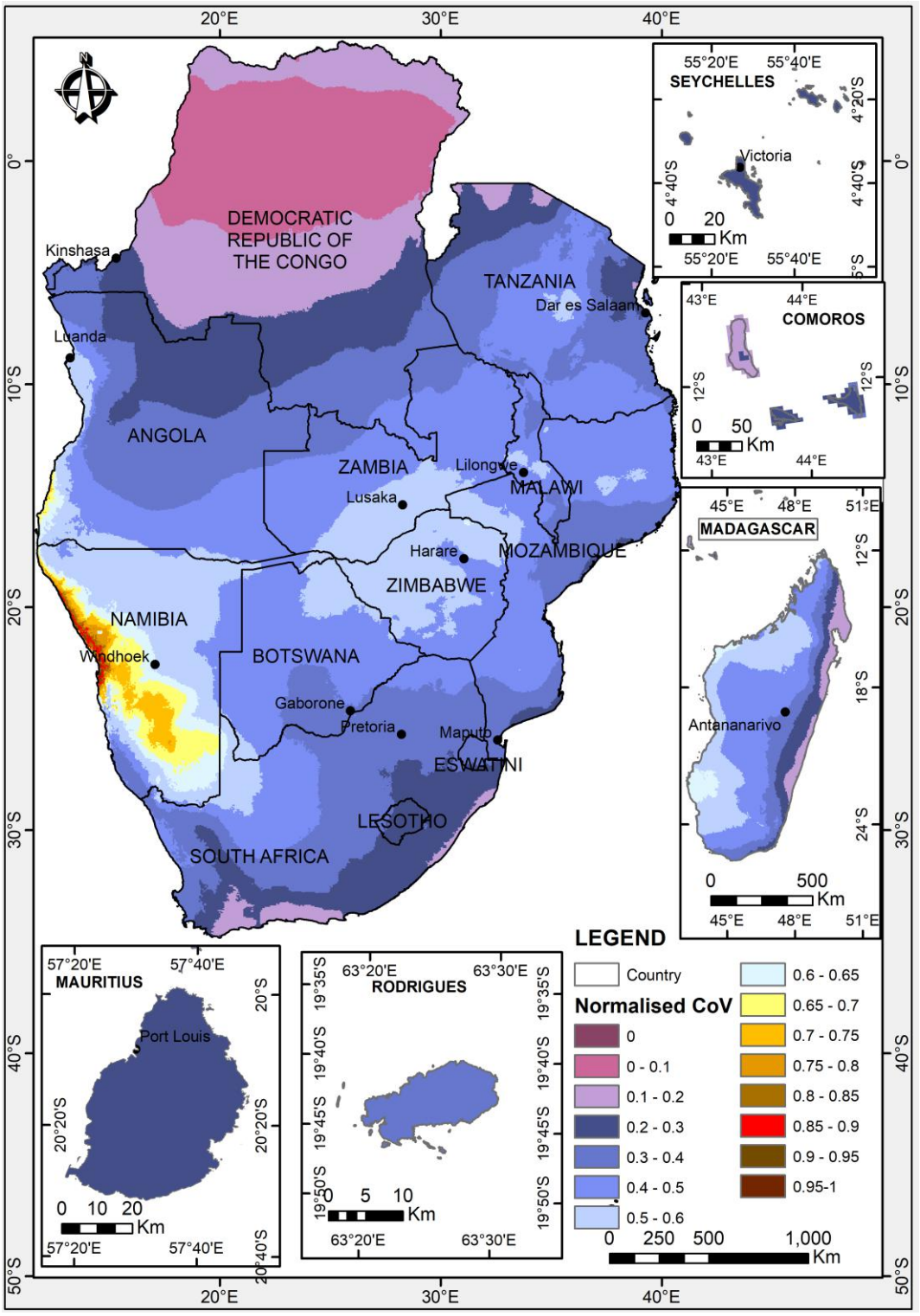

- Figure 3-2)

The number of consecutive dry days- days during which the precipitation was below 1 mm/day in one calendar year (

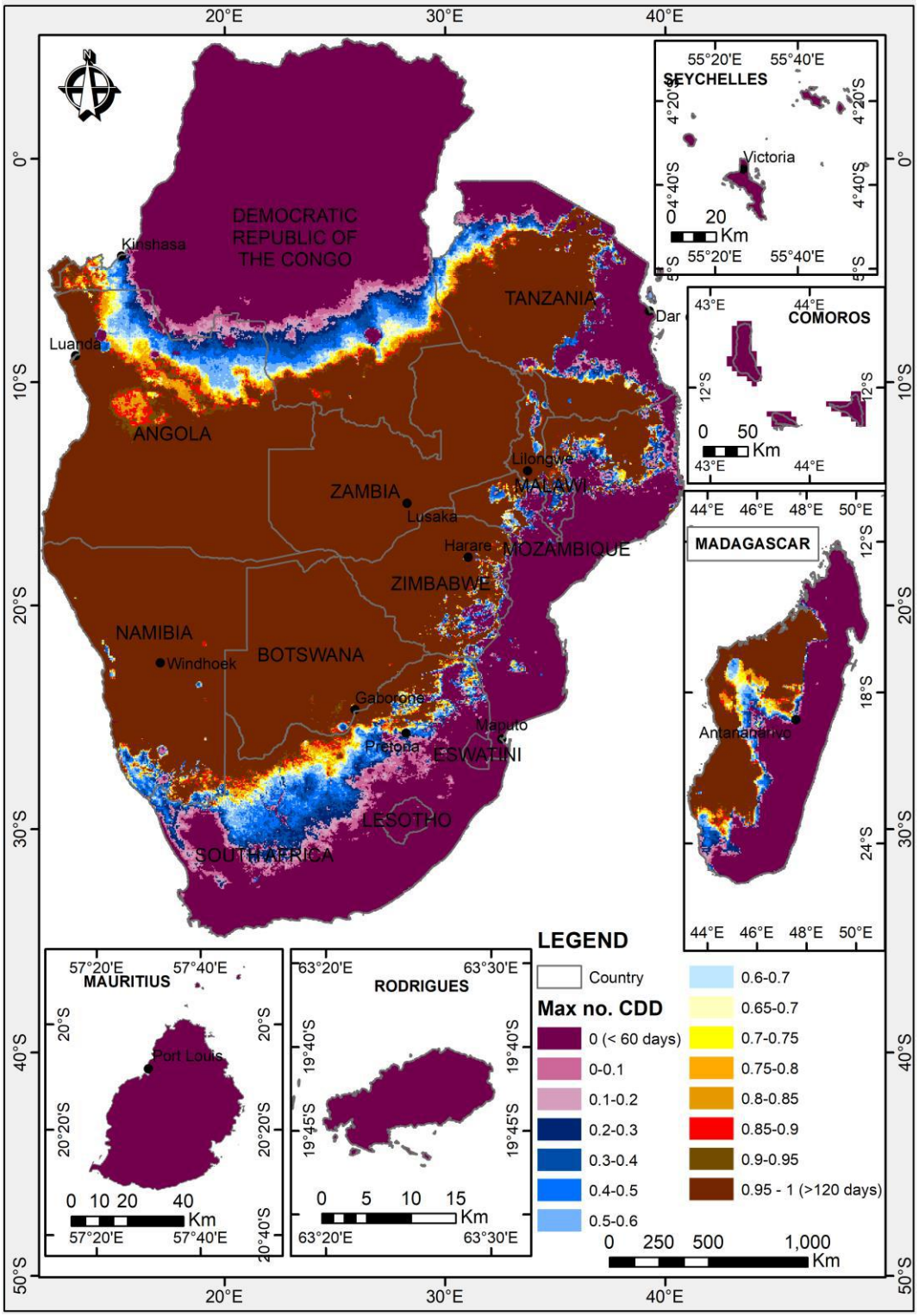

- Figure 3-3)

- **The number of consecutive dry days or days during which the precipitation was below 1 mm/day** over more than one calendar years (to cater for extended dry months) (Figure 3-4)

Table 3-1: Meteorological risk parameters, the ranges and the reclassification values

Parameter	Ranges	Reclassification values
Rainfall amount (P_{ANN})	<1	1-Average rainfall value of grid point
	>1	0
Coefficient of variation (P_{STD})	0 %	0
	100 %	1
	0-100	Rescaled between 0 and 1
Consecutive number of dry days in one calendar year (P_{DRS})	<60 days	0
	>120 days	1
	60-120 days	Rescaled between 0 and 1
Consecutive number of days over more than one calendar year (P_{EXT})	<150 days	0
	>270 days	1
	150-270	Rescaled between 0 and 1

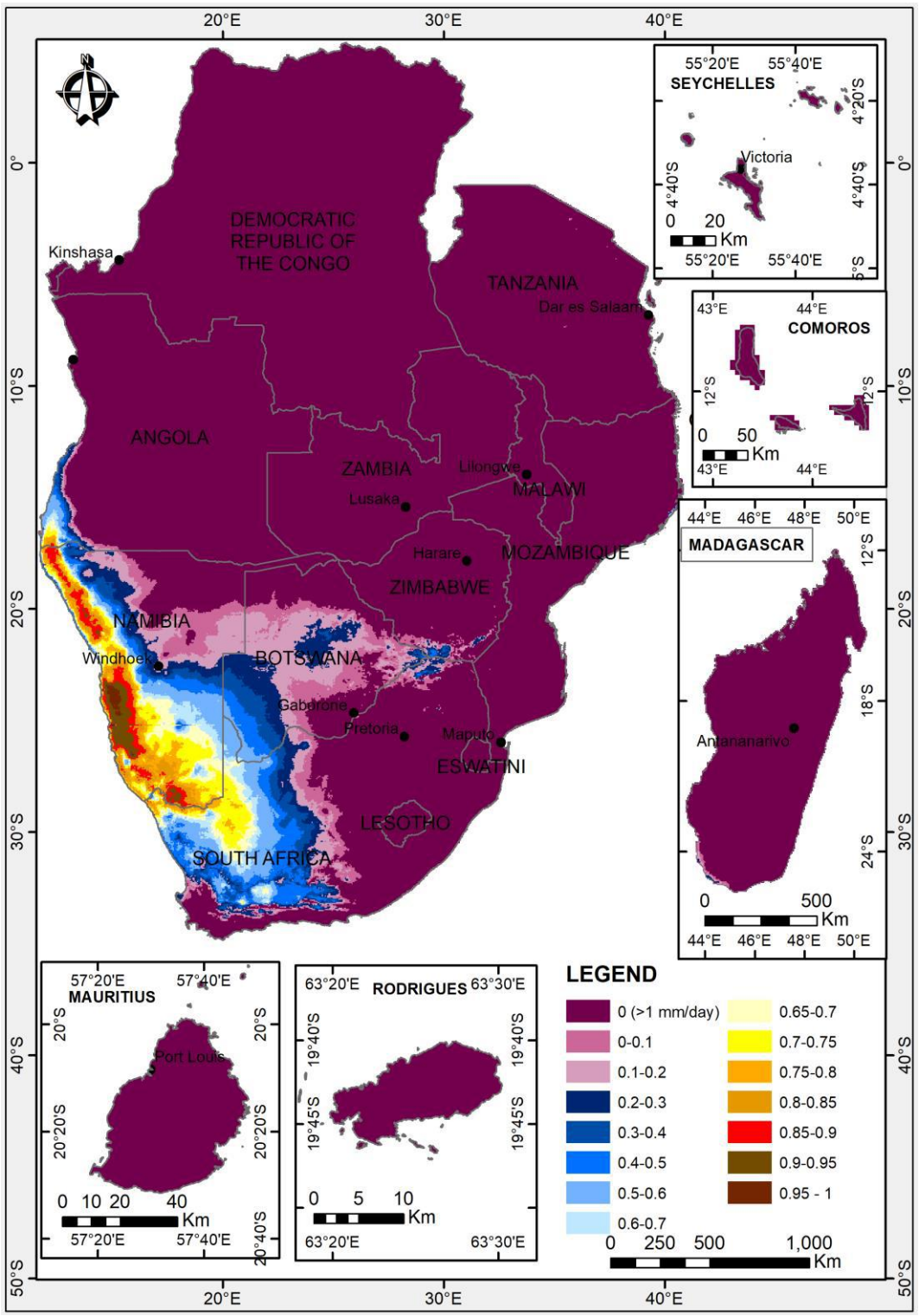

Figure 3-1: **The rainfall amount map showing a scale of 0 – 1, with 1 indicating areas of daily rainfall less than 1mm/day and therefore high groundwater drought risk areas**

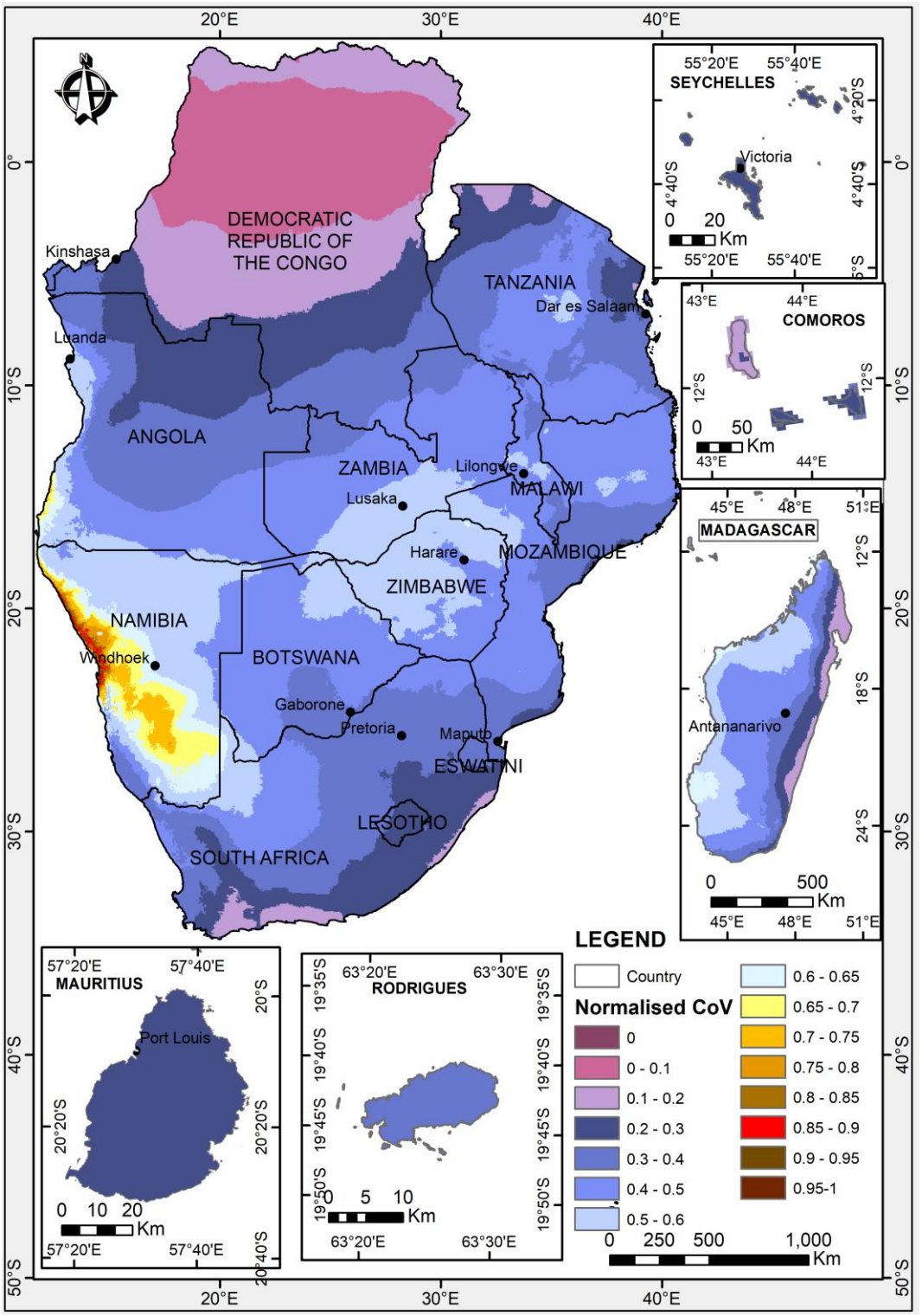

Figure 3-2: The SADC map showing the coefficient of variation of rainfall

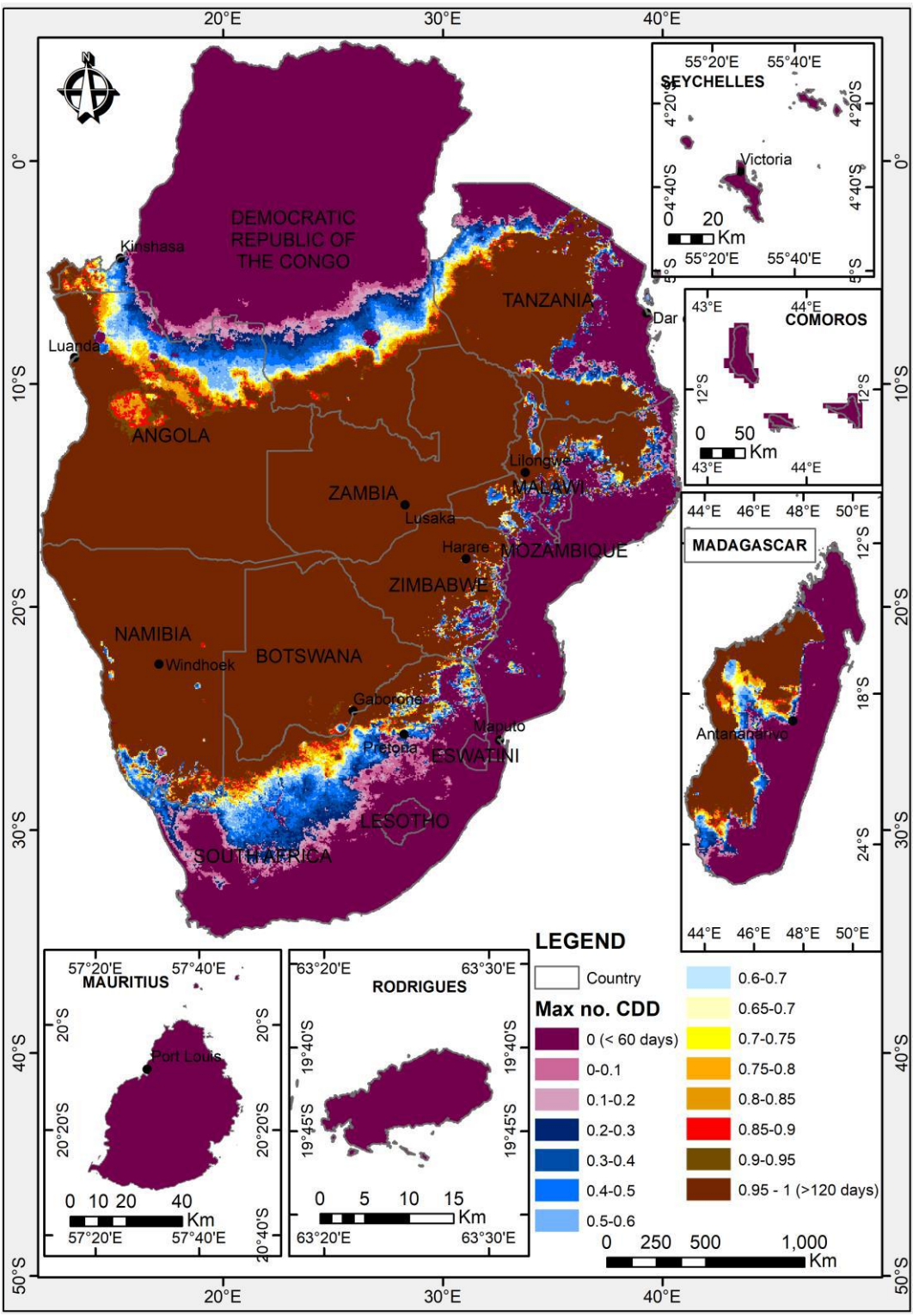

Figure 3-3: **Number of consecutive dry days in one calendar year**

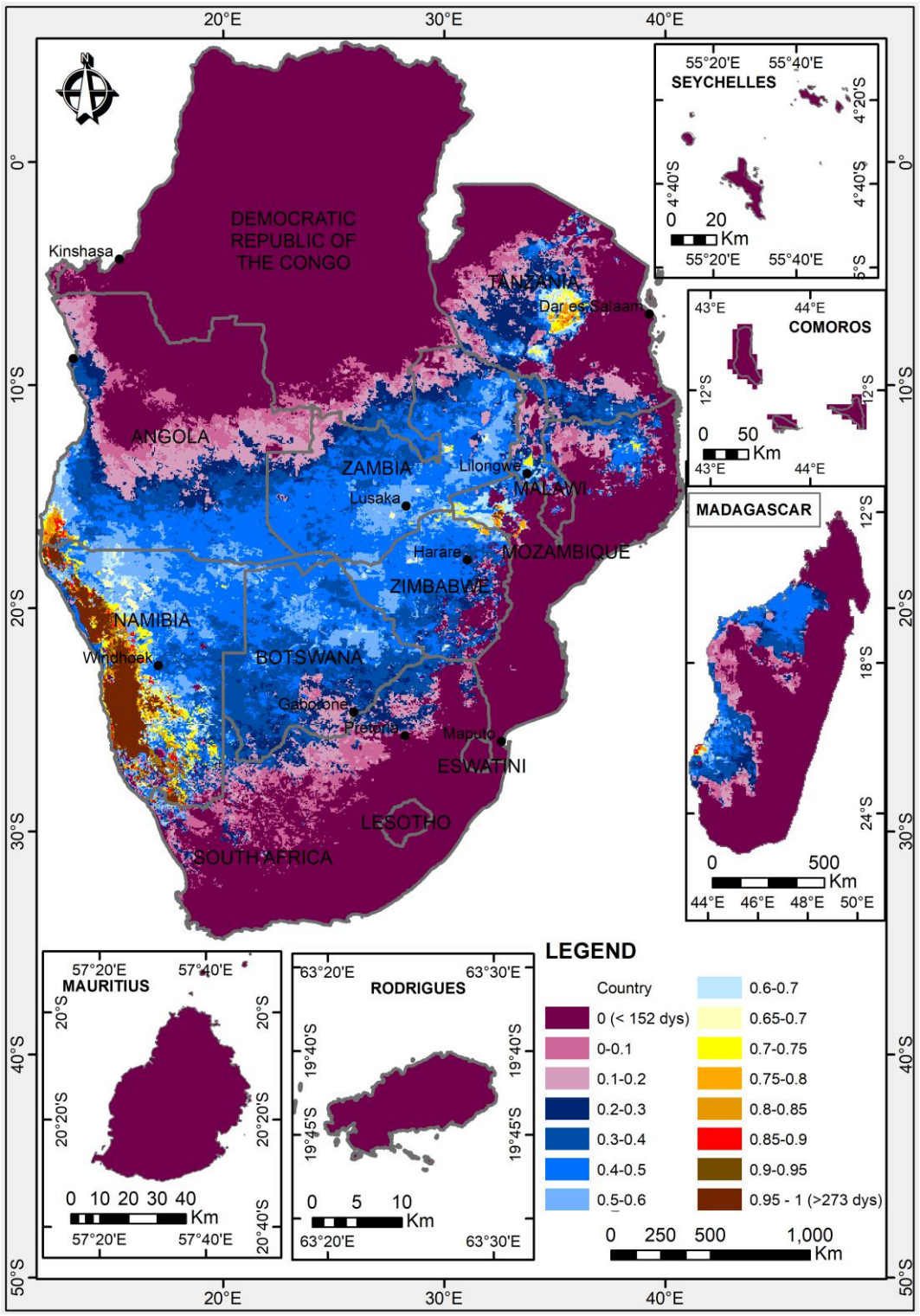

Figure 3-4: Number of consecutive dry days in more than one calendar year

The equation used to calculate meteorological risk adapted from SADC (2011) is given below:

Meteorological risk (M) = 5 *[0.4(PANN) + 0.15 (PDRS) +0.15 (PEXT) +0.3 (PSTD)]

Where

PANN = rainfall amount, assigned the highest weight of 0.4 and has the most effect on drought

PDRS = number of consecutive dry days in one calendar year, assigned the lowest weight of 0.15

PEXT = number of consecutive dry days over more than one calendar year, assigned the lowest weight of 0.15

PSTD = rainfall coefficient of variation, assigned a moderate weight value of 0.3

Sum of all weights = 0.4 + 0.15 + 0.15 + 0.3 =1

A multiplication factor of 5 is used to scale the values between 0 and 5. The meteorological drought risk map is shown in Figure 3-5.

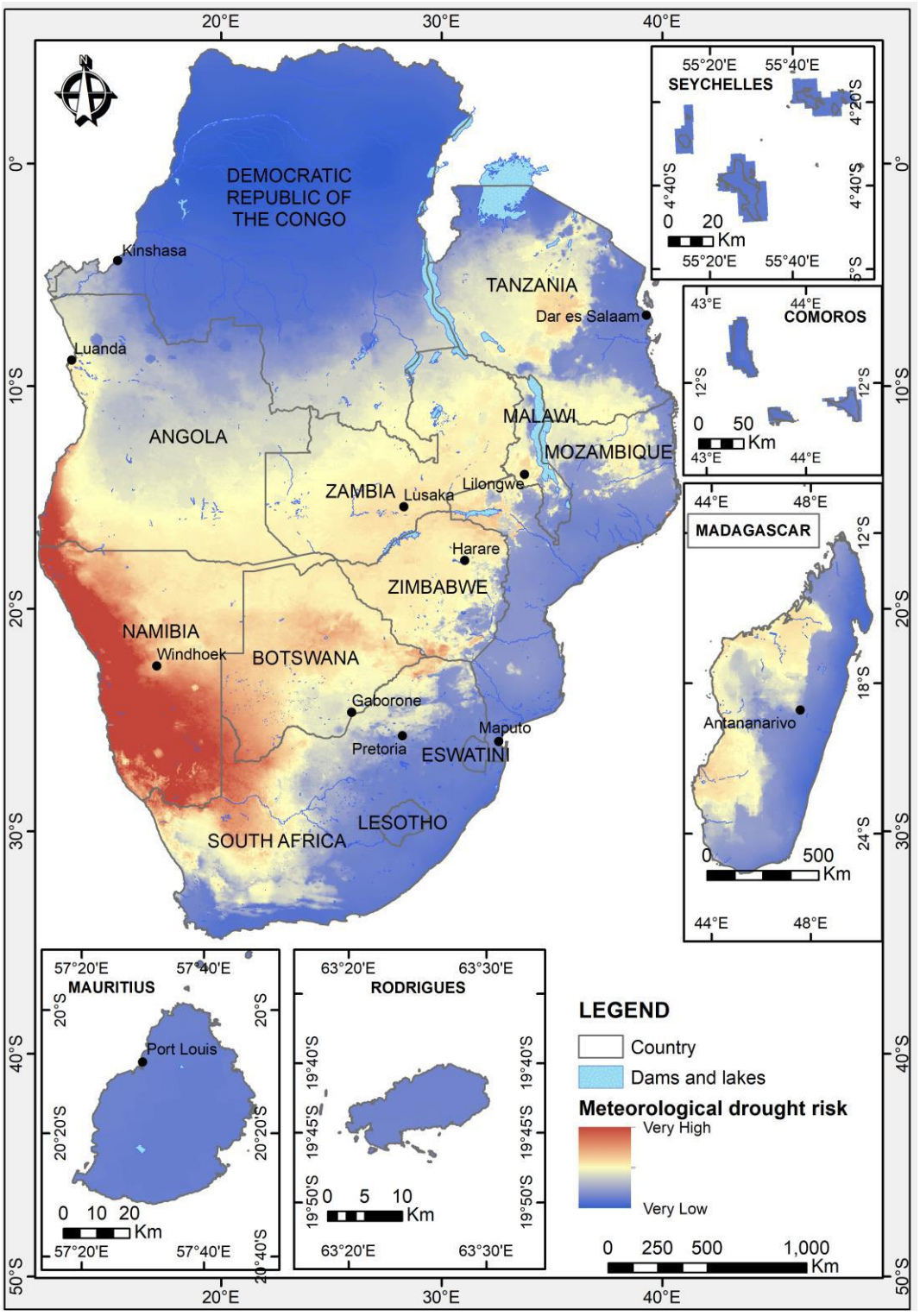

Figure 3-5: Meteorological drought risk map

Another scenario was computed with all the parameters equally weighted. The effects of these results on the climate sensitivity map are discussed in Chapter 4.

3.2. Hydrogeological drought proneness

The hydrogeological drought proneness module relates to the physical factors influencing drought conditions in groundwater systems. The aspects considered are (SADC 2011):

- **Aquifer productivity**- made up of two parameters, aquifer storage capacity and aquifer permeability e.g. a deeper extensive and more productive aquifer will be less drought vulnerable than shallow aquifers
- **Groundwater recharge potential**- areas of high groundwater recharge is less vulnerable to drought

3.2.1. Aquifer productivity

Aquifer productivity describes the potential of aquifers to sustain various levels of borehole water supply and the dominant groundwater flow types in each aquifer (Ó Dochartaigh *et al* 2011). Aquifer storage capacity and aquifer permeability are critical factors in determining aquifer productivity. Aquifer storage covers two aspects of groundwater: the volume of water in the porous system per volume of aquifer (storativity) and the physical extent of the aquifer. Permeability expresses the ease with which water flows in the porous system, and by inference, how much water can be extracted, for a certain power, within a certain time. A practical proxy for this is the well yield, which is expressed in litres per second (L/s) (SADC 2011).

The aquifer types from the SADC Hydrogeology Map (SADC 2010) were used as the input data for aquifer productivity (Figure 3-6; Table 3-2). The map is used to replace both the aquifer permeability and aquifer storage capacity parameters. This is largely, because there are no comprehensive or adequate borehole data per country for the SADC region from which aquifer permeability or storage capacity values can be obtained. The use of the SADC geohydrology map aquifer type data is justified because of the way it was derived as it considered aquifer permeability, flow regimes (transmissivity) and productivity (SADC 2011).

Table 3-2: Aquifer map classes

Aquifer	Reclassification value according to productivity
Low permeability	1
Karst	2
Fissured	3
Unconsolidated intergranular	4
Multi-layered aquifer	5 (most productive=low drought risk)

3.2.2. Groundwater recharge potential

Broadly, groundwater recharge can be defined as an addition of water to the saturated zone with four main modes of recharge distinguished: downward flow of water through the unsaturated zone reaching the water table; lateral and/or vertical inter-aquifer flow, induced recharge from nearby surface-water bodies resulting from groundwater abstraction, and artificial recharge such as from borehole injection or man-made infiltration ponds, dams, etc (Xu and Beekman 2019). The natural recharge by downward flow of water through the unsaturated zone is generally the most important mode of recharge in arid and semi-arid areas. In the GDR map compilation direct groundwater recharge is not calculated but rather a recharge potential map based of the following parameters:

Rainfall: Rainfall is the most important factor of recharge as excessive amounts of surface water are stored and recharged during periods of intense rainfall (

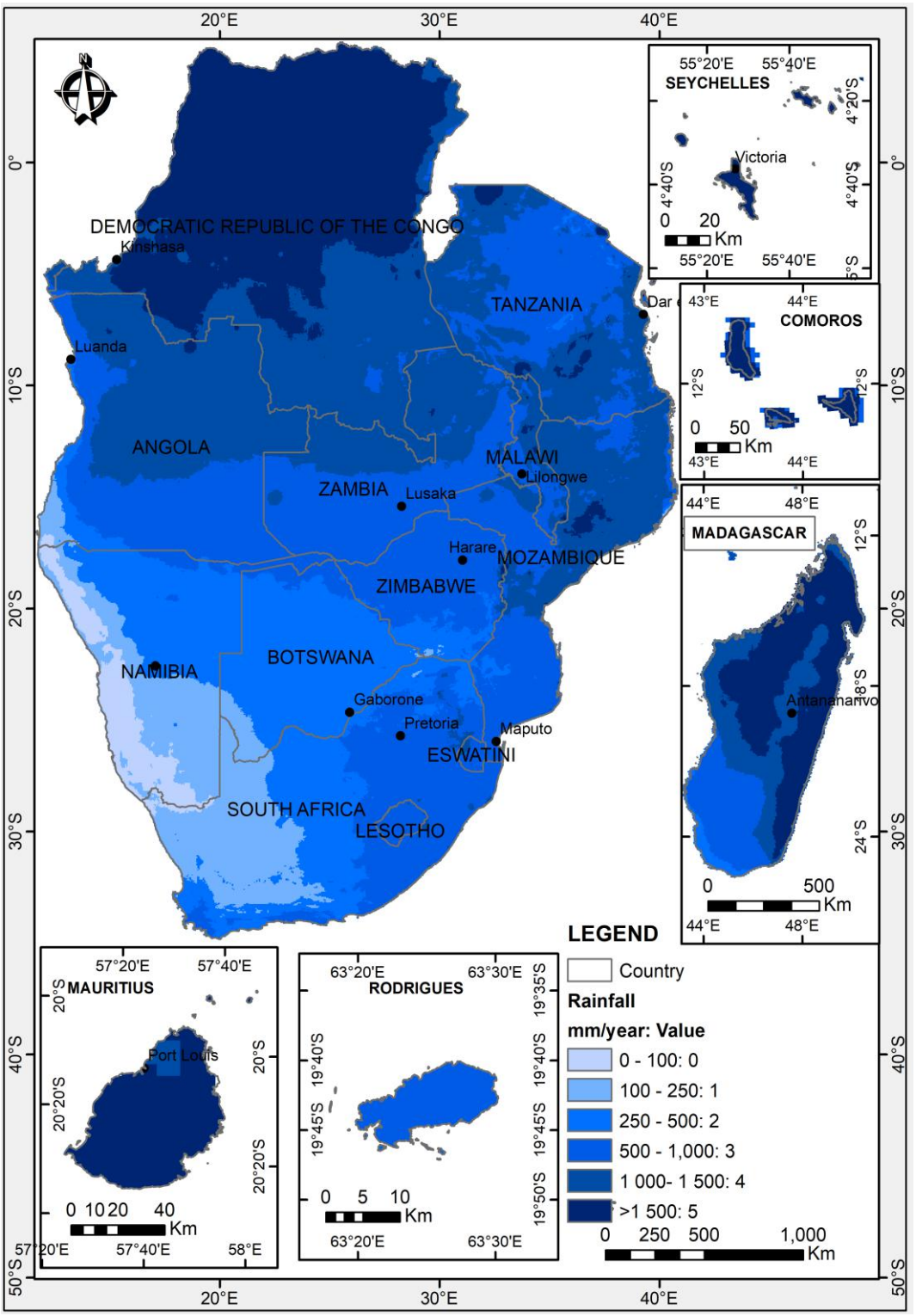

- Figure 3-7). The gridded 5km resolution CHIRPS version 2 mean annual rainfall averaged of 39 years from 1981 to 2019 was used (Funk *et al* 2014). The classes of rainfall (Table 3-3) used are based on various sources (National Park Service 2019, FAO 1989)

Slope: Slope gradient influences the catchment configuration and thus influence runoff, ponding and the infiltration of surface water (Adams *et al* 2004). Low levels in recharge

occur on steep slopes as water flows rapidly downwards providing insufficient time to infiltrate and flat lands facilitate groundwater recharge due to retention of rainwater, providing moderate evaporation conditions (

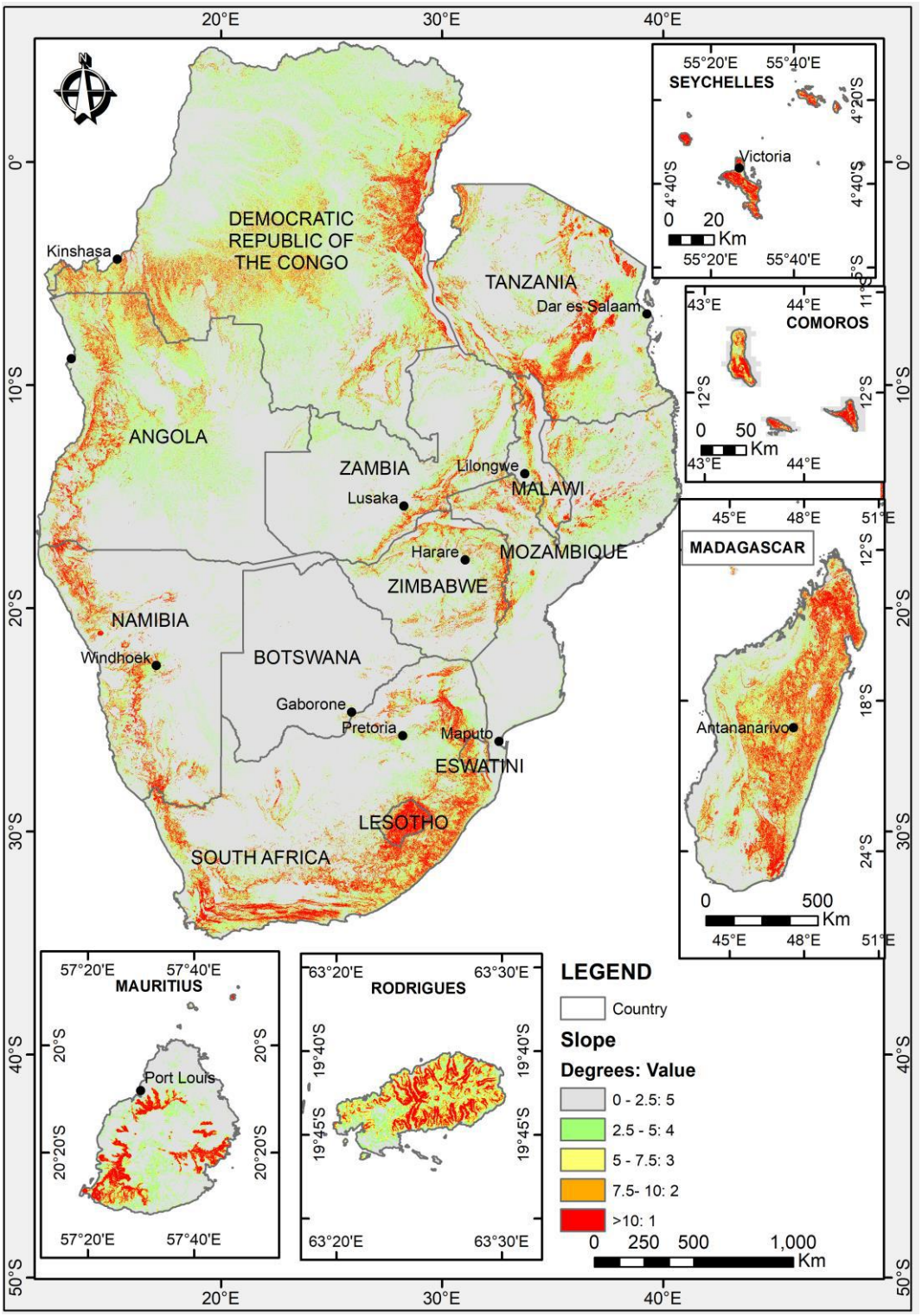

- Figure 3-8). Slope classification is adopted from the SOTER Classification (Table 3-3) which a standard way of classifying slope (Van Engelen and Dijkshoorn 2012, Mogaji *et al* 2015, da Costa *et al* 2019)
- **Vegetation** (Normalized Difference Vegetation Index): NDVI derived from MODIS satellite imagery is used to quantify vegetation by measuring the difference between the near-infrared values (which vegetation strongly reflects) and red light (which vegetation absorbs). The values obtained are between -1 to +1 with higher values representing healthy vegetation and low values low or less vegetation (Figure 3-9; Table 3-3). The assumption is that good vegetation cover enhances infiltration and hence recharge, whereas poor vegetation cover impedes recharge and enhances surface runoff. Global gridded vegetation indices from MODIS are calculated at 16-day and monthly intervals and in this case monthly data at 1 km resolution from the MYD13A2 Version 6 product for the years 2002 to 2019 was averaged and used in the study (Didan *et al* 2015). The NDVI classes used were based on various sources (SADC 2011, Aziz *et al* 2018, Aquino and Oliveira 2012)

Table 3-3: Groundwater recharge parameters and reclassification values

Parameter	Ranges	Description	Values relating to groundwater recharge potential
Mean annual rainfall (mm/year)	0 - 100	Hyper arid	0
	100 - 250	Arid	1
	250 - 500	Semi-arid	2
	500 - 1000		3
	1000 - 1500		4
	>1500	Tropical moist	5
Slope (degrees)	0 - 2	Flat	5
	2 -5	Gently undulating	4
	5 -7.5	Undulating	3
	7.5 - 10	Undulating- sloping	2
	>10	Strongly sloping to extremely steep	1
NDVI	<0	Extreme drought	0
	0 - 0.2	Dry	1
	0.2 - 0.4	Dry-Moderate	2
	0.4 - 0.5	Moderate	3
	0.5 - 0.6	Wet	4
	>0.6	Extremely wet	5

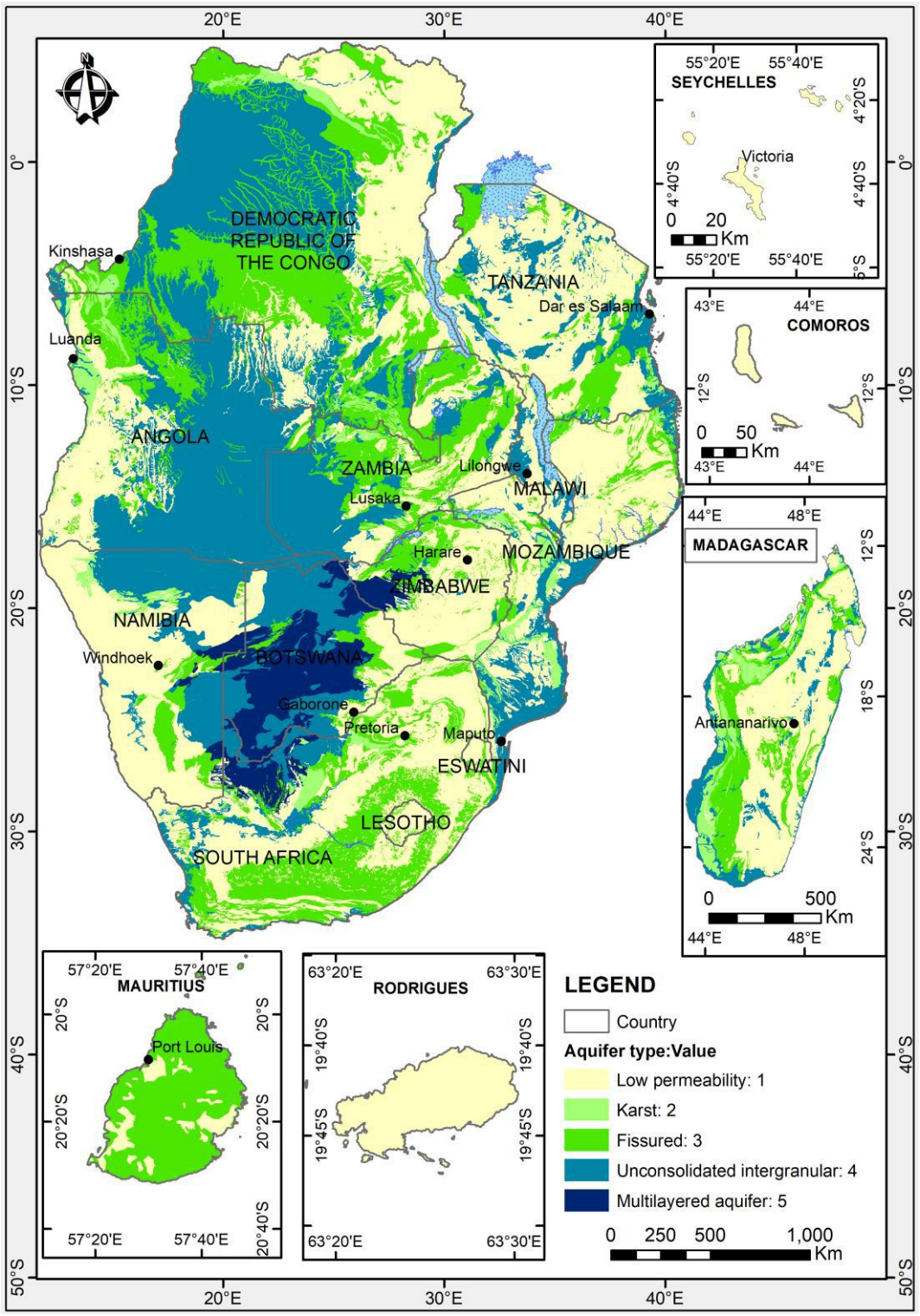

Figure 3-6: **The SADC aquifer type map and the values assigned to the different aquifer types**

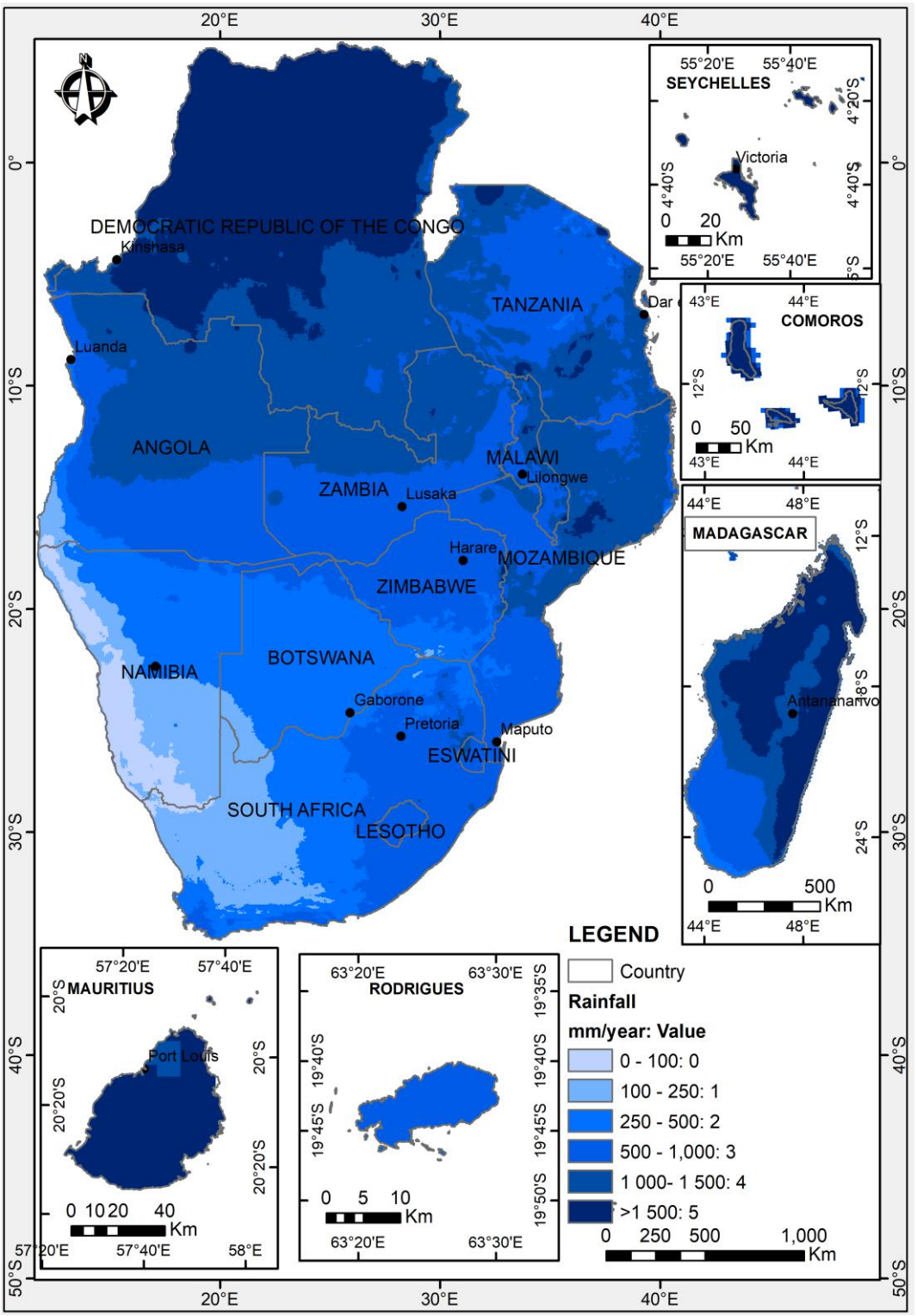

Figure 3-7: **Mean annual rainfall classes and groundwater drought risk values assigned**

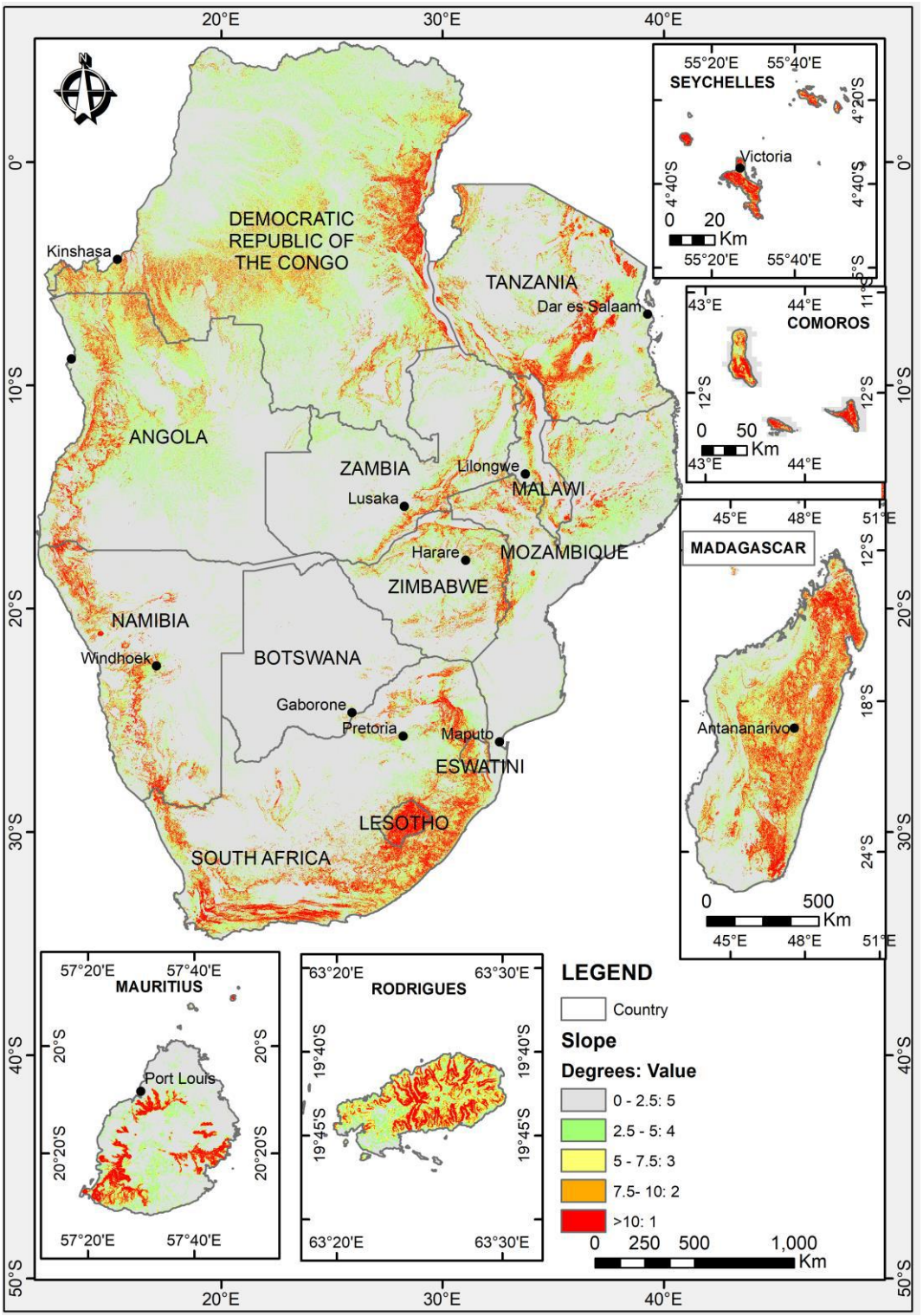

Figure 3-8: **The slope classes assigned values relating to the groundwater recharge potential**

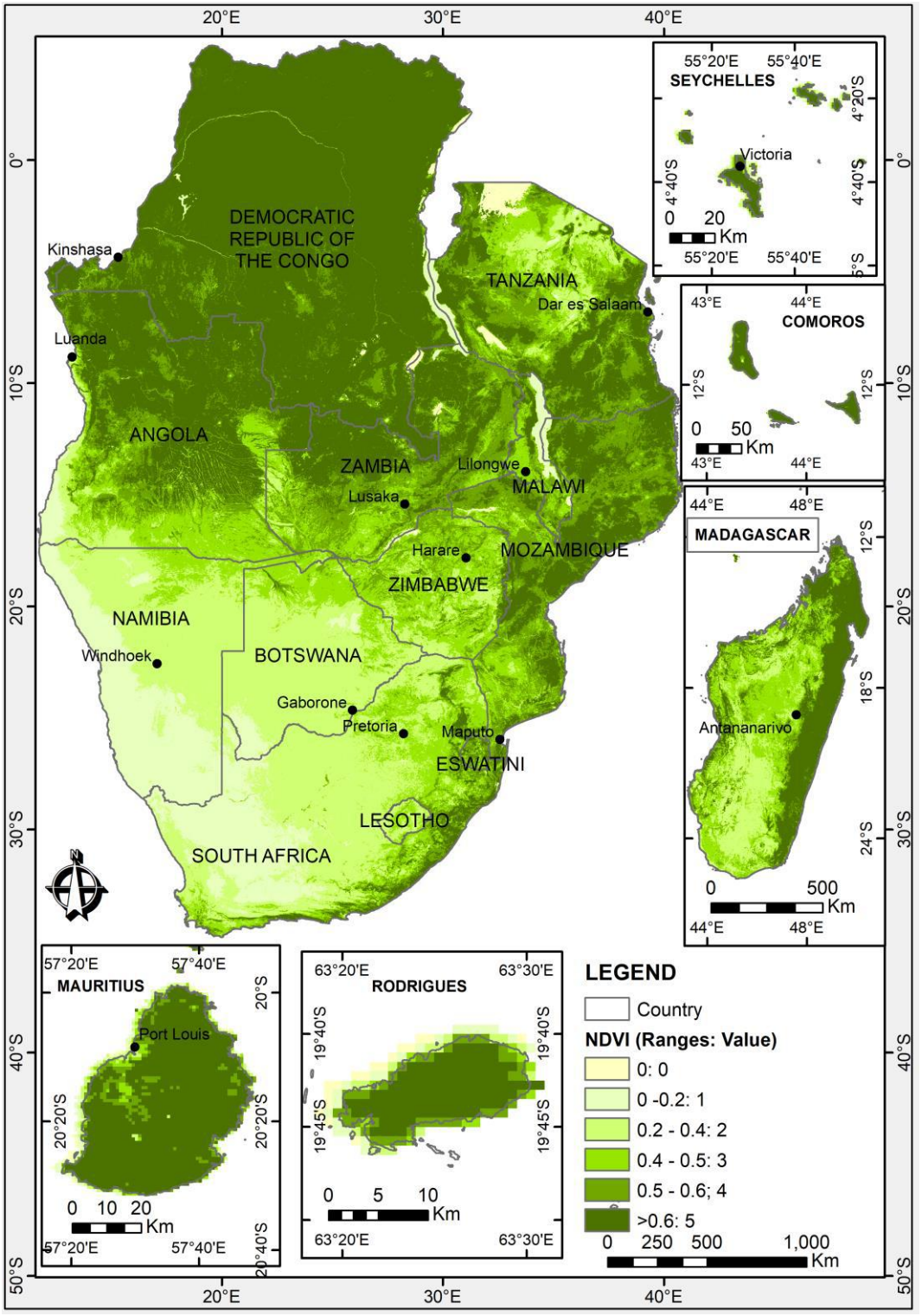

Figure 3-9: NDVI map showing the values assigned according to groundwater recharge potential

The equation for the calculation of the groundwater potential map as adopted from SADC (2011) is as follows:

Groundwater recharge potential = 0.5 * Rainfall + 0.35 *NDVI + 0.15* Slope

The groundwater recharge potential map is given in Figure 3-10.

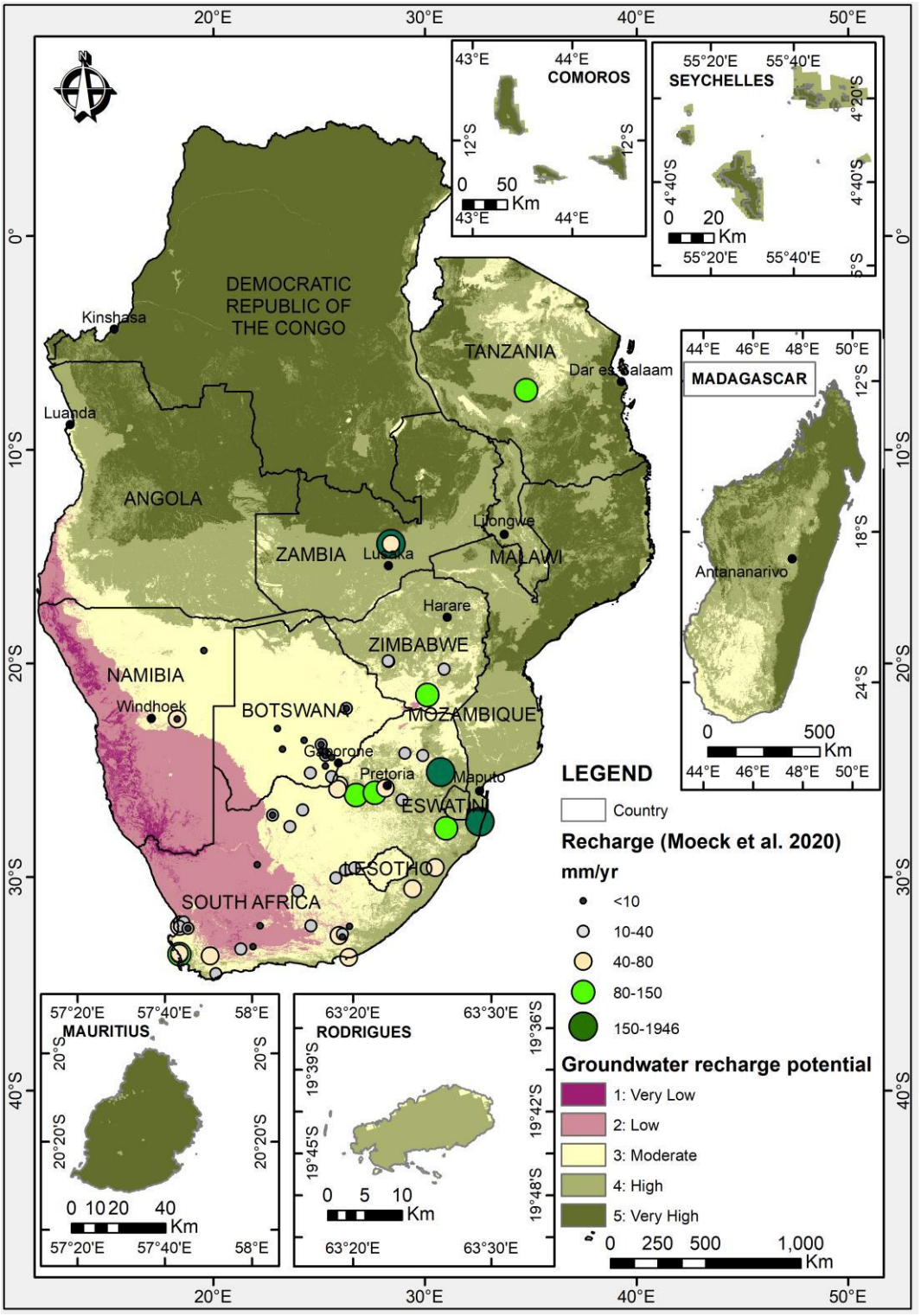

Figure 3-10: **The groundwater recharge potential map based on the mean annual rainfall**

A second scenario was computed with all parameters. i.e. slope, NDVI and rainfall equally weighted. The effects of these results on the groundwater recharge potential map are discussed in Chapter 4.

3.2.2.1. Consideration of evapotranspiration in groundwater recharge potential

The above approach oversimplifies groundwater recharge processes by generalizing relationships between climate and hydrological fluxes but remains the only viable option to simulate large scale processes due to long model running times and lack of data (Moeck *et al* 2020). The water availability on the surface for infiltration and the potential of the subsurface system to intake water are the two major controls on recharge (Mohan *et al* 2018). Evapotranspiration (ET) is a dominant component of the water balance and potential evaporation is much higher than rainfall in most areas throughout SADC. Moeck *et al* (2020) analysis of a global dataset of recharge rates and other global-scale datasets, such as climatic or soil-related parameters, using correlation analysis, showed that climatic forcing functions, particularly annual precipitation and seasonality in temperature and precipitation, are the most important predictor variables of groundwater recharge rates followed by soil and vegetation factors. In general, higher precipitation rates and stronger precipitation seasonality increase the potential for recharge by increasing the availability of water at the surface whilst, global variability in evapotranspiration has less of an effect on groundwater recharge.

To take the evapotranspiration into account in the algorithm we used the aridity index (Table 3-4). The Global Aridity Index dataset is freely available at ~1 km resolution for the years 1970-2020 (Trabucco and Zomer 2018). Aridity is usually expressed as a generalized function of precipitation, temperature and reference evapotranspiration (ET0). An Aridity Index (UNEP 1997) can be used to quantify precipitation availability over atmospheric water demand. The datasets are derived by dividing the mean annual precipitation with the mean annual reference evapotranspiration. The data is classified based on various sources (UNEP 1997, FAO 1993) (Figure 3-11).

Table 3-4: The global aridity index and reclassification values

Parameter	Ranges	Description	Values relating to groundwater recharge potential
Global aridity Index (mm/year)	<0.05	Hyper arid	0
	0.05 – 0.2	Arid	1
	0.2 -0.5	Semi-arid	2
	0.5-0.65	Dry sub-humid	3
	0.65-0.75	Humid	4
	>0.5	Hyper-humid	5

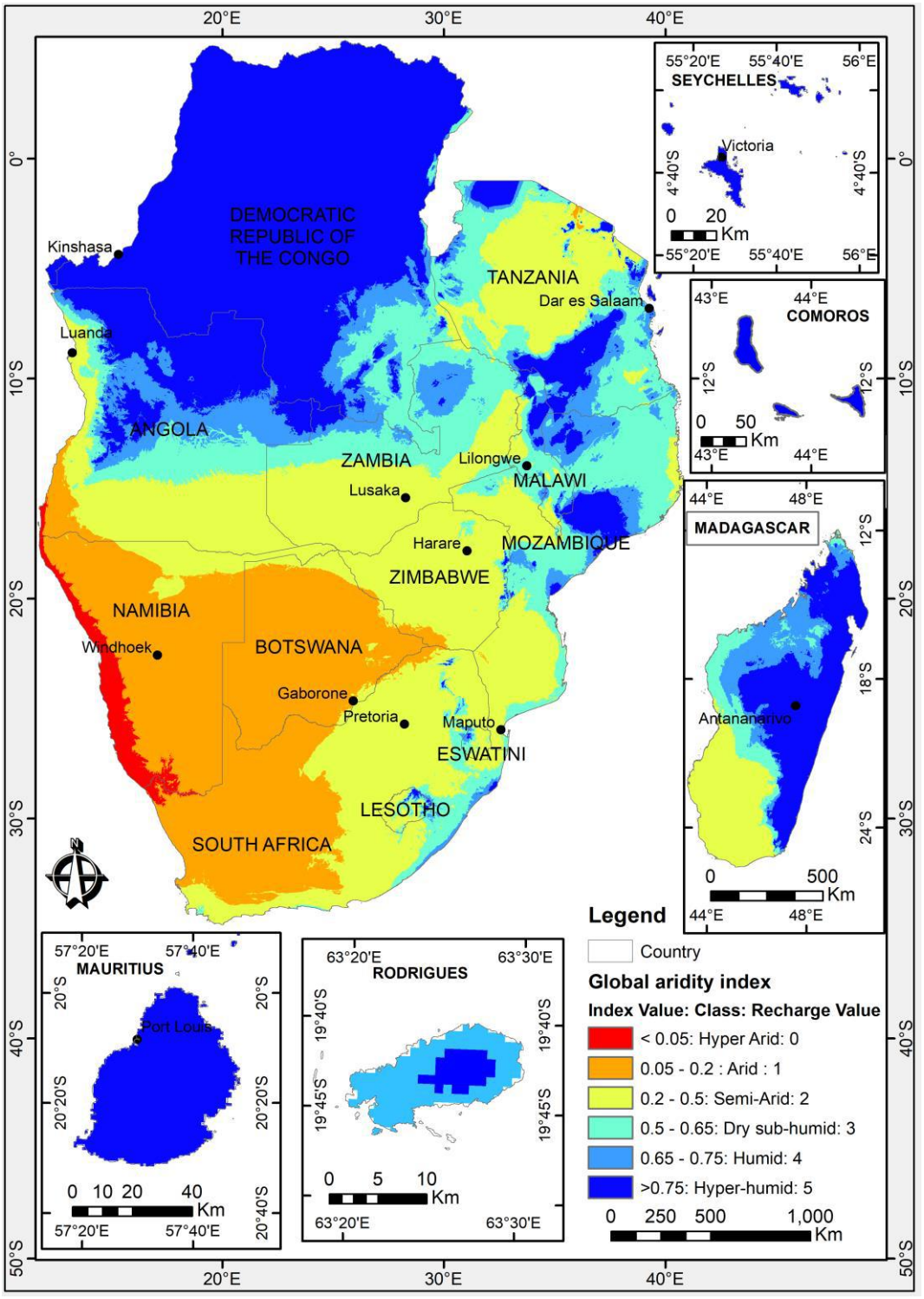

Figure 3-11: Global aridity index map

A second groundwater recharge potential map was created by substituting the mean annual rainfall with the aridity index (Figure 3-12).

The equation for the calculation of the groundwater potential map as adopted from SADC (2011) is as follows:

Groundwater recharge potential = 0.5 * Aridity index + 0.35 *NDVI + 0.15* Slope

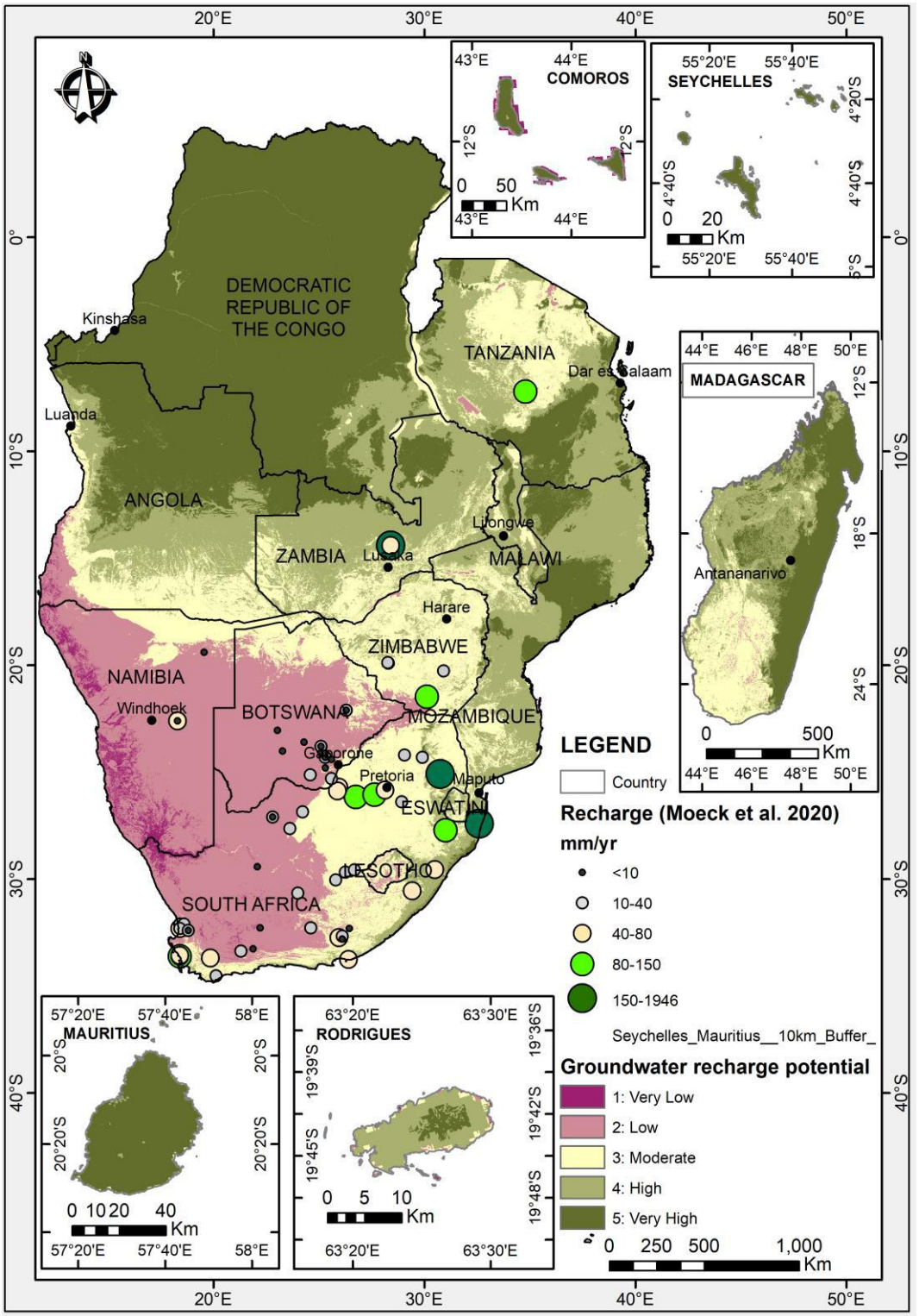

Figure 3-12: **The groundwater recharge potential map based on the aridity index**

3.2.3. Calculation of hydrogeological drought proneness

The equation for the calculation of the hydrogeological drought proneness is as follows:

Hydrogeological drought proneness = 0.5 * Aquifer productivity + 0. 5 *Groundwater recharge potential

The hydrogeological drought proneness map is given in Figure 3-13.

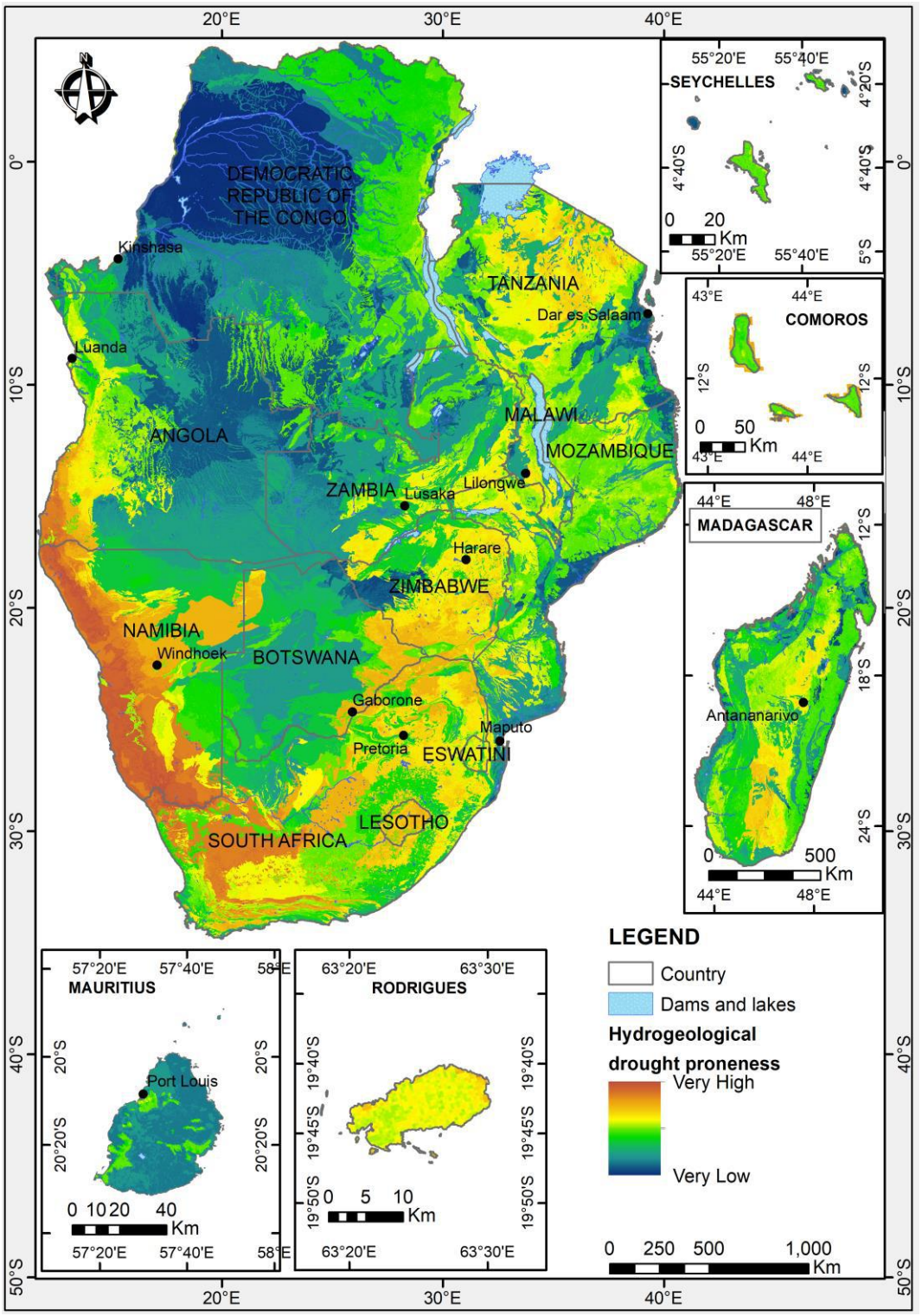

Figure 3-13: **The hydrogeological drought proneness map based on the mean annual rainfall data**

Another hydrogeological drought proneness map was created based on the groundwater recharge potential map created using the aridity index. The results and comparisons of the two maps will be discussed in Chapter 4 using sensitivity analysis.

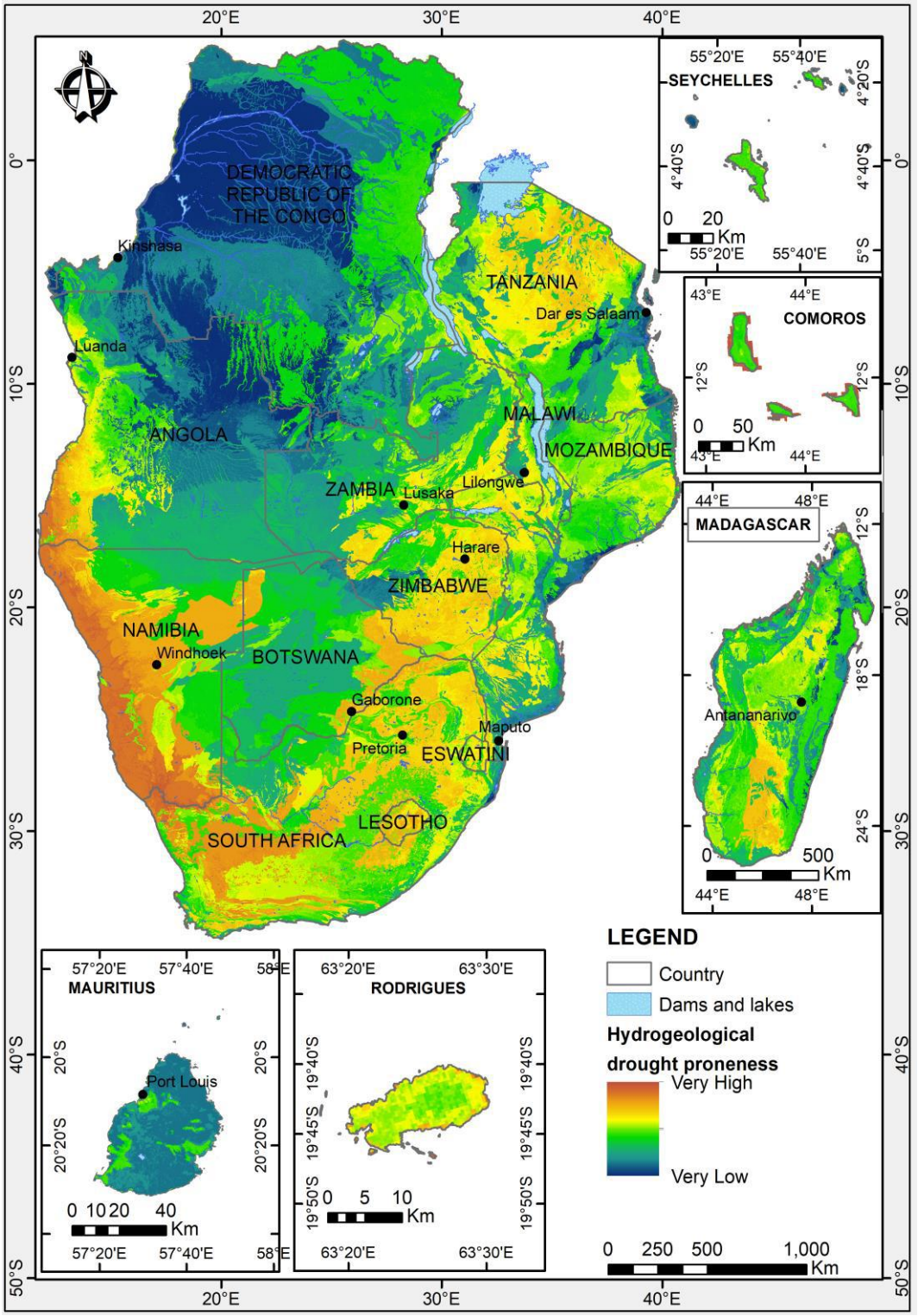

Figure 3-14: **The hydrogeological drought proneness map based on the aridity index**

3.3. Groundwater storage risk

Satellite-based GRACE provides data and information of available terrestrial water storage anomalies and combining the soil moisture from Global Land Data Assimilation System (GLDAS) offers an approach to estimate groundwater storage changes for a region (Singh and Saravanan 2020). Understanding groundwater storage changes is critical as groundwater storage represents a buffer for achieving groundwater resilience under extreme climate events e.g. extended drought conditions. A groundwater storage sensitivity module is incorporated in the GRiMMS algorithm using GRACE-derived groundwater storage anomalies by relating to the GRACE Groundwater Drought Index (GGDI).

Box 3-1: GRACE Tellus mission

The GRACE Tellus mission represents a breakthrough to measure and monitor changes in the Earth's cryosphere, hydrosphere and oceanographic components[1]. The GRACE Tellus mission consists of twin satellites measuring changes in Earth's gravity field. GRACE and GRACE-Follow On (FO) level - 1 instrument data is fed to three processing centres NASA's Jet Propulsion Laboratory (JPL), GeoforschungsZentrum Potsdam (GFZ), and Center for Space Research at University of Texas (CSR). These three processing centres are the primary centres responsible for delivering GRACE level – 2 to level – 4 data products. These products include, monthly changes in terrestrial water storage, monthly ocean bottom pressure changes, monthly gravitation field anomalies, and much more, from land mass changes data (Wahr *et al* 1998). Each centre relies on various post-processing algorithms to derive monthly gravity field changes (Level – 2), which in turn are used to derive the above data products. The result is three different solutions for GRACE derived data products (Sakumura *et al* 2014).

Thomas *et al* (2017) utilised GRACE-deficit analysis approach to characterize groundwater drought. In this case to characterise groundwater drought in the Central Valley, California due to anthropogenic effects and natural drought responses. Normalized GRACE-derived groundwater storage deviations were shown to quantify groundwater storage deficits during the GRACE record, which was defined as the GGDI. The GGDI is calculated by normalising the results of removing the monthly mean from each monthly observation. The GGDI provides a measure of the deviation in groundwater storage from normal conditions. Hence, negative GGDI indicate groundwater storage drought conditions, while positive GGDI indicate groundwater storage surplus conditions. The GGDI allow for the identification of groundwater storage drought event, intensity, duration and frequency (Thomas *et al* 2017).

The GGDI is however, a timeseries analysis of GRACE derived groundwater storage anomalies. In this form it is not suited for incorporation in the GRiMMS algorithm, which is a composite mapping overlay analysis. Instead thematic layers representing spatial distributions are more appropriate. In this regard we extend the GGDI methodology by extracting a set of parameters from the GGDI

[1] https://grace.jpl.nasa.gov/

timeseries, that can be used to explain the spatial distribution of the sensitivity of groundwater storage to drought so as to derive a groundwater storage risk. To do this a set of descriptive core indices are developed:

- **Percentage of the time –series in a groundwater storage drought** – this is used as a proxy to explain duration of groundwater storage in deficit
- **Mean negative GGDI** – is used to explain the mean intensity of groundwater storage deficit conditions
- **Trend GGDI** – used to indicate changes in groundwater storage conditions

3.3.1. Data

3.3.1.1. GRACE derived terrestrial water storage (ΔTWS)

At present, there are two major level - 1 GRACE post-processing products representing terrestrial water storage changes:

1. spherical harmonics (SH) based solutions
2. Mass concentration blocks (mascon) based solution

Both versions where downloaded and used in the analysis of the GRACE data. The SH version rely on resolving earth gravity field using a set spherical harmonic (Stokes) coefficients at approximately monthly intervals, complete to degree and order 120 (Swenson and Wahr 2006, Swenson *et al* 2008). The mascon version depend on a surface spherical cap mascon based solution to directly estimate mass variations from the inter satellite range-rate measurements (Watkins *et al* 2015). The SH version used are the Release 06 version 03 of GRACE and GRACE-FO Level – 3 monthly terrestrial water storage anomalies, from April 2002 – November 2019[2]. The data are provided on a global 1°x1° grid with ocean signals masked. Optional land grid scaling factors have not yet been applied to the data. All three post-processing solutions are downloaded and the arithmetic mean of the three used for further analysis. The mascon version used in this application is the Release 06 version 02 of GRACE and GRACE-FO level – 3 monthly terrestrial water storage anomalies, for April 2002 – March 2020, from the Center for Space Research at University of Texas[3] (Save *et al* 2016). The data are provided on a global 0.25°x0.25° grid, with ocean signals masked. No optional gain factors need to be applied to this data.

[2] Available from https://podaac.jpl.nasa.gov/GRACE?sections=about%2Bdata
[3] (http://download.csr.utexas.edu/outgoing/grace/RL06_mascons/CSR_GRACE_GRACE-FO_RL06_Mascons_all-corrections_v02.nc

3.3.1.2. GLDAS NOAH-derived terrestrial water storage (TWS)

The GRACE ΔTWS data detailed above include water storage in the entire terrestrial water column - water stored as groundwater, soil moisture, canopy water storage, snow-water storage and surface water bodies (Rodell *et al* 2007). To extract the groundwater signal, the various terrestrial water storage components must be removed from the grace signal (Rodell *et al* 2007). The GLDAS in combination with land surface modelling is designed to provide optimal fields of land surface fluxes, through using remote sensing and ground based observations (Rodell *et al* 2004). The GLDAS provide data on various land surface states such as evapotranspiration, soil moisture, land surface energy fluxes to name a few. There are 5 land-surface model derivatives of GLDAS, Noah, CLM, VIC, Mosaic, and Catchment land surface models. Together the various models provide data on land surface states as 1° or 0.25° gridded data products at 3 hourly, daily or monthly intervals from 1948 – present.

Two different datasets are downloaded from the GLDAS NOAH model. Specifically, the first dataset (GLDAS TWS 1) monthly averages from April 2002 – March 2020 for soil moisture (SM), canopy water storage (CW), and snow water equivalent thickness (SWE), on 0.25°x0.25° grid, were extracted[4]. The second dataset (GLDAS TWS 2) presents already aggregated GLDAS NOAH terrestrial water storage anomalies. This dataset provides monthly observation at 1°x1° global grids and does not require additional processing[5].

3.3.1.3. Scaling factors

Estimation of GRACE ΔTWS SH has noise and correlated errors. Various post-processing filters are applied during level – 1 processing to reduce or remove these errors. However, during this process some of the true geophysical signal, especially at finer spatial scales, is lost. Signal attenuation is necessary to ensure comparative analysis of GRACE derived hydrological data. The filtered GRACE data typically has a native resolution ~300km, which is far more course than complimentary datasets such as GLDAS NOAH TWS. When comparative analysis is performed without accounting for the signal loss during GRACE filtering, potential erroneous observations can be made. This mismatch in spatial scale can be accounted for by restoring the signal loss (Landerer and Swenson 2012). Landerer and Swenson (2012) developed a method to calculate a set of scale factors, one for each grid cell, that can be used to restore the GRACE signal lost during post-processing (Landerer and Swenson 2012).

[4] https://disc.gsfc.nasa.gov/datasets/GLDAS_NOAH025_M_2.1/summary?keywords=GLDAS
[5] https://podaac-tools.jpl.nasa.gov/drive/files/allData/tellus/L3/gldas_monthly/netcd

A set of scale factors derived from National Centre for Atmospheric Research's Community Land Model (NCAR CLM) version 4, based on Landerer and Swenson (2012)[6]. The current release (Release 05) of this set of scale factors is package as a 1°x1° gridded latitude and longitude product, complimenting the GRACE gridded data product. This set of scale factors were computed for GRACE Release 05. However, the scale factors are independent of GRACE data proper, and only depend on the GRACE filters used. Considering that the spherical harmonic coefficients fields have changed based on the adoption of satellite laser ranging (Cheng and Tapley 2004), the use of non-complementary scaling factors can introduce additional uncertainty into the model. Nonetheless, these are the only available scaling factors for the GRACE ΔTWS SH, and should dampen the signal loss to some degree, that accompanies the GRACE data processing.

3.3.1.4. MODIS evapotranspiration data

For the downscaling, the predictant variable was chosen as evapotranspiration. Evapotranspiration data from the Terra/MODIS mission, was collected. Specifically, data were extracted from the MOD16A2GF dataset. This dataset that has a temporal resolution of 8-days and spatial resolution of 500m, and contain layers for composited ET, LE, Potential ET (PET), and Potential LE (PLE). However, composited ET was used, which is a measurement of actual ET. The temporal coverage of the data collected was from April 2002 - to November 2019. The data is first converted to metres of equivalent water thickness, then aggregated into monthly cumulative ET, based on a 32-day month. Finally, a single month (May 2002), was used as a test sample, for further analysis.

3.3.1.5. Groundwater level data

Depth to groundwater level data were collected for various boreholes across the SADC region. In particular, the data cover localities in Botswana, Malawi, Mozambique, Namibia, and South Africa (Figure 3-15). Combined, there are over 2,500,000 groundwater level records in the dataset, following pre-processing of the raw data. This include data for a total of 4390 borehole across the region, with temporal range spanning 1936 to 2020. Groundwater level data are used to validate the GRACE ΔGWS and the GGDI, by calculating correlation coefficients between monthly groundwater level values and the GGDI.

[6] Available from https://podaac-tools.jpl.nasa.gov/drive/files/allData/tellus/_retired/L3/grace/land_mass/RL05/netcdf

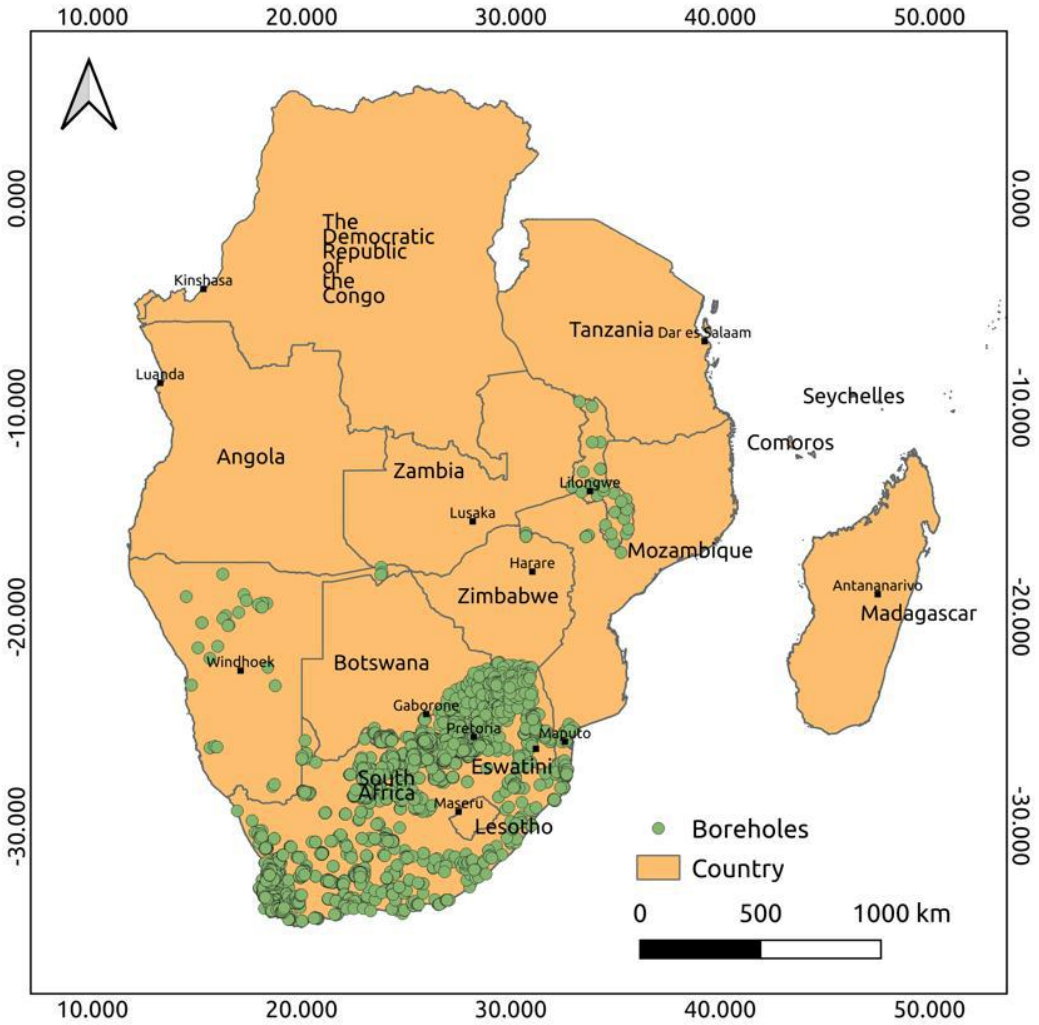

Figure 3-15: Groundwater level data points in SADC

3.3.2. Pre-processing of data

In the following sections the pre-processing steps that were carried out to transform the data for comparative analysis are discussed.

3.3.2.1. Mascon data pre-processing

Due to inconsistencies in satellite data collection, GRACE data typically has a number of missing observations in the time series. There are 216 months in the observation period (2002/04 - 2020/03), while data exist for only 184 months. Gaps in the data where filled by substituting the monthly mean. Firstly, the observation where grouped according to calendar month, and the

mean for each group (calendar month) was calculated. These values were substituted for the corresponding missing months in the time series. Thereafter the data was clipped according to the outline of SADC region (Figure 3-16).

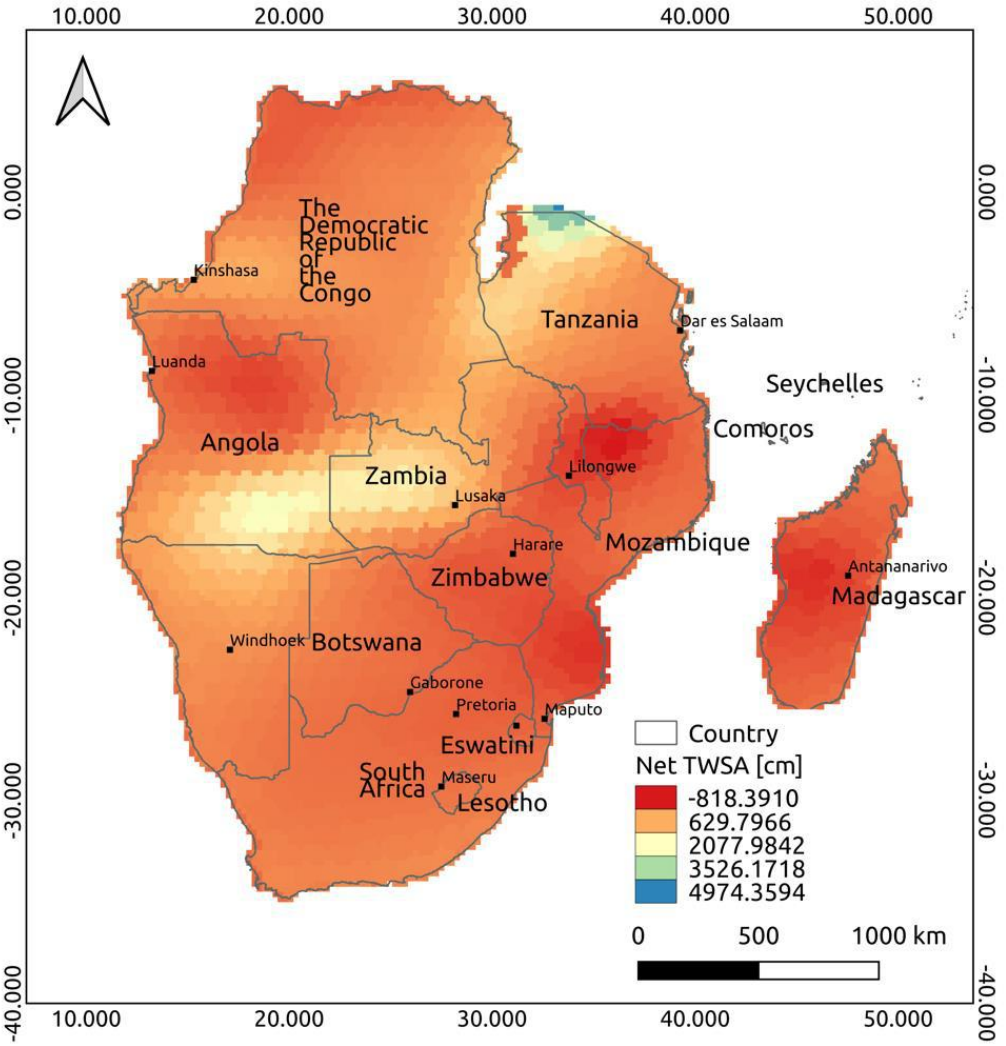

Figure 3-16: Net ΔTWS according to GRACE ΔTWS Mascons

3.3.2.2. Spherical harmonics data pre-processing

For the GRACE ΔTWS SH the solutions from CSR and GFZ are presented with duplicate co-ordinate labels. Hence, these solutions had to be curated by removing the duplicate coordinate values. In addition, the time stamps for the CSR and GFZ solutions where different than the JPL solution. To reconcile this difference, the time stamps were all set according values in the JPL solution. The arithmetic mean of the three solutions was calculated for use in the further analysis (Sakumura *et al* 2014). Exactly like the mascon version, this version also contains the same temporal data

gaps. Gaps in the data where filled by substituting the monthly mean. Firstly, the observation where grouped according to calendar month, and the mean for each group (calendar month) was calculated. These values were substituted for the corresponding missing months in the time series. Thereafter the data were descaled by applying the scaling factors described above. There is one scaling factor for each grid cell in the GRACE ΔTWS SH data. The same scaling factors is applicable to every time step, for each grid cell. The application of the scaling factors was done by multiplying the scale factor by the corresponding grid cell for every time step (Landerer and Swenson 2012). Finally, the data was clipped according to the outline of the SADC region (Figure 3-17).

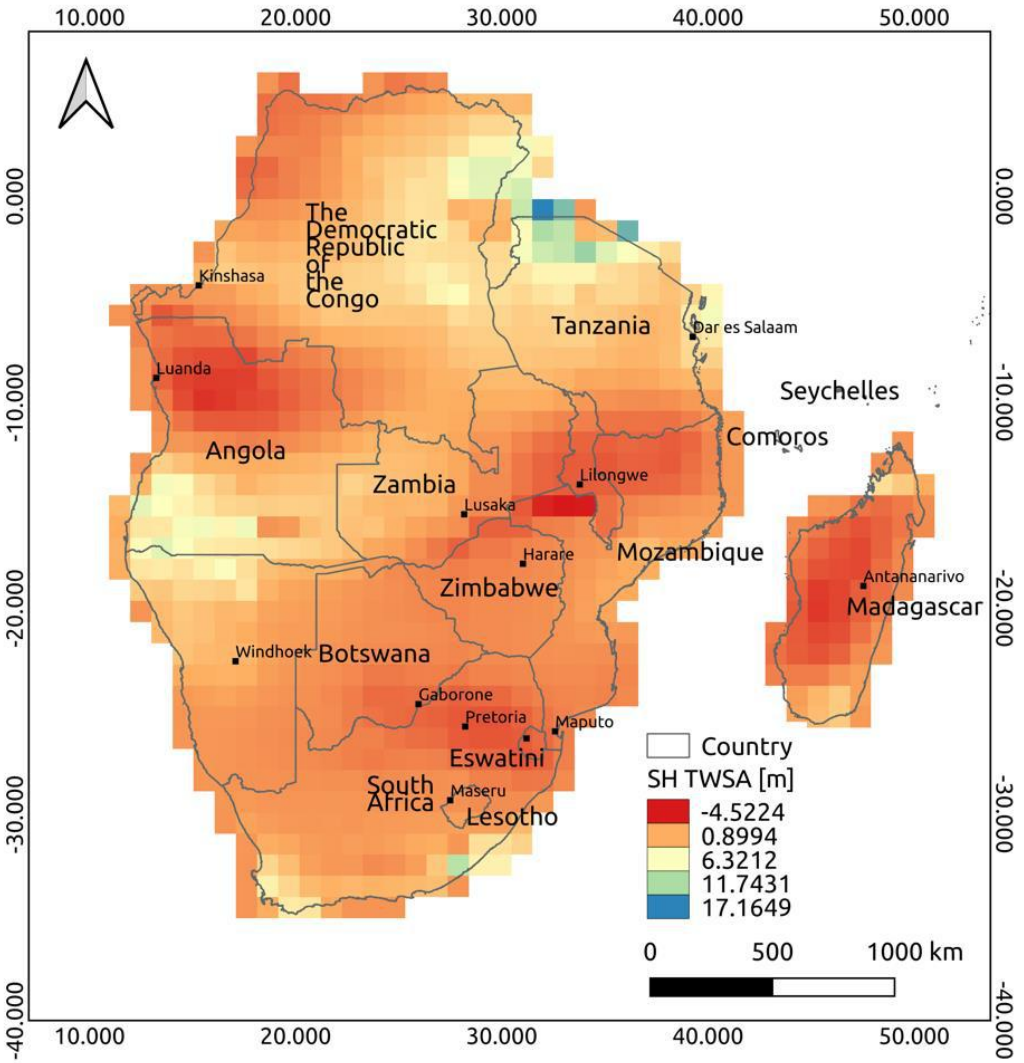

Figure 3-17: **Net ΔTWS according to GRACE ΔTWS SH**

3.3.2.3. GLDAS NOAH data pre-processing

For the GLDAS TWS 1, the data are presented in units of kg/m^2. All the units where converted to cm. This is to ensure compatibility to the GRACE ΔTWS mascon units, which is in cm. There after the individual components (SM, SWE, CW) were aggregated, by summation. This value reflects the land surface component of the total terrestrial water budget. However, GRACE data reflects anomalies relative to a mean baseline period (2004-2009). For the GLDAS TWS 1 data to be compatible to the GRACE data, anomalies must be calculated relative to this same baseline period. Firstly, the mean GLDAS TWS 1 value was calculated for the months between 2004 –2009. This mean value is then subtracted from each monthly time-step in the GLDAS TWS 1 timeseries. This new value reflects GLDAS ΔTWS 1 relative the baseline period. Finally, the data was clipped according to the outline of SADC region (Figure 3-18).

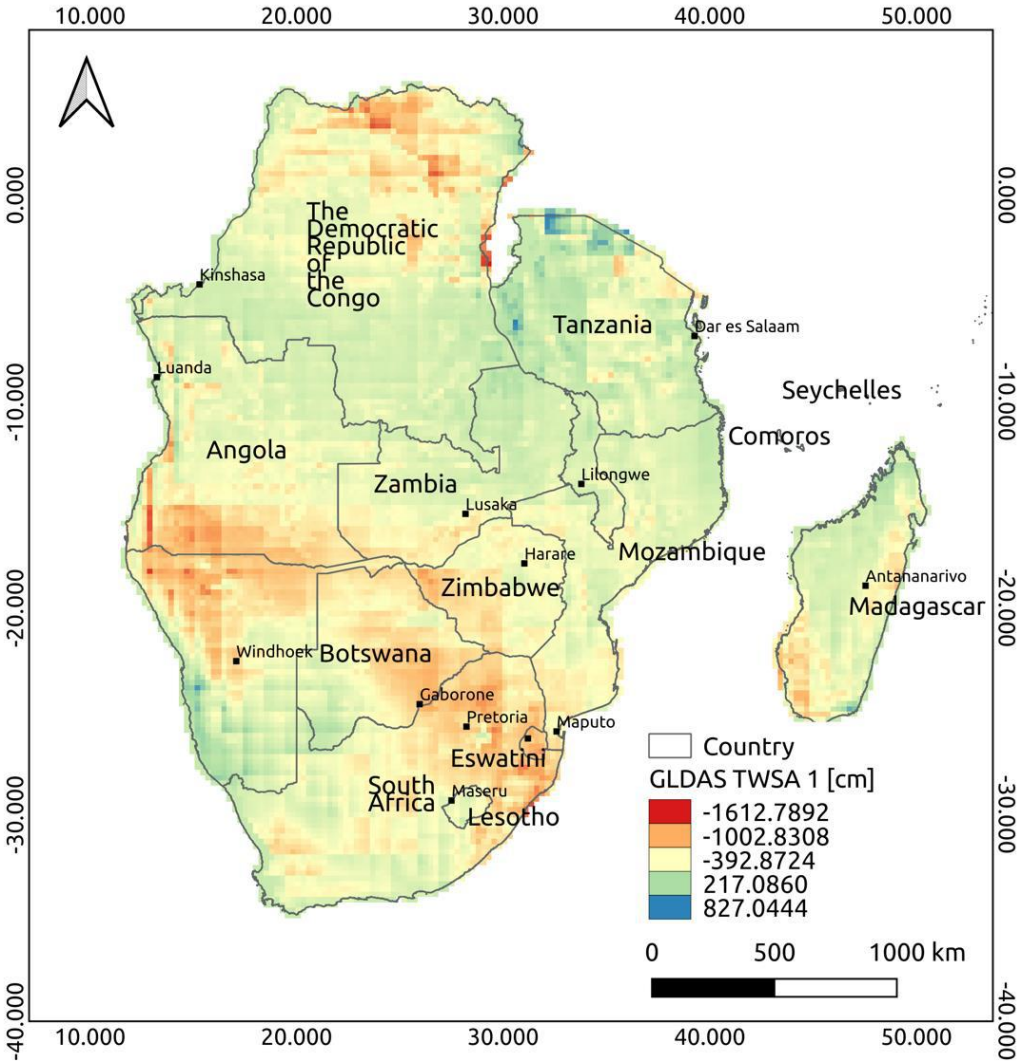

Figure 3-18: Net GLDAS ΔTWS 1

For the GLDAS TWS 2 dataset, the co-ordinate reference system is inconsistent with the GRACE data. THE GRACE data is centred on the antimeridian, while GLDAS TWS 2 is centred on the prime meridian. Hence, for this dataset, the co-ordinate reference system is changed so that the data is centred on the antimeridian. There after the data are converted from units of mm, to units of m. This GLDAS ΔTWS 2 is now compatible with the GRACE ΔTWS SH. As this dataset already represent anomalies relative to the mean baseline, no further pre-processing is needed. Finally, the data was clipped according to the outline of SADC region (Figure 3-19).

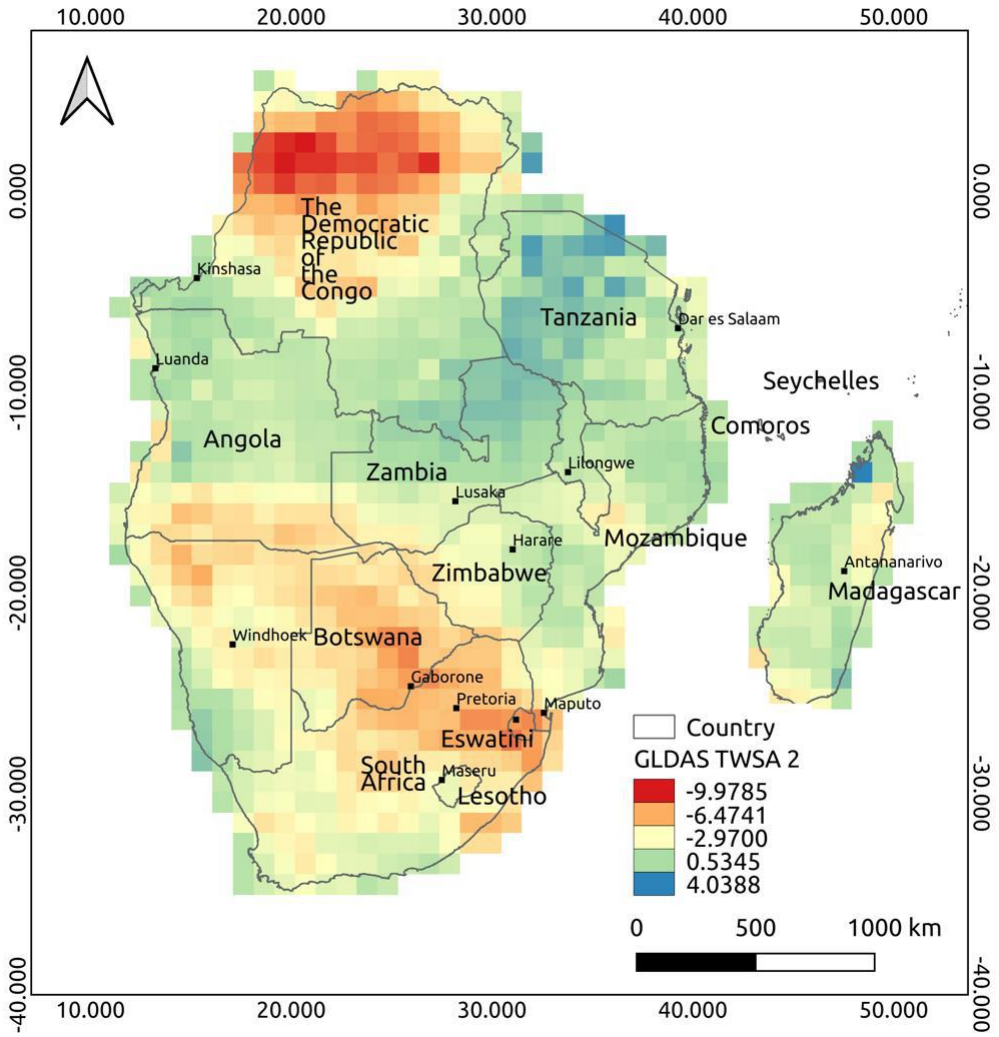

Figure 3-19: Net GLDAS ΔTWS 2

3.3.2.4. Groundwater level data pre-processing

The groundwater level data were received from the data providers as tabular spreadsheets in Microsoft excel and csv formats. The data were pre-processed and combined in the following manner:

1) Spreadsheet were pre-processed by removing auxiliary data such as logger information, elevation data, borehole status, and renaming table headers in a uniform manner. This is done to produce a regular set of spreadsheets that include only depth to water level, borehole identification, observation date, and co-ordinates.
2) Individual spreadsheet was then combined, into a single dataset.
3) The dataset is curated by removing, duplicate data records, records with missing values, and erroneous depth to water level observations, such that only records with a borehole identification, date, and co-ordinates remain.
4) Conversation of co-ordinates into decimal degree units, and conversion of depth to water level data to metres below ground surface.
5) In some cases, both phreatic and semi-confined depth to water level data were collected. In this case the mean of the two is used as the depth to groundwater level.

The above pre-processing resulted in a curated and cleaned data records, however, the presence of outliers and possible erroneous data might persist in the data. To address this, outliers where removed using a z-score approach. Any record that was 3 standard deviation above or below the mean was removed. Thereafter, a sample of the data, April 2002 to March 2020 was extracted from the dataset. This range is intended to match the GRACE data time range. The data record for this sample contain considerable temporal gaps in the time-series for many boreholes. This sample was aggregated into monthly averages, and only those boreholes with data for 150 and more month in between April 2002 and March 2020, were selected for further analysis. Temporal gaps were filled using a linear interpolation method (only up until the most recent month for a particular borehole).

To compare groundwater level data to the GRACE ΔGWS and GGDI we process the groundwater level data in the same manner as the GRACE data. Firstly, a mean depth to groundwater level data for the baseline period (2004-2009) is calculated per borehole. This baseline reflects the same baseline period as the GRACE data. Every monthly record was then subtracted from the corresponding baseline for each borehole. This new value now reflects monthly depth to groundwater level anomalies (ΔGWL) relative to the baseline period. The processing up to this point is used to validate the GRACE ΔGWS. Thereafter the groundwater level deviation is calculated by subtracting the groundwater level anomalies from the average anomaly for a

calendar month for each borehole. This value reflects the deviation of the groundwater level anomaly compared to normal conditions. The groundwater level deviation is then normal according to the mean and standard deviation. This normalized groundwater level deviation is correlated with the GGDI.

3.3.2.5. MODIS data pre-processing

The MODIS data has units of kg/m^2/day. The data is first converted to metres of equivalent water thickness, by dividing by 1000. Thereafter, the data are aggregated into monthly cumulative ET, based on a 32-day month. Finally, a single month (May 2002), was used as a test sample, for further analysis.

3.3.3. Calculating the GRACE-derived groundwater storage anomalies (ΔGWS)

In-order to determine the ΔGWS signal within the GRACE ΔTWS mascon data, the various terrestrial water components must be removed from the model. In this case a water mass balance approach was used (Rodell *et al* 2007). In this case the ΔGWS = ΔTWS – Δ (SM + SWE + CW). For every timestep the corresponding GLDAS ΔTWS 1 is subtracted from the GRACE ΔTWS mascon data (Figure 3-20). It is important to note that the GLDAS ΔTWS 1 data be subtracted from the GRACE ΔTWS mascon data, and the GLDAS ΔTWS 2 data be subtracted from the GRACE ΔTWS SH data (Figure 3-21), as these set are complimentary. These two versions of ΔGWS are used for different applications. Although it is quite reasonable to assume the terrestrial water constitutes most of the GRACE ΔTWS signal. Changes in surface water storage and biomass can have an effect (Rodell *et al* 2007). However, these components are not included in the model.

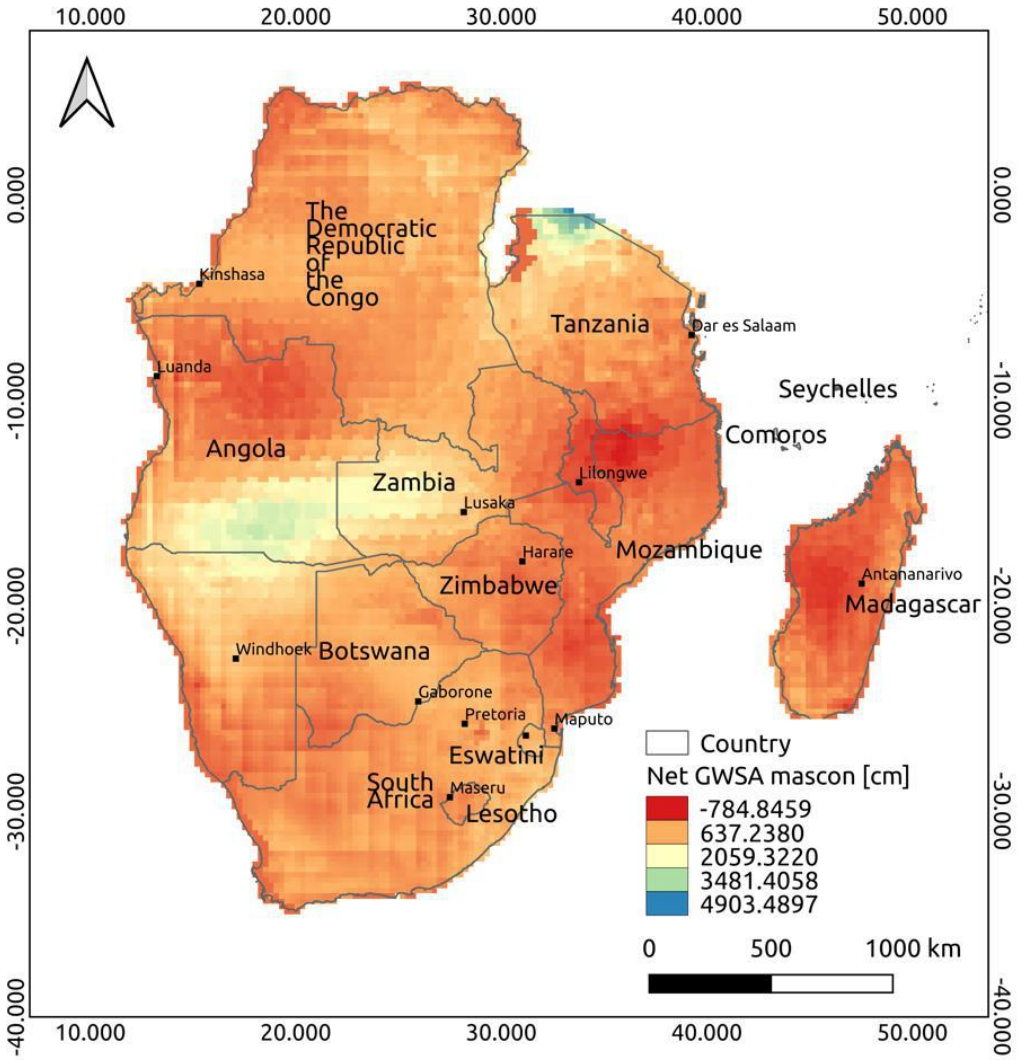

Figure 3-20: **Net GRACE ΔGWS for Mascon version**

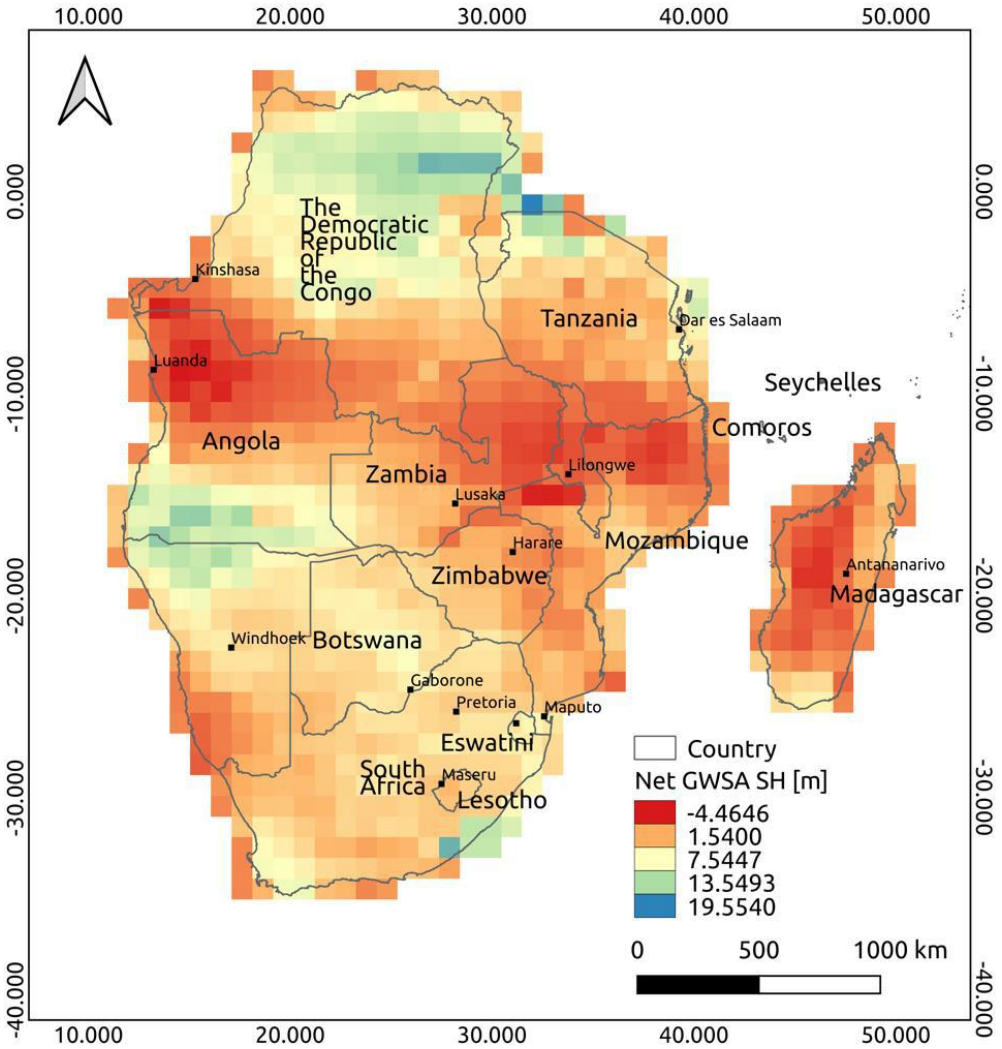

Figure 3-21: **Net GRACE ΔGWS according to SH version**

3.3.4. Validation

To ground truth GRACE ΔGWS mascon data, a correlation analysis was performed with ΔGWL. A total of 894 boreholes were used in this analysis, following the pre-processing. For every borehole, the underlying pixel values were selected. Both a Pearson's and Spearman rank correlation where performed for each sample set (i.e. normalized groundwater level deviations and GRACE ΔGWS mascon data) (Figure 3-22, Figure 3-23).

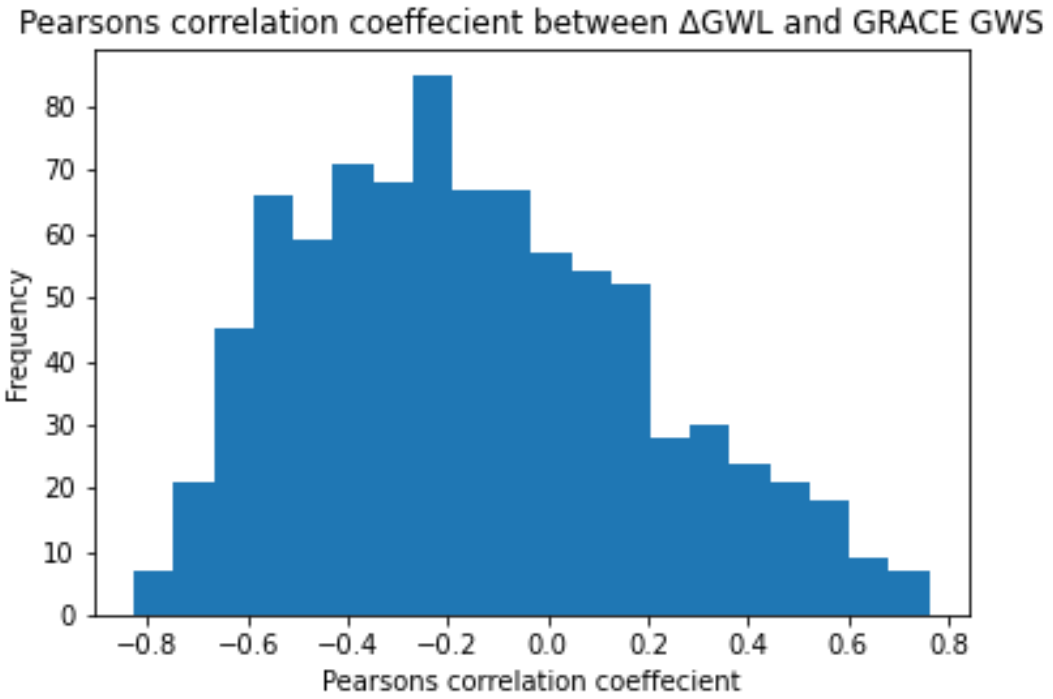

Figure 3-22: **Histogram of the Pearson's correlation coefficient between groundwater levels and GRACE ΔGWS Mascons**

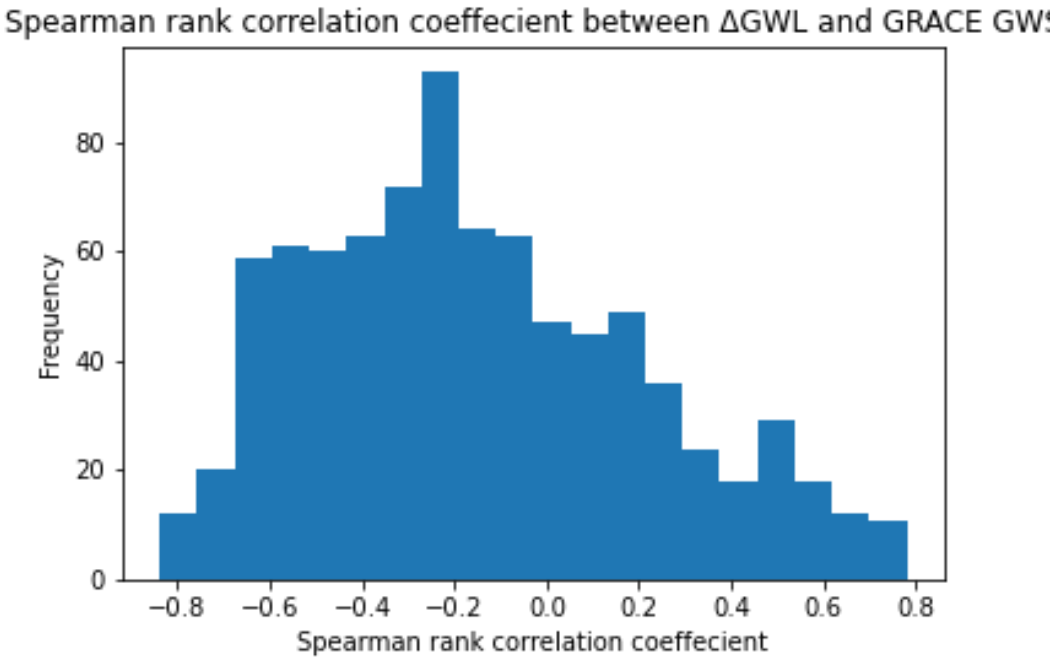

Figure 3-23: **Histogram of the Spearman's rank correlation coefficient between groundwater levels and GRACE ΔGWS Mascons**

The results presented in the histograms above indicate an overall poor correlation between GWL and GRACE ΔGWS mascons. Majority of the correlations are centred around –0.7 to 0. Ideally, strong positive correlation as more favourable, to ensure GRACE mimics local groundwater storage trends. In fact, only a small number of boreholes have a correlation above 0.7. This indicates no plausible correlation between the datasets. However, GRACE data is not expected to resolve small scale or even local changes in groundwater storage, as the GRACE signal is smoothed to ~300km, prior to release. It must also be noted that the preferred approach is to derive local groundwater storage anomalies from boreholes records to compare to GRACE ΔGWS (Frappart and Ramillien 2018). However, the lack of specific yield data and groundwater level data across SADC makes this approach difficult to implement.

3.3.5. Downscaling

An attempt was made to test a downscaling method on the entire SADC. The following sections describes the application of attempting to downscale GRACE ΔGWS SH from a ~110km resolution to a ~5km resolution. For this application a method developed by Yin *et al* (2018) was used to test a regional downscaling of GRACE ΔGWS, using evapotranspiration data as the predictant. The approach relies on a correlative relation method. MODIS evapotranspiration data was used for this analysis and is substituted in the following equation:

$$GWS_{local} = GWS_{GRACE\_min} + \frac{ET_{local} - ET_{avg\_min}}{ET_{avg} - ET_{avg\_min}} (GWS_{GRACE} - GWS_{GRACE\_min})$$

where GWS_{local} is the downscaled GWS at a local scale; GWS_{GRACE} is the gridded GRACE ΔGWS SH at the standard resolution of approximately 110 km (1°); GWS_{GRACE_min} is the minimum gridded ΔGWS among the 211 months from 2002 to 2019; ET_{local} is the ET at a local scale; ET_{avg} is the upscaled ET with the same spatial resolution as the gridded GRACE data; ET_{avg_min} is the minimum ET among the 211 months from 2002 to 2019 at a resolution of approximately 110 km. However, according to Yin *et al* (2018) this method only applies where there is a strong correlation between evapotranspiration and GRACE groundwater storage anomaly.

Firstly, the MODIS ET data is upscaled using a linear interpolation algorithm (ET_{avg}). Thereafter the minimum ET_{avg} along the time series for each pixel is determined (ET_{avg_min}). Following this, the minimum GRACE ΔGWS SH along the time series for each pixel is determined (GWS_{GRACE_min}). A single time step (May 2002) was extracted from the time-series to perform the downscaling. This was because the processing is computational extensive. The values were then substituted as per the formula above. The results of the downscaling were not satisfactory, in terms of spatial

smoothing. The original pixel dimension is persisting as an artefact in the downscaled data (Figure 3-24). It is possible that the correlation between MODIS ET and GRACE ΔGWS SH is poor, which is affecting the efficiency of the algorithm. Additionally, the execution of the algorithm through the programming code may not be optimized. This requires additional experimentation.

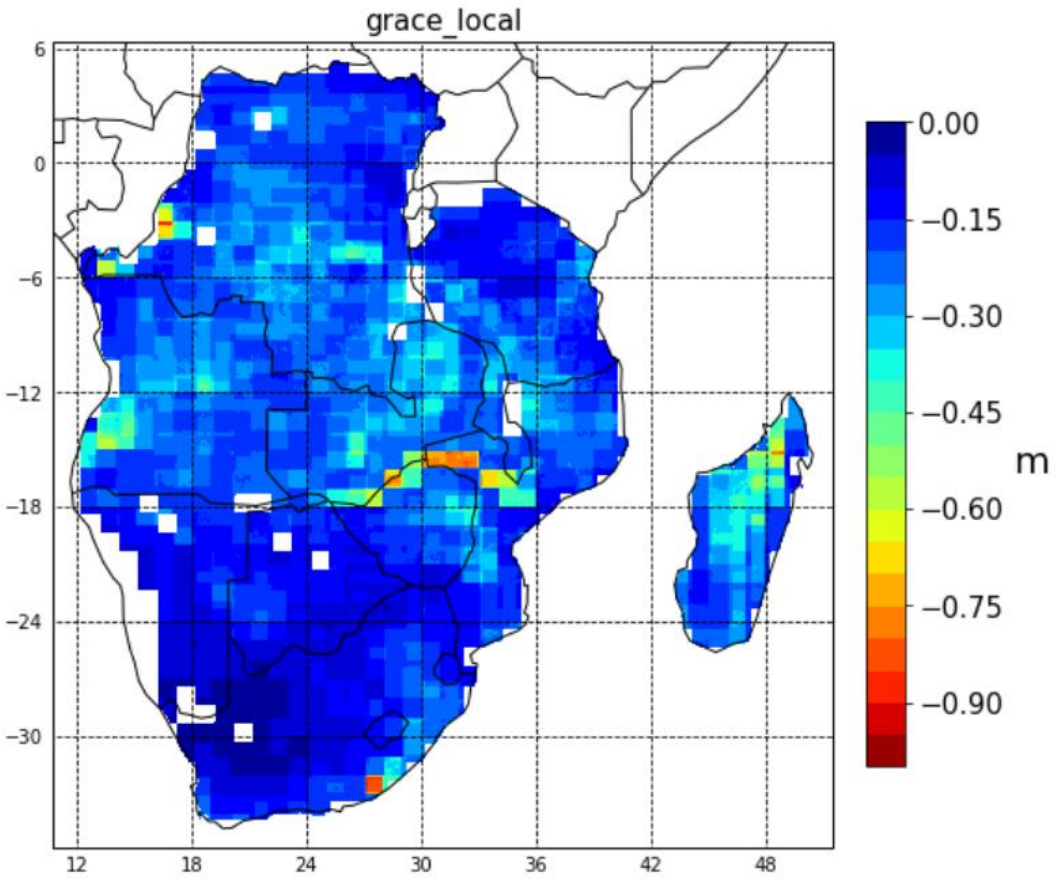

Figure 3-24: Result of GRACE ΔGWS downscaling, for May 2002

3.3.6. Calculating GGDI

The GGDI is calculated using the GRACE ΔGWS mascons (at 0.25° x 0.25° resolution) (Figure 3-25). The GGDI is calculated as follows:

The monthly average values are calculated. The is simply the average groundwater storage change for each of the unique months of the year (n=1, ...12). Each monthly GRACE GWS value is subtracted from its corresponding average to derive the Groundwater Storage Deviation (GSD). The GSD provides us with an indication of deviations from normal groundwater storage conditions. positive deviation indicates a surplus of groundwater storage, while negative deviations indicate a deficit of groundwater storage. A deficit infers the presence of drought

conditions. The GSD is normalized according to mean and standard deviation. The normalized GSD is the GGDI.

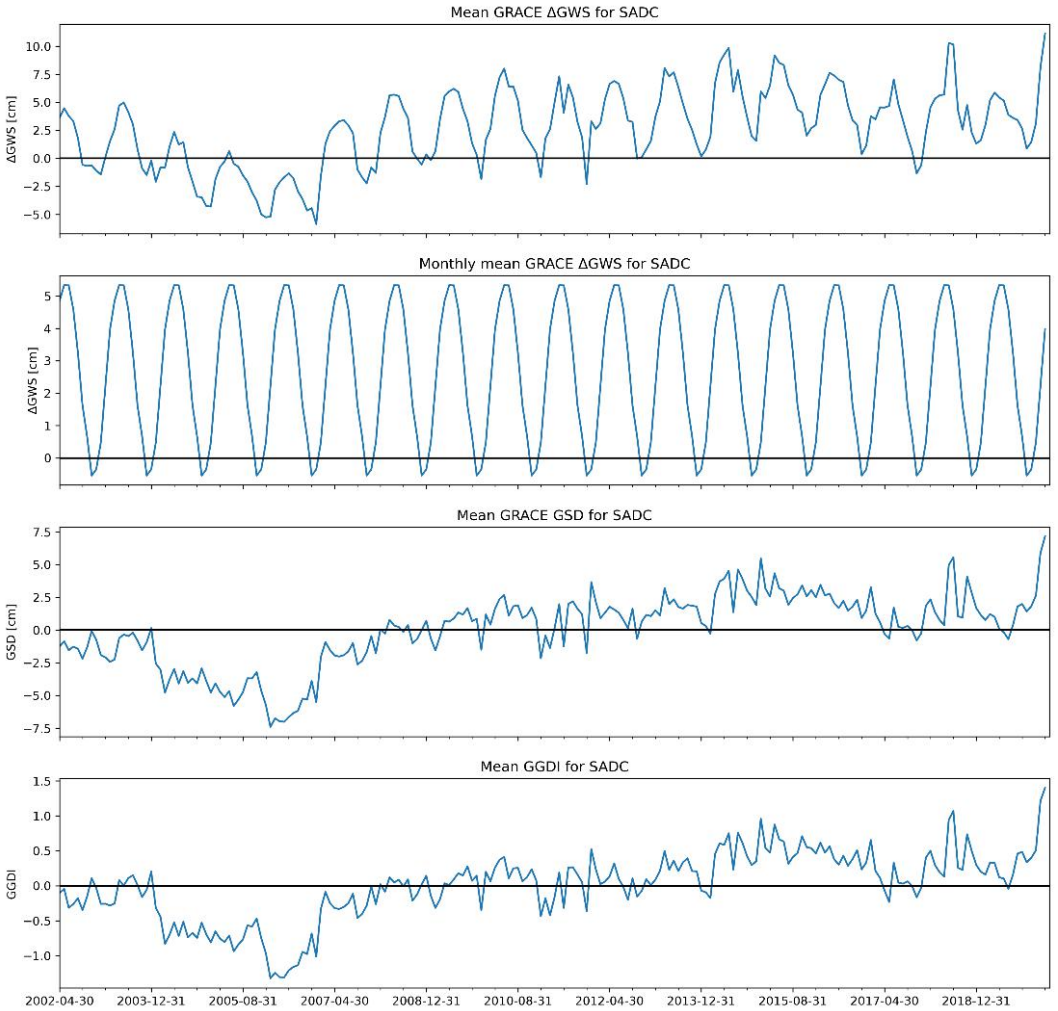

Figure 3-25: **Schematic of the calculation of the GGDI. (Top: Mean GRACE GWS for SADC; Second from top: Monthly average of GWS for SADC; Third from top: The Mean GSD for SADC, which is the monthly mean subtracted from the GRACE GWS; Bottom: the Mean GGDI, which is the normalized GSD)**

3.3.7. Validation of GGDI

Following the creation of the GGDI for SADC, a second validation is performed to ensure that the GGDI provides a representative analysis of on the ground conditions. Here we use groundwater level time series processed in the same manner as the GRACE data, up until the GGDI. This groundwater level dataset is essentially a groundwater level indicator, that mimics the GGDI. Figure 3-26 displays the Pearson's correlation coefficient results between the groundwater level deviations for 894 boreholes and the GGDI. Figure 3-27 displays the Spearman's rank correlation coefficient results between the groundwater level deviations for 894 boreholes and the GGDI.

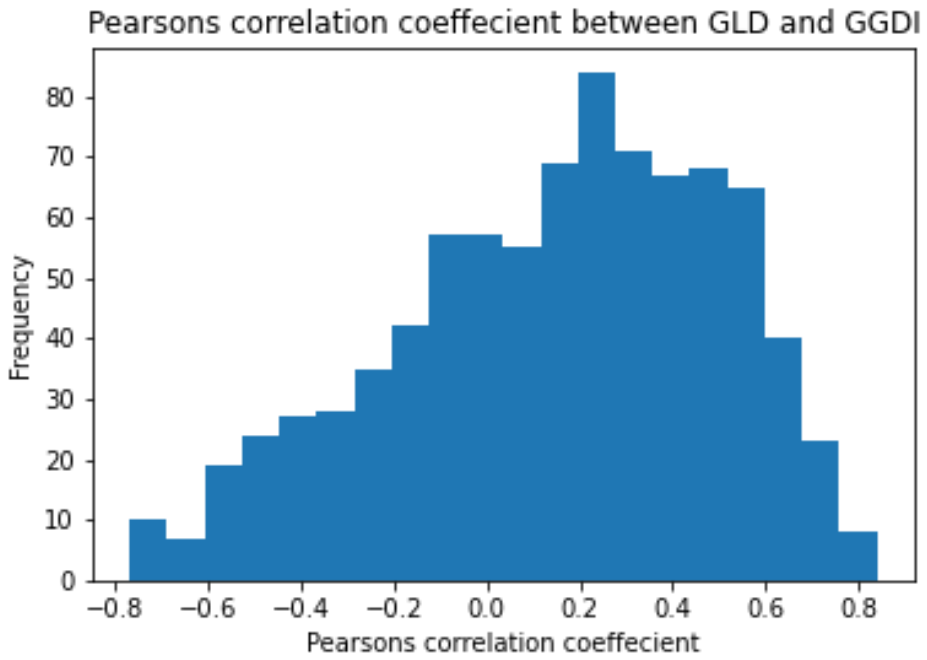

Figure 3-26: **Histogram of the Pearson's correlation coefficient between groundwater levels deviations and GGDI**

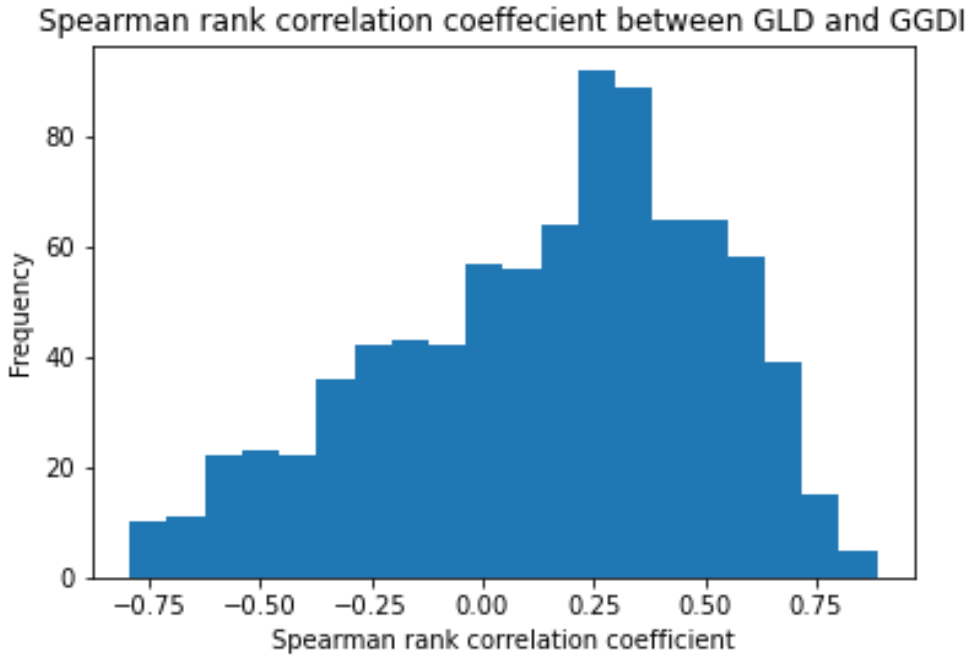

Figure 3-27: **Histogram of the Spearman's rank correlation coefficient between groundwater levels deviations and GGDI**

In this case the correlations results are markedly improved over the correlation results for the GRACE GWS data. Overall, there is a high number of boreholes that have a high positive correlation. Here, high positive correlation is preferred, as this demonstrates similar trends between the GGDI and the groundwater level deviations. The better correlations results seen here, may also be due to the fact that the data has been normalized. In comparison to the previous validation which has was done without normalization of the data.

3.3.8. Groundwater storage risk

The percentage negative GGDI, mean negative GGDI and trend GGDI were not classified but rather rescaled linearly to values between 1 and 5 (with 1 indicating low groundwater drought risk and 5 indicating high groundwater drought risk). This classification system is only applicable to the SADC region.

3.3.8.1. Percentage negative GGDI

This factor explains the percentage of the time-series that is in a groundwater storage deficit, or drought, according to the GGDI. This layer is developed by calculating the number of months with a negative GGDI value, divided by the total number of months in the time series, and expressed as a percentage. This is done for every pixel, along its time series. The data is then resampled from a ~25km resolution (native resolution of GRACE mascon data) to a ~5km resolution using a linear interpolation algorithm. Spatial distributions reflect differences in the lengths and frequency of drought conditions along the time series. In regions were groundwater storage drought conditions are more numerous have been classed as more sensitive, compared to region that experience fewer groundwater storage drought conditions (Figure 3-28).

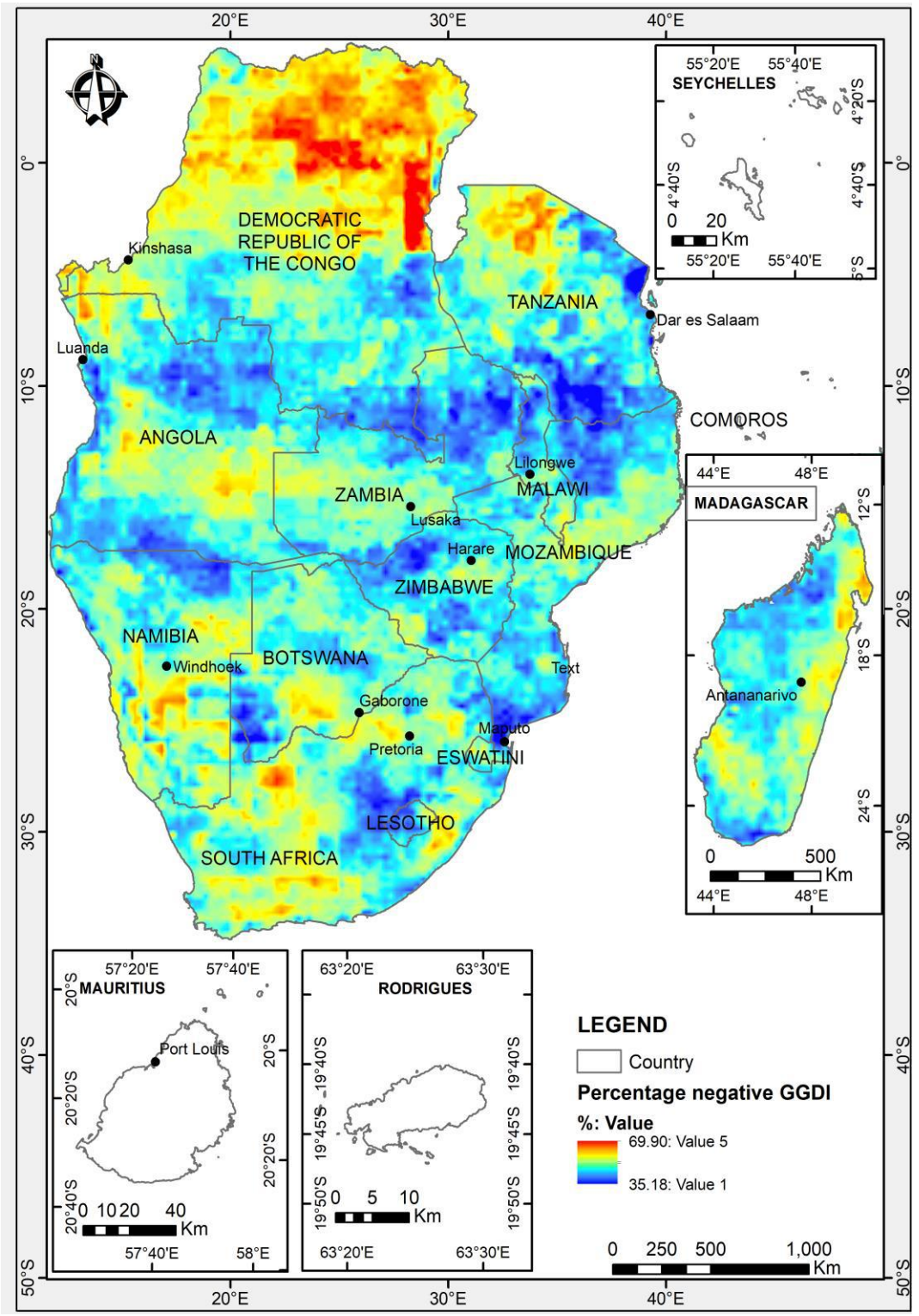

Figure 3-28: **The percentage negative GGDI with values in red showing areas more sensitive to drought**

3.3.8.2. Mean negative GGDI

This factor explains the mean intensity of groundwater storage drought conditions according the GGDI. The larger the GGDI value, the larger the deviation from normal conditions - the more intense the groundwater storage drought conditions. This layer is developed by calculating the arithmetic mean for only negative GGDI values along the time-series for every pixel. The data is then resampled from a ~25km resolution to a ~5km resolution using a linear interpolation algorithm. Spatial distributions reflect differences in the mean intensity of groundwater storage drought conditions. Regions that have a higher mean intensity are more sensitive, compared to

regions that have a lower mean intensity (

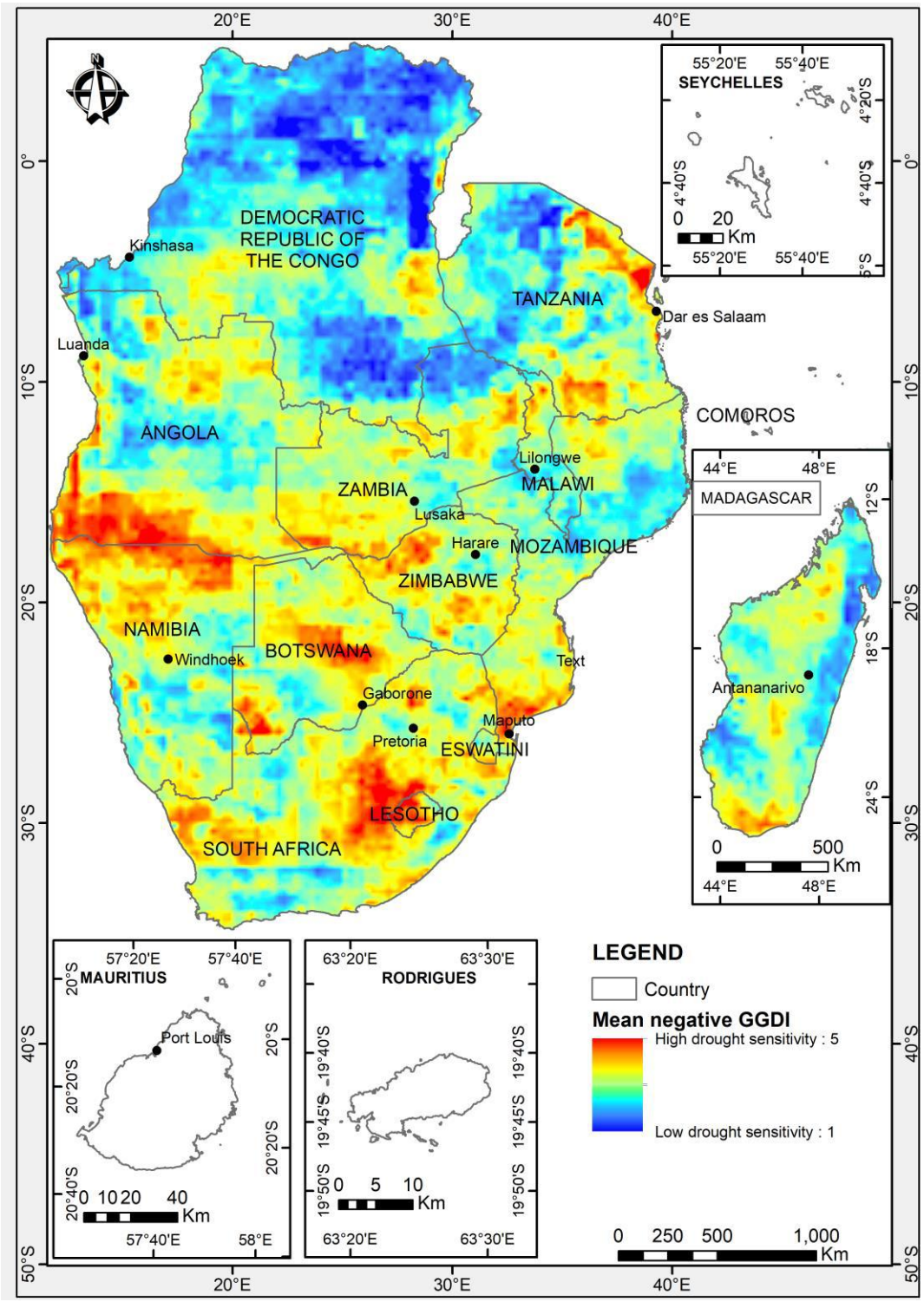

Figure 3-29).

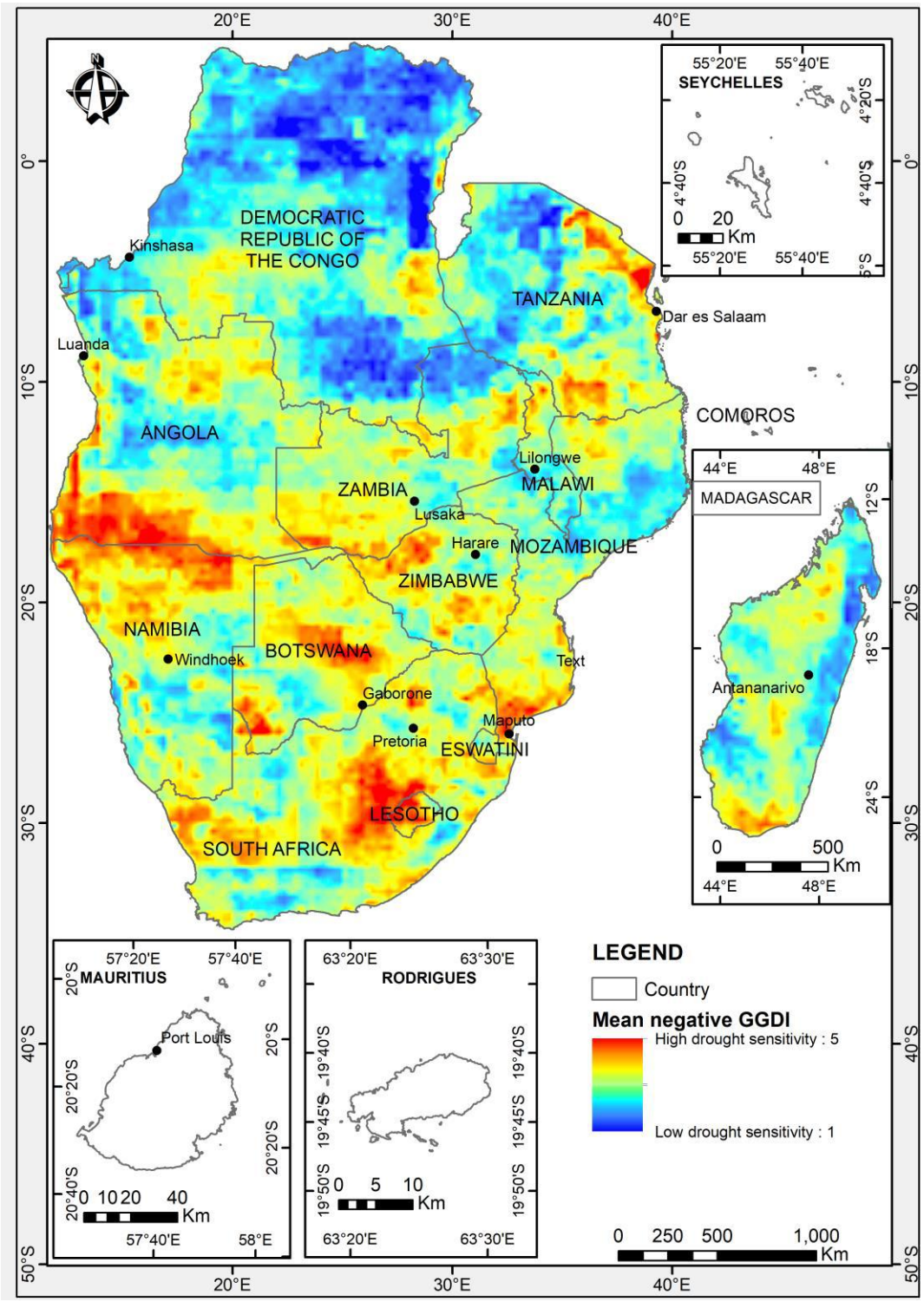

Figure 3-29: **The mean negative GGDI with values in red showing areas more sensitive to drought.**

3.3.8.3. Trend GGDI

This factor explains the trend in the GGDI. To develop this layer the time-series was first de-seasonalised, using the Loess smoothing (STL) (Cleveland *et al* 1990). This is a common step in

time-series analysis, is required to reduce the effects on seasonality on GRACE data (Rodell *et al* 2018). There after the linear regression model was fitted to the de-seasonalised GGDI. In this case, we use the slope of the linear regression line to reflect the trend in the time –series. The data is then resampled from a ~25km resolution to a ~5km resolution using a linear interpolation algorithm. Positive slopes indicate an increasing trend in the GGDI (i.e. The GGDI is trending toward more positive values) (Figure 3-30). This means that groundwater storage drought conditions are becoming less intense or shifting towards a surplus in groundwater storage. The data is rescaled where high positive slopes, indicate a lower sensitivity, while lower negative slopes indicate higher sensitivity.

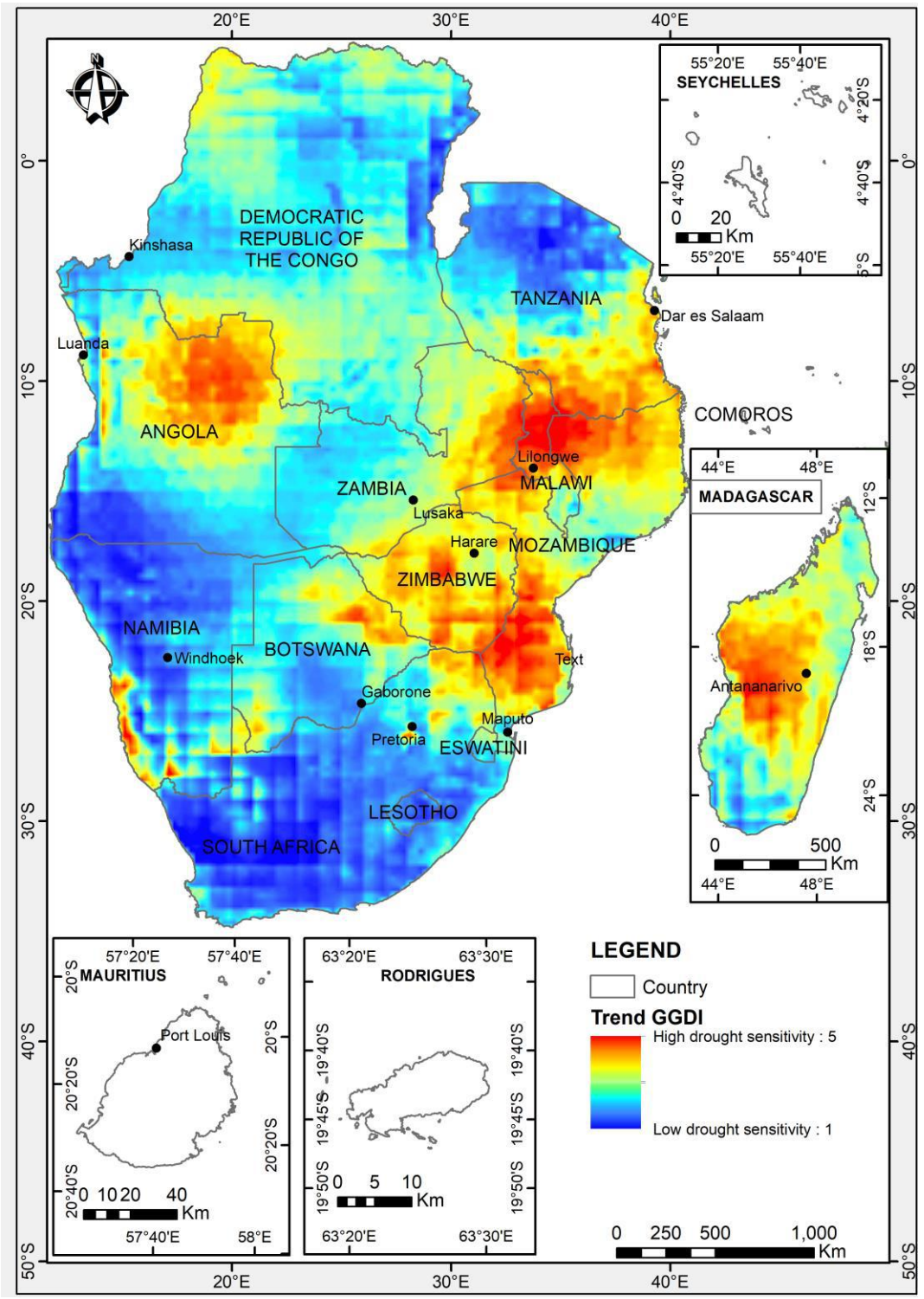

Figure 3-30: **The linear regression trend of the GGDI with values in red showing areas more sensitive to drought**

3.3.8.4. Calculation of groundwater storage risk

Groundwater storage risk = 0.4 * negative GGDI + 0.3 *mean negative GGDI + 0.3*trend GGDI

The groundwater storage risk is given in Figure 3-31.

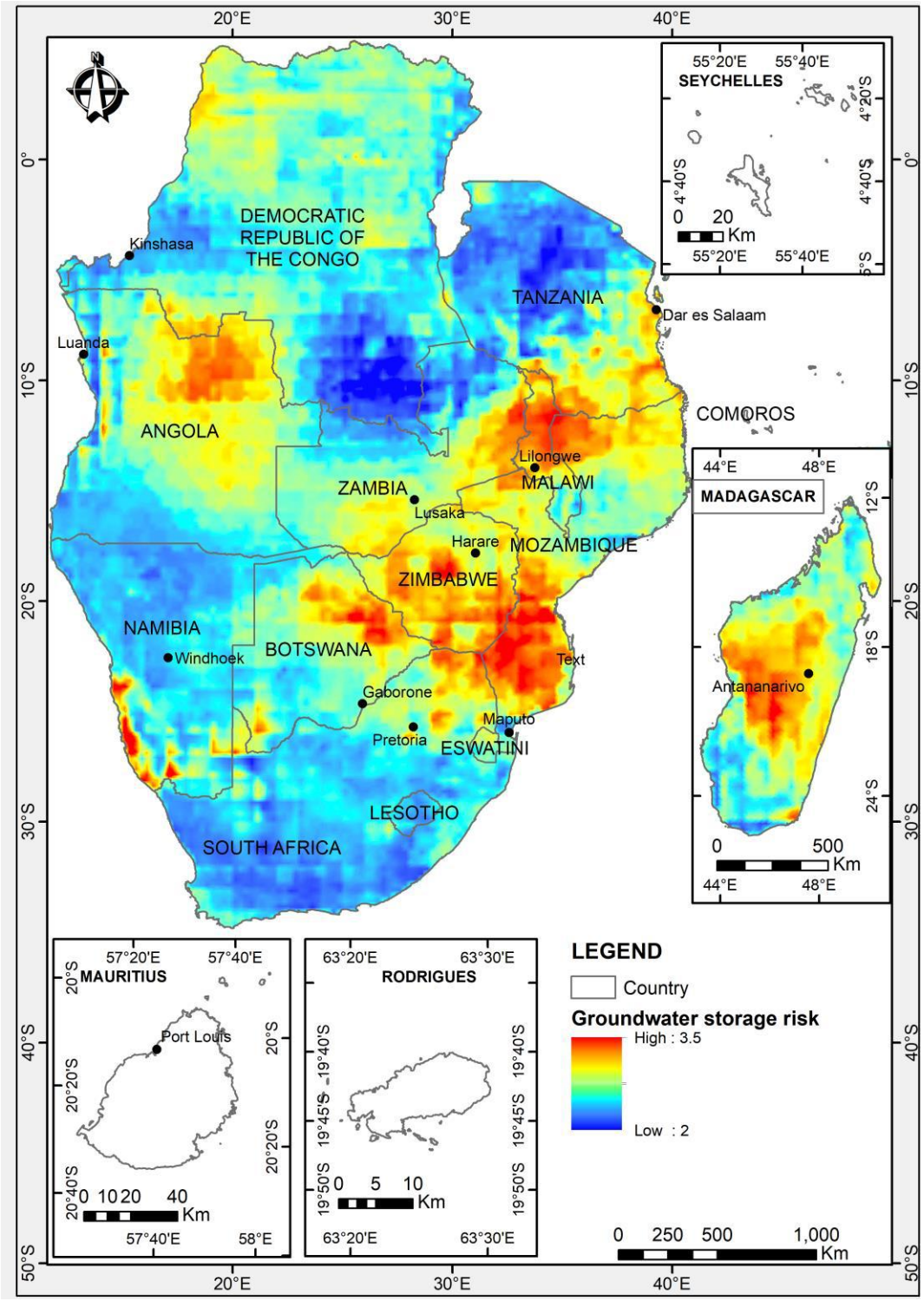

Figure 3-31: **The groundwater storage risk map based on the GGDI parameters.**

In Figure 3-31 warm colours (reds) represent areas of high groundwater storage risk, while blue colours indicate areas of lower groundwater storage risk. Based on the three groundwater storage risk factors, regions in southern Mozambique, Zimbabwe, Malawi, Northern Angola, and parts of the Namibian coast have high groundwater storage risk. This implies that these regions experiencing groundwater storage deficits, greater extreme groundwater storage changes, and possible negative trends in groundwater storage drought conditions, compared to the lower risk regions.

3.4. Human groundwater drought vulnerability

Hydrogeological groundwater vulnerability is made up of the following parameters:

- Groundwater dependence- dependence and groundwater demand is governed by use for domestic, livestock and irrigation purposes. Higher population, irrigation densities and livestock densities imply higher drought risk and closeness to surface water imply less drought vulnerability as surface water is regarded as an alternative source of water
- Human capacity for drought preparedness- this depends on individual and societal knowledge and ability to survey hydrogeology conditions and mitigate the hazards. Three types of human capacity and preparedness are considered: society, science and government. This parameter was not used at this level as the data is not detailed enough and is only available at country scale

Population density map shows the amount of people per square area. The Gridded Population of the World, Version 4 (GPWv4) data was used. It models the distribution of the human population on a continuous raster surface. The primary sources of data are population censuses and administrative data and these are converted into a grid using areal weighting (CIESIN 2016). The ranges used are based on (SADC 2011) and are meant to enhance the variations in the SADC region.

Irrigation density is based on the version 5 “Global Map of Irrigated areas” map. The information is provided at a spatial resolution of ~10 x 10 km and includes percentages of areas irrigated with groundwater, surface water or non-conventional sources of water. The groundwater component of the data was used. The ranges used are based on (SADC 2011) which were based on Siebert *et al* (2010) and are meant to be used with the map.

The FAO livestock density data are available that show the densities per livestock type i.e. of cattle, sheep, buffalo, goats, pigs and chicken and is presented in animals per km^2 (Gilbert *et al* 2018). To produce one map of combined livestock density, this was done by weighting the

different maps according to water use by the different livestock types. These are differentiated as the water usage by various livestock differs. In the report by SADC (2011), the following equation was derived and was used in this study to create a weighted average map representing livestock density.

Weighted livestock density = [Cattle*0.5] + [Pigs*0.2] + [Sheep*0.1] + [Goat*0.1] + [Poultry*0.01]

The map was proven to be correct and was verified by using livestock water requirements data from various literature sources (Table 3-5). The ranges were the ones used in the original global maps with some variation to highlight the variations in the SADC region (Robinson *et al* 2014).

Table 3-5: Estimates of livestock water requirements from various sources

Animal	Average water Requirement Range (L/day) per animal	Reference
Cattle	4.9-115	Ward and McKague, 2007
	5.55	South African Department of Agriculture and Rural Development, Province of KwaZulu-Natal
	40-140	State of New South Wales through the Department of Trade and Investment, Regional Infrastructure and Services 2014
Pig	1-22.7	Ward and McKague, 2007
	5-23	South African Department of Agriculture and Rural Development, Province of KwaZulu-Natal
	2-45	Government of Western Australia, Department of Primary Industries and Regional Development,2019
Horses	13-59	Ward and McKague, 2007
	40-50	State of New South Wales through the Department of Trade and Investment, Regional Infrastructure and Services 2014
	20-90	Government of Western Australia, Department of Primary Industries and Regional Development 2019
Sheep	6.3-11.4	Ward and McKague, 2007
	4-11	South African Department of Agriculture and Rural Development, Province of KwaZulu-Natal
	4-12	State of New South Wales through the Department of Trade and Investment, Regional Infrastructure and Services 2014
	2.5-7	Government of Western Australia, Department of Primary Industries and Regional Development 2019
Goats	4-10	Victoria Department of Environment and Primary Industries,2001
	5-6	FAO,1977
	5-20	Government of Western Australia, Department of Primary Industries and Regional Development 2019
Chickens	0.005-0.32	Ward and McKague, 2007
	0.008-0.4	South African Department of Agriculture and Rural Development, Province of KwaZulu-Natal
	0.25	FAO,1984

For distance to rivers, perennial rivers were used. Rivers are considered alternative sources of water supply, proximity to a surface water body reduces the vulnerability to groundwater drought. The ranges used were the same as those used in SADC (2011).

Table 3-6: Groundwater dependence parameters and reclassification values

Parameter	Ranges	Reclassification values relating to drought risk
Population density (people per km^2)	0	0
	0-10	1
	10-50	2
	50-100	3
	100-250	4
	>250	5
Livestock density (livestock per km^2 weighted according to water demand)	0	0
	0-5	1
	5-25	2
	25-50	3
	50-100	4
	>100	5
Irrigation density (% of area irrigated by groundwater)	0	0
	0 - 0.1	1
	0.1-1	2
	1-2.5	3
	2.5-5	4
	>5	5
Distance to perennial rivers (km)	0	0
	0-1	1
	1 - 2.5	2
	2.5 - 5	3
	5 - 10	4
	>10	5

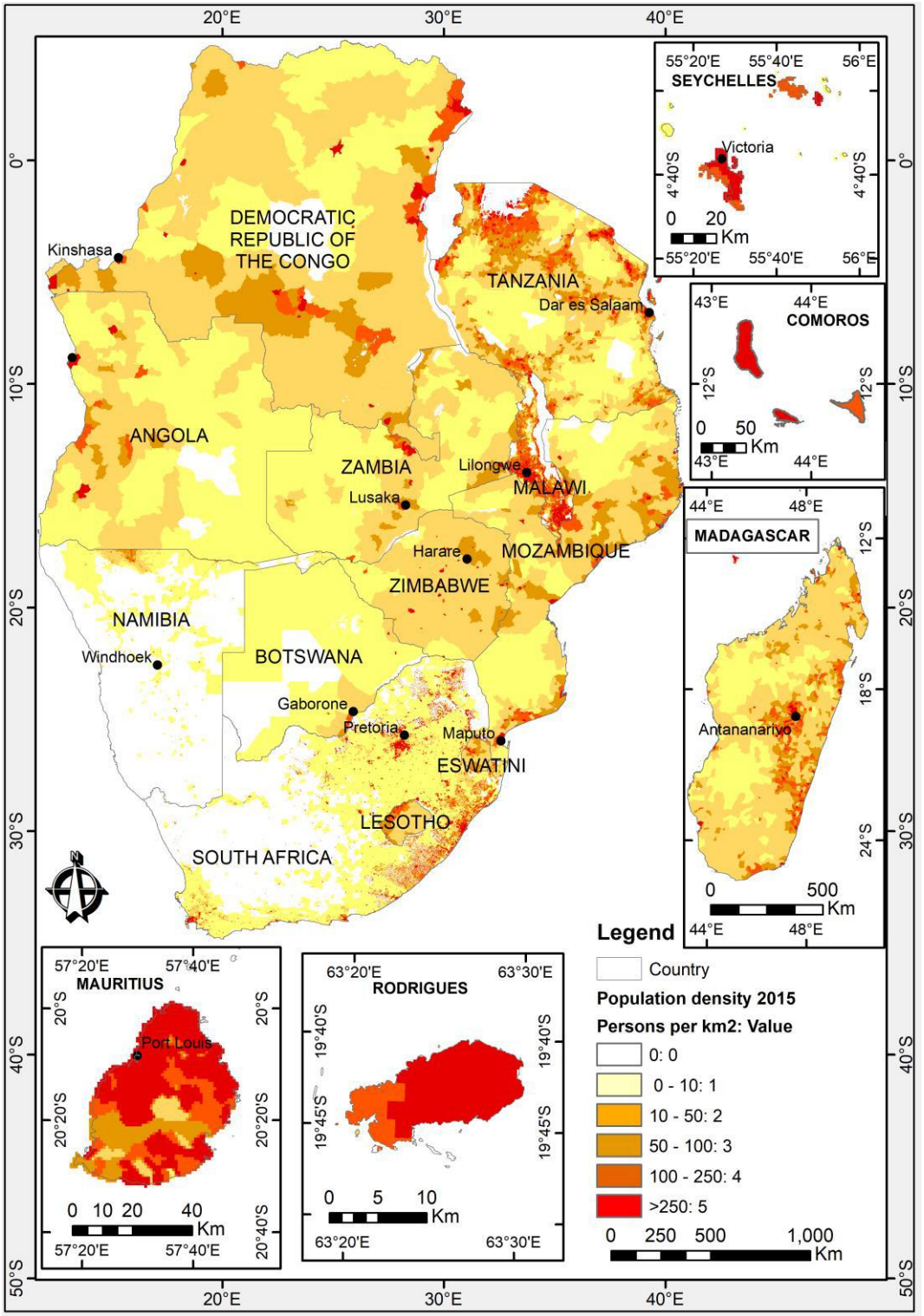

Figure 3-32: **The population density map of the year 2015.**

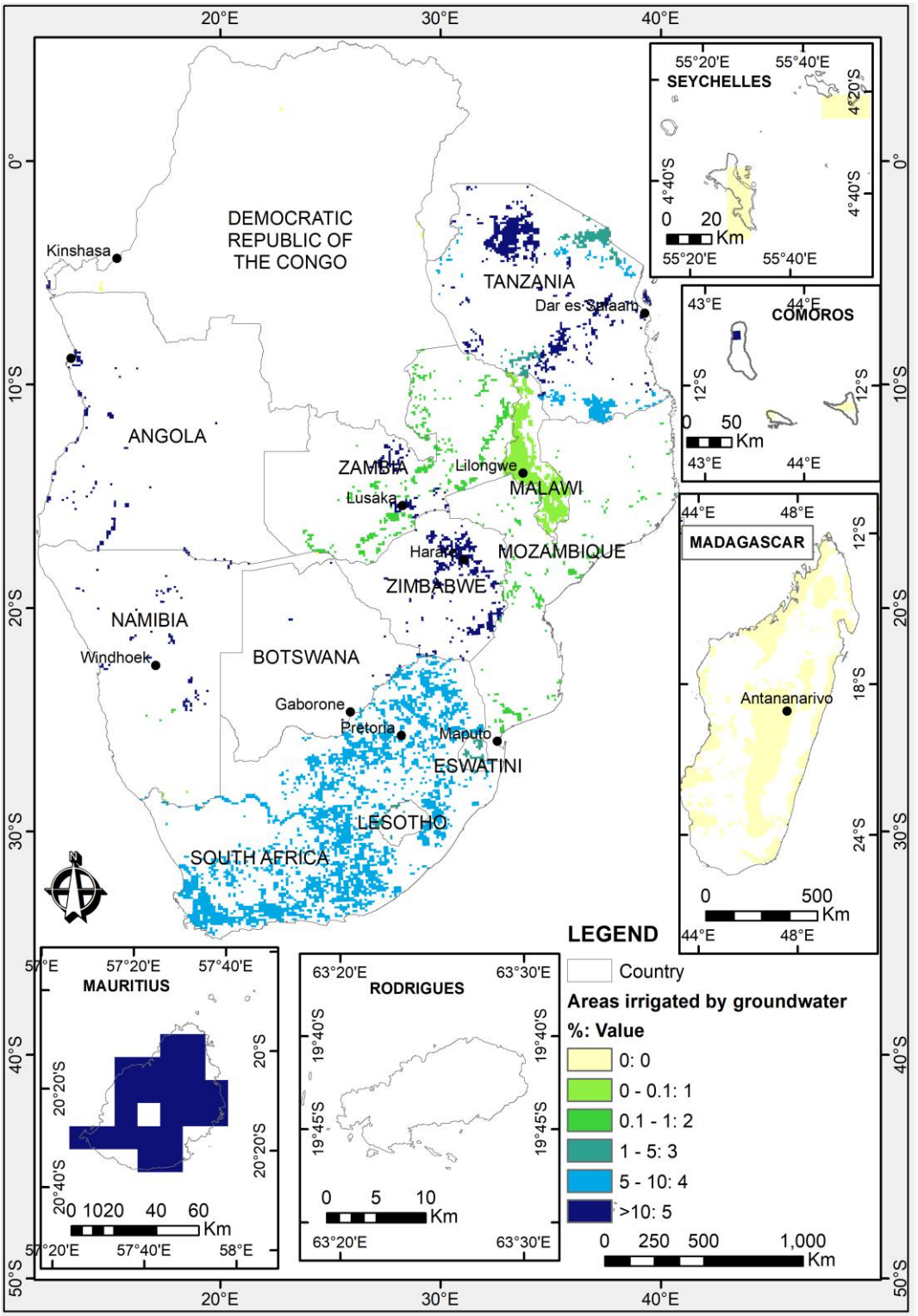

Figure 3-33: **The map showing the percentages of areas irrigated by groundwater**

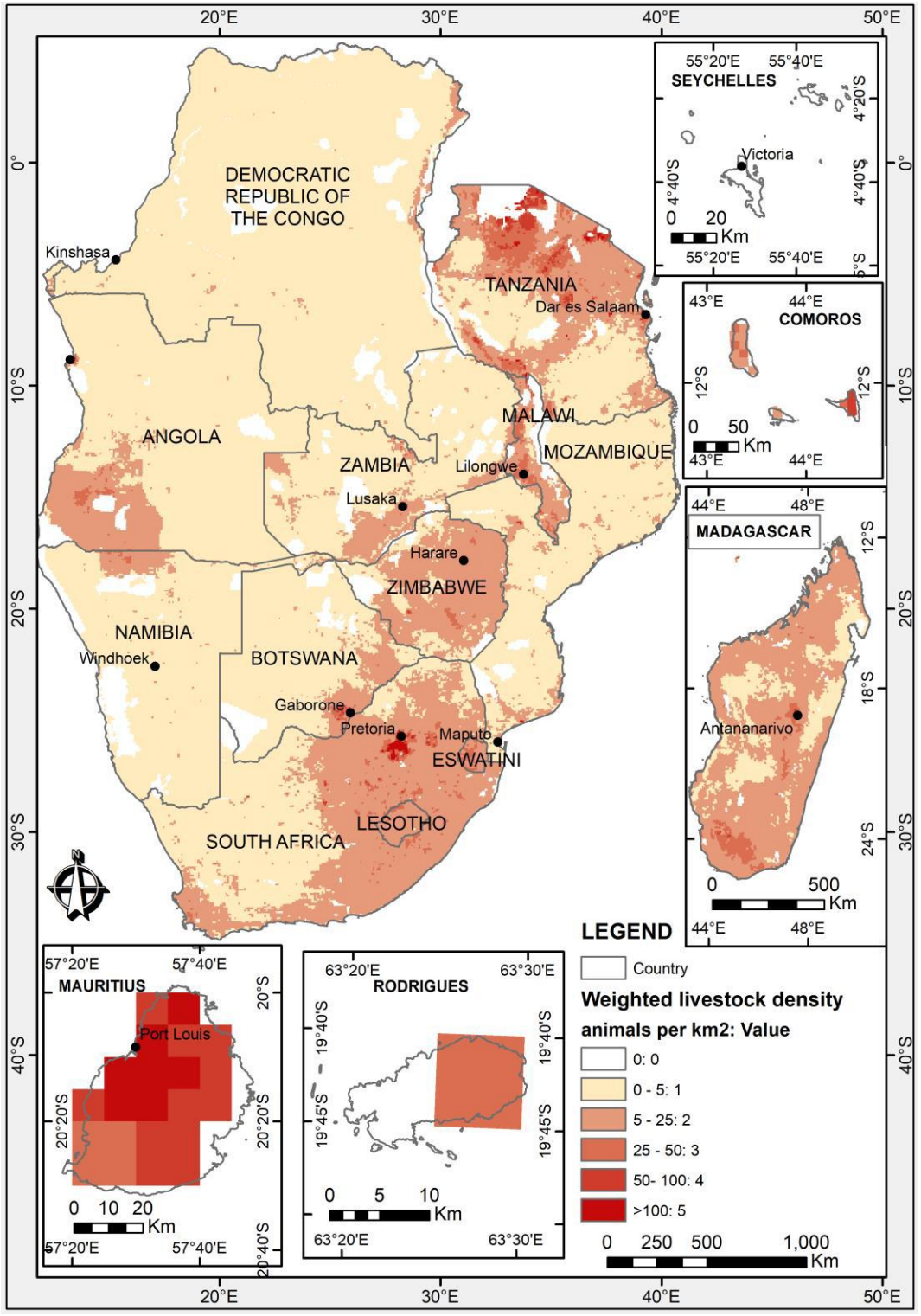

Figure 3-34: **The weighted livestock density map**

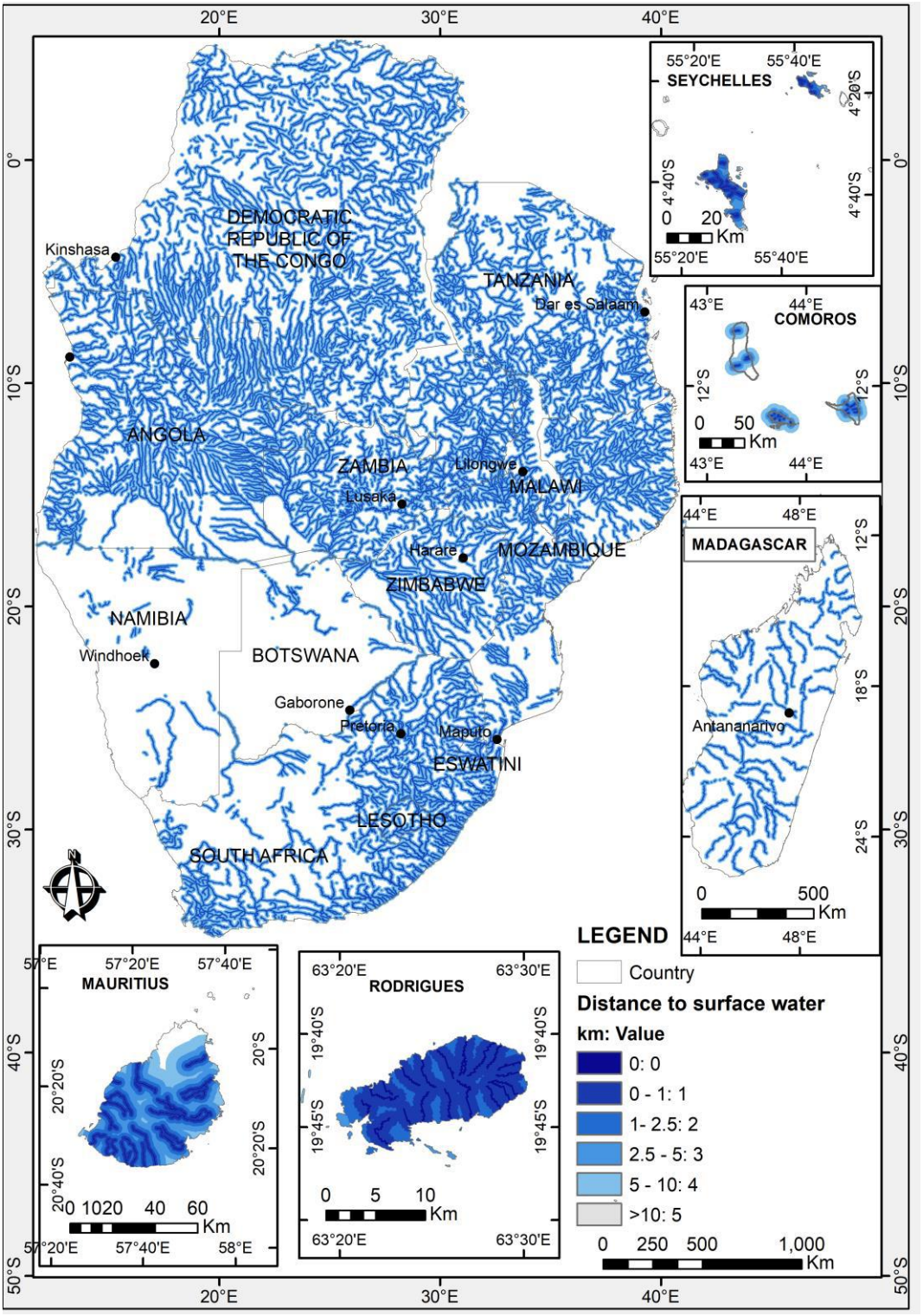

Figure 3-35: Map showing the distances to perennial rivers

All parameters are weighted equally and used to calculate the human groundwater drought vulnerability using the equation below:

Human groundwater drought vulnerability = 0.25*Population density + 0.25*Livestock density + 0.25*Irrigation density + 0.25*Distance to rivers

The human drought vulnerability is given in Figure 3-36.

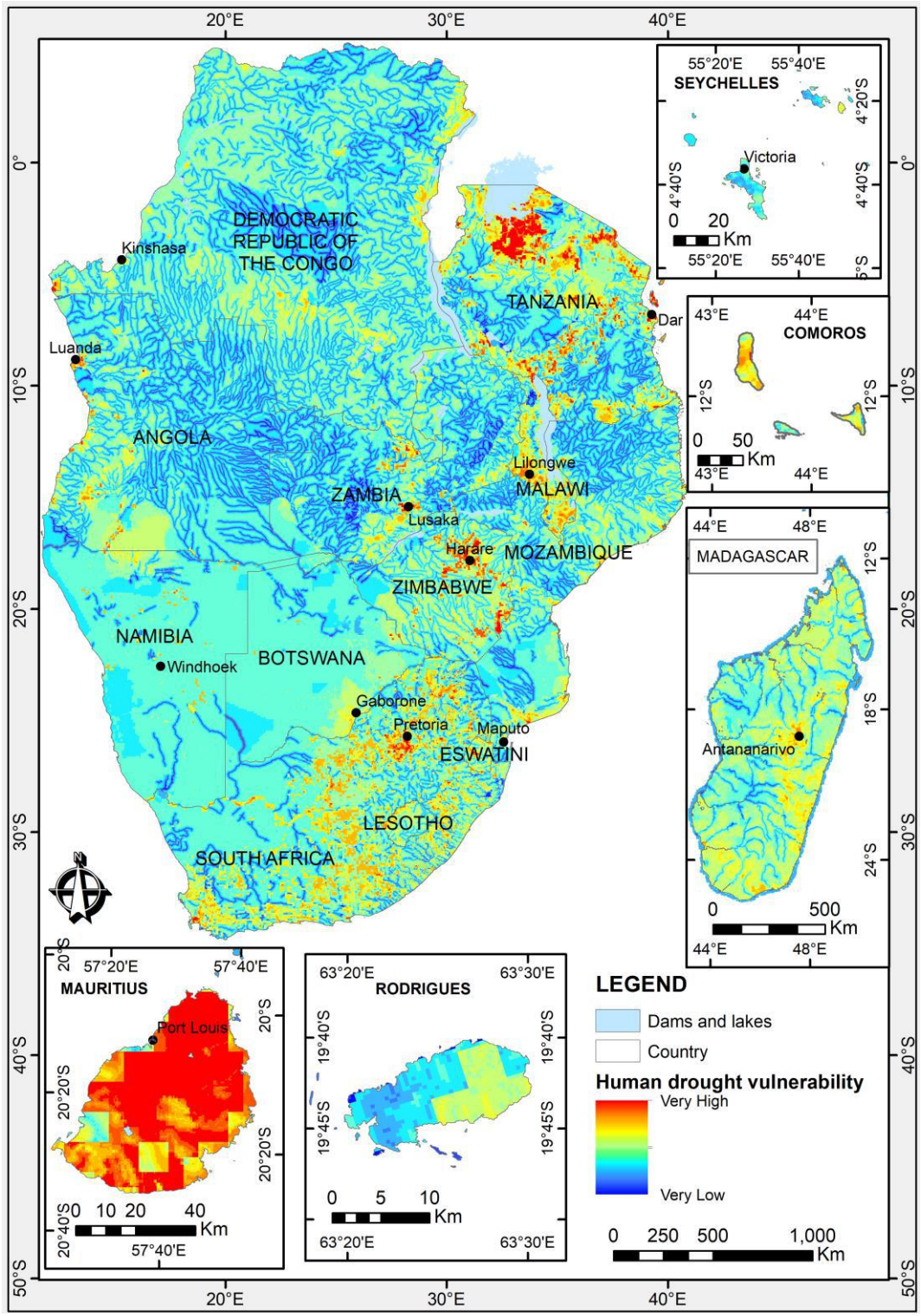

Figure 3-36: **The human groundwater drought vulnerability map**

3.5. Groundwater drought risk map

The groundwater drought risk is calculated as follows (SADC 2011):

Groundwater drought risk (G) = P x w_P + V x w_V

Where:

P = Physical groundwater drought risk

V = Human groundwater drought vulnerability

w_P= weight assigned to P = 0.5

w_V = weight assigned to V = 0.5

w_P + w_V =1

Physical groundwater risk (P) =M x w_M + H x W_H

Where:

M = Meteorological groundwater drought risk

H= Hydrogeological drought proneness

w_M = weight assigned to M = 0.5

w_H = weight assigned to H =0.5

w_M + w_H = 1

The results presented in this section are based on a scenario in which all the parameters are equally weighted. Alternative scenarios are discussed in Chapter 4.

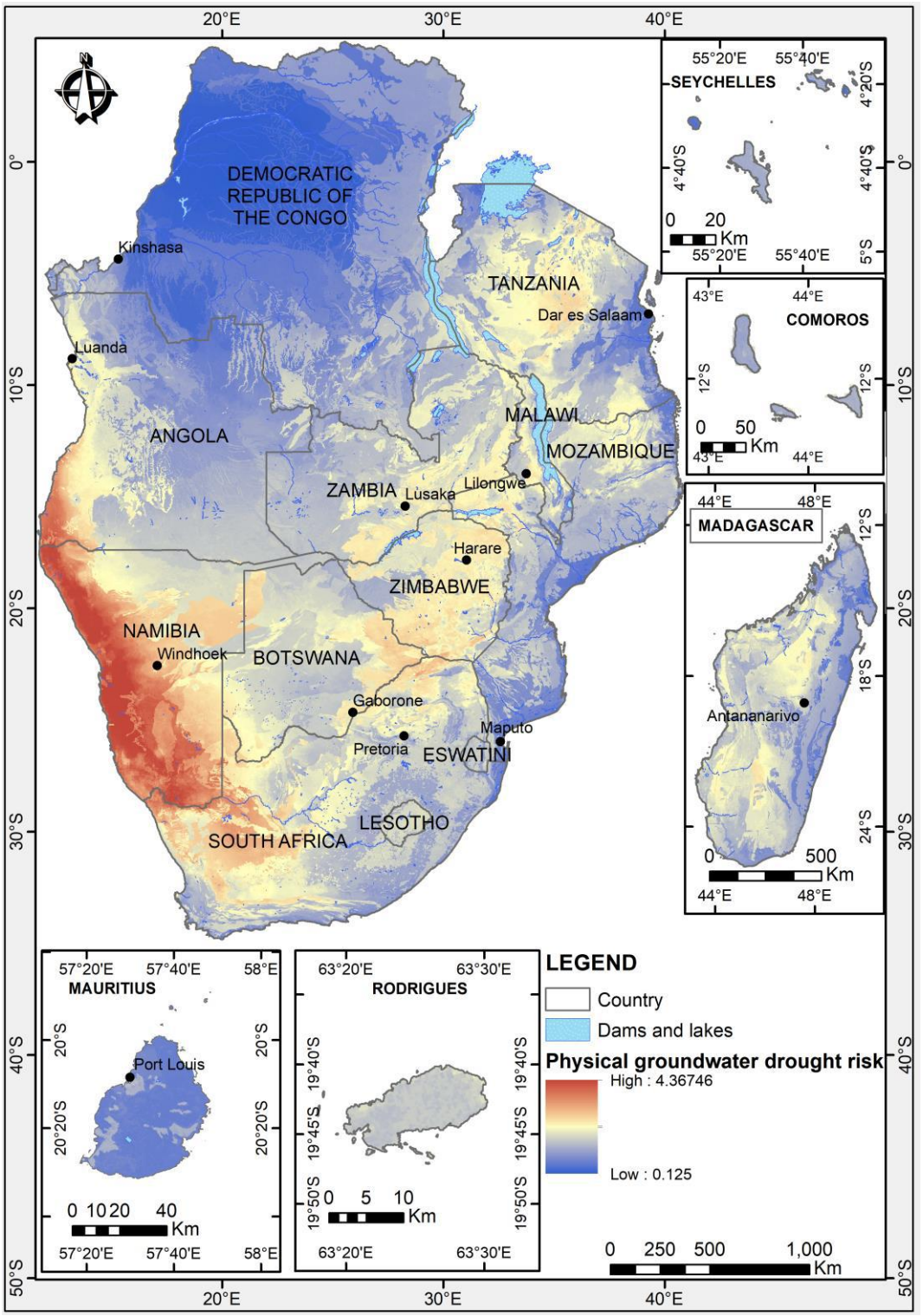

Figure 3-37: **Physical groundwater drought risk map (SADC 2011)**

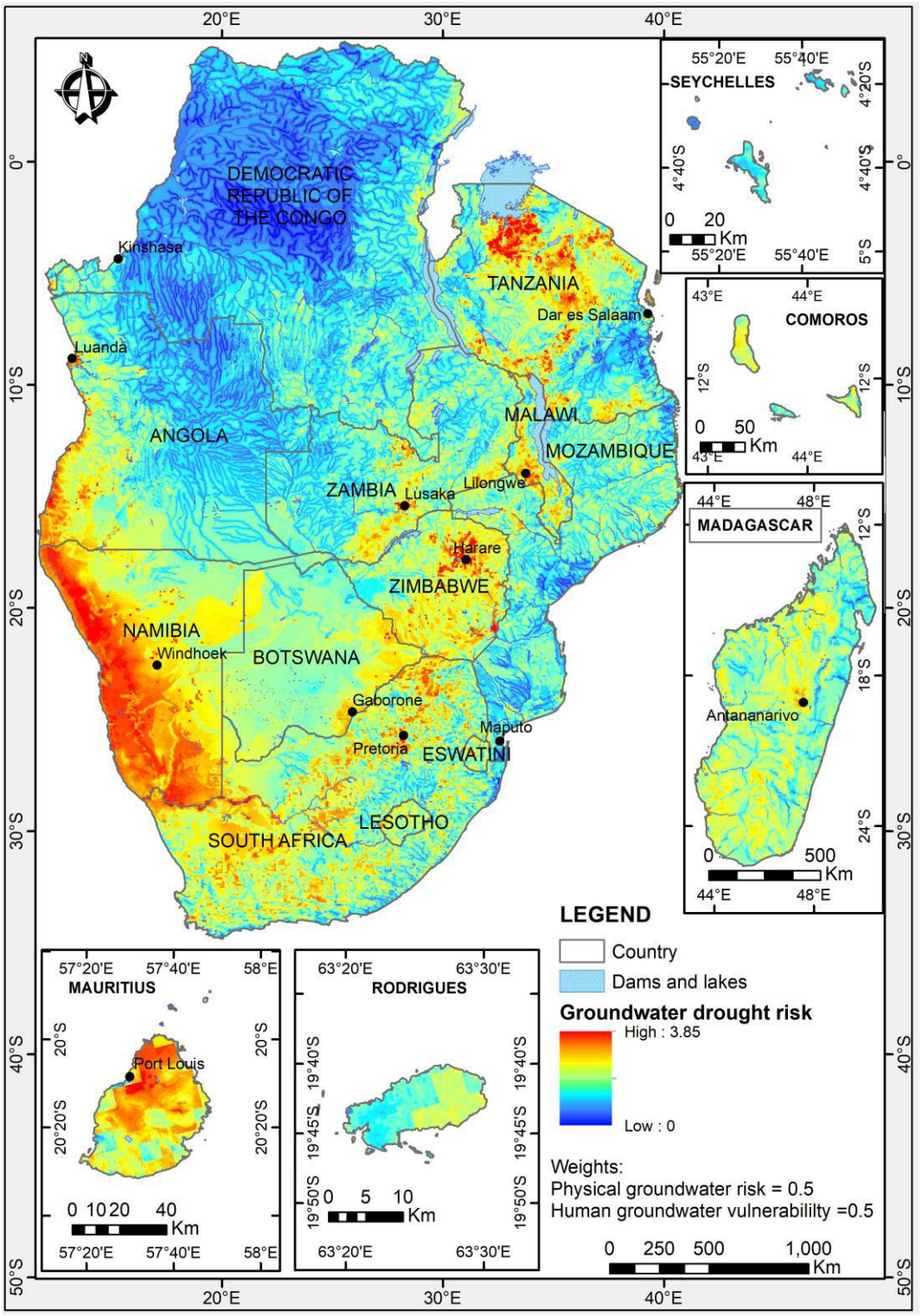

Figure 3-38: **The 2020 groundwater drought risk map without the inclusion of the GGDI parameters**

Scenario 1 (groundwater drought risk map including GGDI parameters):

Updated groundwater drought risk (G) = P x w_P + V x w_V + S x w_S

Where:

P = Physical groundwater drought risk

V = Human groundwater drought vulnerability

S = Groundwater storage sensitivity

w_P = weight assigned to P = 0.34

w_V = weight assigned to V = 0.33

w_S = weight assigned to S = 0.33

$$\mathbf{w_P + w_V + w_S = 1}$$

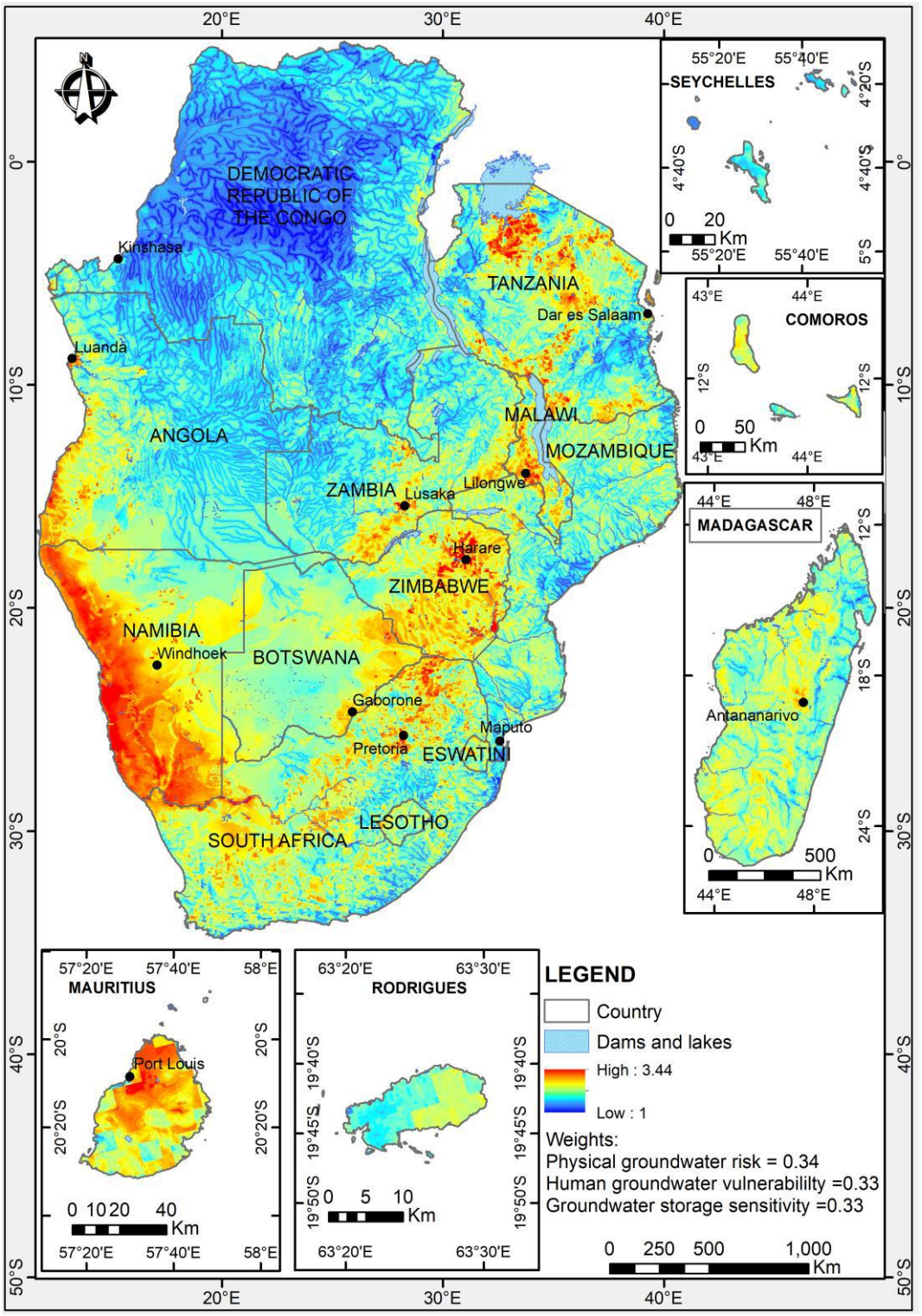

Figure 3-39: **Updated groundwater drought risk map including the GGDI parameters with all parameters equally weighted**

4. SENSITIVITY AND SCENARIO ANALYSIS

Sensitivity analysis (SA) measure the uncertainty or variations in the output results obtained from models applied (Saltelli et al 2008 as cited by Thapa *et al* 2018). In more general terms it measures the robustness associated with the model output as a result of variations in input variables. It facilitates the understanding of the influence of individual input parameters on the model's output by estimating the change in the output map with each change in inputs. The model output can be affected by the following factors:

- The number of input parameters
- Inaccuracies related to inputs, weights, and ranks assigned
- The nature of the overlay performed

4.1. Sensitivity analysis in weighting parameters

GIS based composite mapping approaches have been criticised for not explicitly specifying the weighting methods, using subjective weighting and not evaluating parameter weights (Hagenlocher *et al* 2019). Hagenlocher *et al* (2019) recommend exploring the different weighting options and comparing the results using sensitivity analysis to evaluate their effects on the results. This was the approach undertaken to assess the weighting of the following submodules:

- The climate sensitivity: two scenarios were tested, one in which all parameters were weighed equally and one in which the weights were varied according to SADC (2011)
- The groundwater recharge potential calculation: two scenarios were tested; one in which all parameters were weighed equally and one in which the weights were varied according to SADC (2011)

The scenarios are listed in Table 4-1 and Table 4-3.

Table 4-1: Climate sensitivity scenarios

Scenario	Parameters	Weights
Met 1	Rainfall amount (PANN)	0.4
	Consecutive dry days one calendar year (PDRS)	0.15
	Consecutive dry days more than one calendar year (PEXT)	0.15
	Coefficient of variation (PSTD)	0.3
Met 2	Rainfall amount	0.25
	Consecutive dry days one calendar year	0.25
	Consecutive dry days more than one calendar year	0.25
	Coefficient of variation	0.25

The resulting climate sensitivity maps from the two scenarios were subtracted to obtain a difference map. The results show that the most significant changes are in the low to medium drought risk ranges and the changes in the very low and very high classes are mostly below 20%.

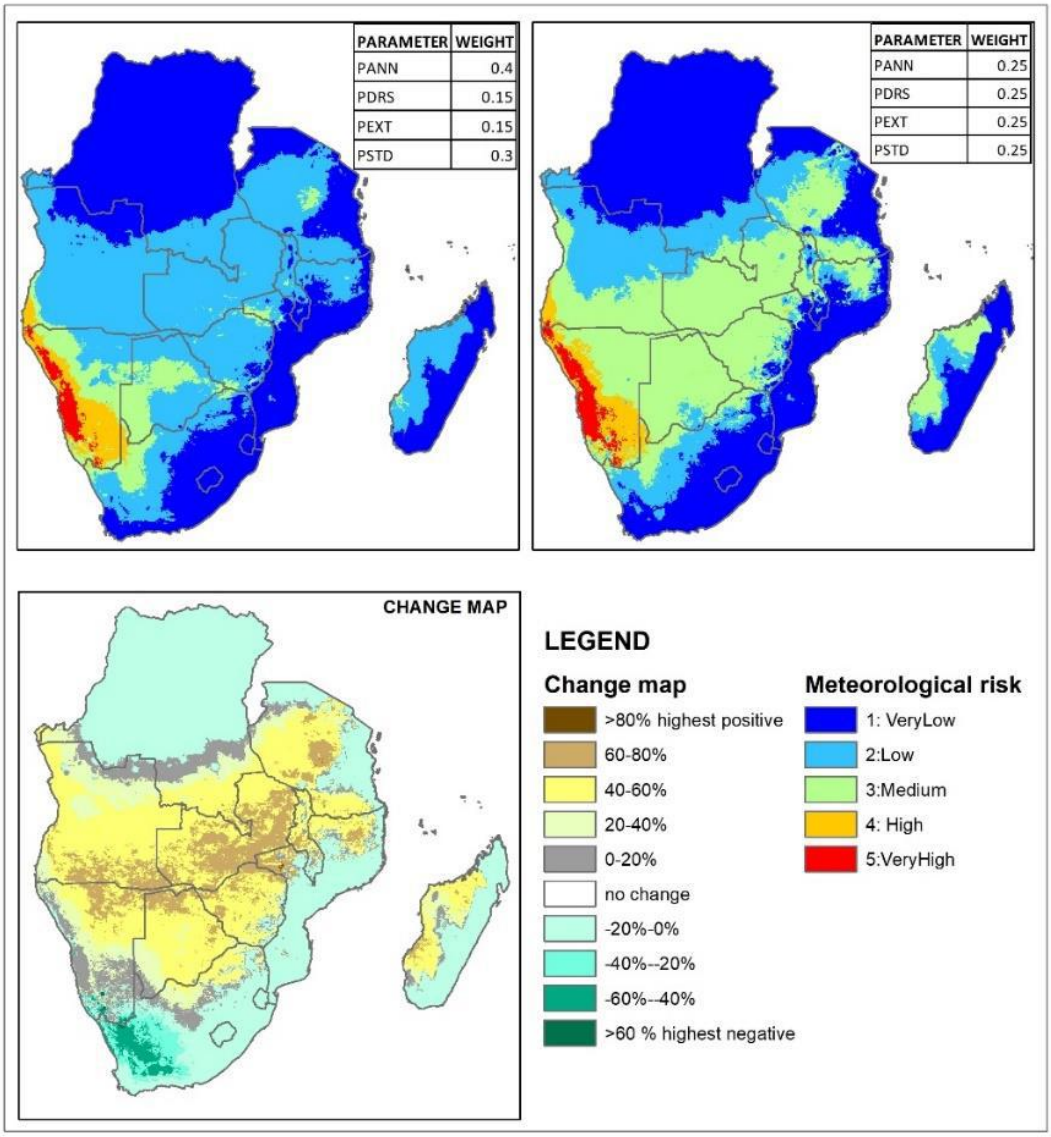

Figure 4-1: **A comparison of the two meteorological drought risk weighting scenarios.**

The changes in the meteorological drought risk classes were also assessed and the results presented in the Table 4-2 were obtained. The results compare the meteorological risk classes from both scenarios and show that the high and very high meteorological risk areas would also be classified as high and very high meteorological drought risk areas under both weighting scenarios (e.g. 100% of the area was classified in the range 4-5 or very high meteorological drought risk in both weighting scenarios). The largest image differences occur in the low to medium meteorological drought risk classes where the total class change for range 1-2 is 62 %, i.e. 62% of the areas were classified as low in one scenario and as medium in the second scenario.

Table 4-2: Meteorological drought risk weighing scenarios

Percentages	Range 0-1	Range 1-2	Range 2-3	Range 3-4	Range 4-5
Range 0-1	94	2	0	0	0
Range 1-2	6	37	6	0	0
Range 2-3	0	61	83	5	0
Range 3.4	0	0	11	79	0
Range 4-5	0	0	0	16	100
Total	100	100	100	100	100
Range Changes (%)	6	**62**	17	21	0

The groundwater recharge potential scenarios are shown in Table 4-3.

Table 4-3: Groundwater recharge potential scenarios

Scenario	Parameters	Weights
GW_rech 1	Rainfall	0.5
	NDVI	0.35
	Slope	0.15
GW_rech 2	Rainfall	0.34
	NDVI	0.33
	Slope	0.33

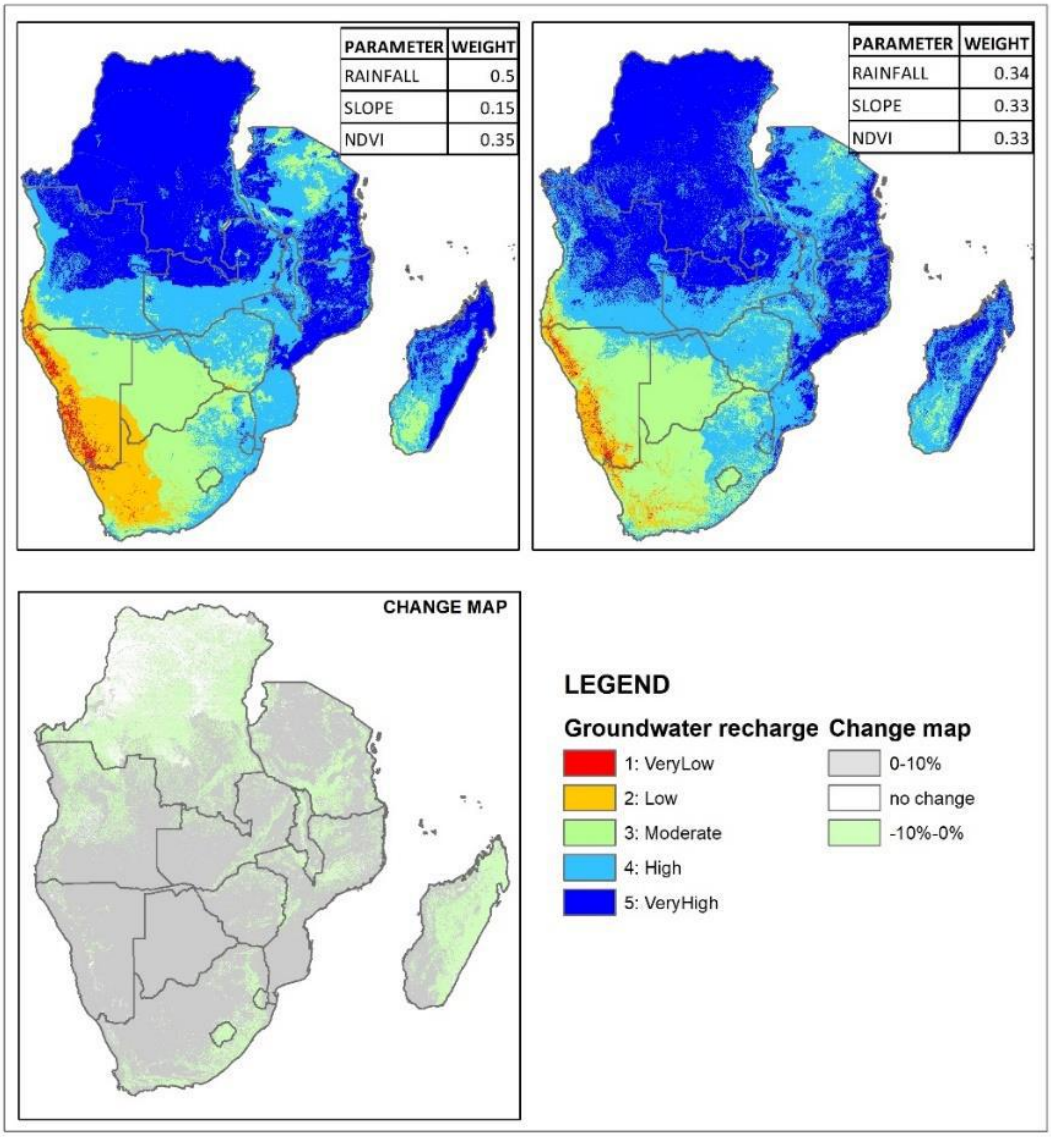

Figure 4-2: **A comparison of the two groundwater recharge weighting scenarios.**

The result of subtracting the two maps show that the differences between the values of the two maps are less than or equal to 10% (Figure 4-2). The changes in the classes were also assessed and the results in the Table 4-4 were obtained. The results compare the recharge classes from both scenarios and show that the high to very high groundwater recharge potential areas would be classified as high recharge potential maps under both weighting scenarios (e.g. 93% of the area was classified in the range 4-5,very high groundwater recharge potential, in both weighting scenarios). The large image differences occur in the very low and low groundwater recharge classes (ranges 0-1 and 1-2) where the class changes are 61 % and 67 % respectively.

Table 4-4: Groundwater recharge potential image difference statistics

Percentages	Range 0-1	Range 1-2	Range 2-3	Range 3-4	Range 4 -5
Range 0-1	39	0	0	0	0
Range 1-2	61	33	0	0	0
Range 2-3	0	67	67	4	0
Range 3-4	0	0	33	91	7
Range 4-5	0	0	0	5	93
Total	100	100	100	100	100
Range changes (%)	**61**	**67**	33	9	7

A correlation analysis was also conducted between the two scenarios and an independent global dataset from Moeck *et al* (2020). The result shows that the map from scenario 1 (with rainfall highly weighted) correlates better with the 80 points in the SADC region from the global recharge dataset with a moderate positive correlation coefficient of 0.65 (Table 4-5).

Table 4-5: Correlation analysis between the different weighting scenarios and Moeck *et al* (2020)

	Moeck et al. 2020 dataset	Equal (GW_rech 2)	Original (GW_rech 1)
Moeck et al. 2020 dataset	1		
Equal (**GW_rech 2**)	0.48	1	
Original (**GW_rech 1**)	0.65	0.85	1

4.2. Sensitivity analysis for different macro-level scenarios

Sensitivity analysis was also used to assess the variations in the different weighting of the input parameters on the groundwater drought risk map. The most appropriate way of running such sensitivity analysis is by changing the weights of the criterion/criteria by specific percentage increments and calculating a map for each scenario. This process can generate hundreds of scenario maps (Chen *et al* 2009). For these scenarios, the pixel class changes are analysed and the following statistics can computed on the final drought risk maps: the mean, median minimum, maximum, range, standard deviation and the coefficient of variation on each cell. The following information can be derived from such statistics (Grandmont *et al* 2012, Quinn *et al* 2015):

- the mean and minimum can show the most vulnerable areas, irrespective of the weightings of the parameters
- low values of range and standard deviation for areas of high vulnerability indicate the robustness of the model identifying the most vulnerable areas

- the coefficient of variation (the standard deviation divided by the mean) map accurately represents areas where the predicted ratings are most sensitive to the choice of layer weights, the higher the coefficient of variation the more sensitive to parameter weights.

This extensive scenario analysis was beyond the scope of the study and was not conducted. There was no need to perform such extensive analysis as this was previously done in SADC, 2011 and the results of the analysis were reviewed by regional experts who concluded that the groundwater drought risk map was representative of the status quo in the region. The five scenarios listed in Table 4-6 were the only ones explored.

Table 4-6: Parameter weights for all scenarios

Scenario	Submodules	Sub_sub_modules	Parameters	Scenario 1 Weights	Scenario 2 Weights	Scenario 3 Weights	Scenario 4 Weights	Scenario 5 Weights
GDR 2	Climate Sensitivity	Meteorological risk	Rainfall amount	0.4	0.25	0.4	0.4	0.4
			Consecutive dry days one calendar month	0.15	0.25	0.15	0.15	0.15
			Consecutive dry days more than one calendar month	0.15	0.25	0.15	0.15	0.15
			Coefficient of variation	0.3	0.25	0.3	0.15	0.3
	Hydrogeological drought proneness	Groundwater recharge potential	Slope	0.15	0.33	0.15	0.15	0.15
			NDVI	0.35	0.33	0.35	0.35	0.35
			Mean annual rainfall	0.54	0.34	0.5	0.5	-
			Aridity index	-	-	-		0.5
	Hydrogeological drought proneness	Groundwater recharge potential (derived from rainfall)		0.5	0.5	0.5	0.5	-
		Groundwater recharge potential (derived from the aridity index)		-	-	-	-	0.5
		Aquifer productivity		0.5	0.5	0.5	0.5	0.5
	Human groundwater drought vulnerability	Groundwater dependence	Population density	0.25	0.25	0.25	0.5	0.25
			Irrigation density	0.25	0.25	0.25	0.2	0.25
			Distance to river	0.25	0.25	0.25	0.15	0.25
			Livestock density	0.25	0.25	0.25	0.15	0.25
Groundwater drought risk map								
Module								
Physical groundwater drought risk				0.34	0.34	0.34	0.34	0.34
			Meteorological risk	0.5	0.5	0.75	0.5	0.5
			Hydrogeological drought proneness	0.5	0.5	0.25	0.5	0.5
Groundwater storage sensitivity				0.33	0.33	0.33	0.33	0.33
Human groundwater drought vulnerability				0.33	0.33	0.33	0.33	0.33

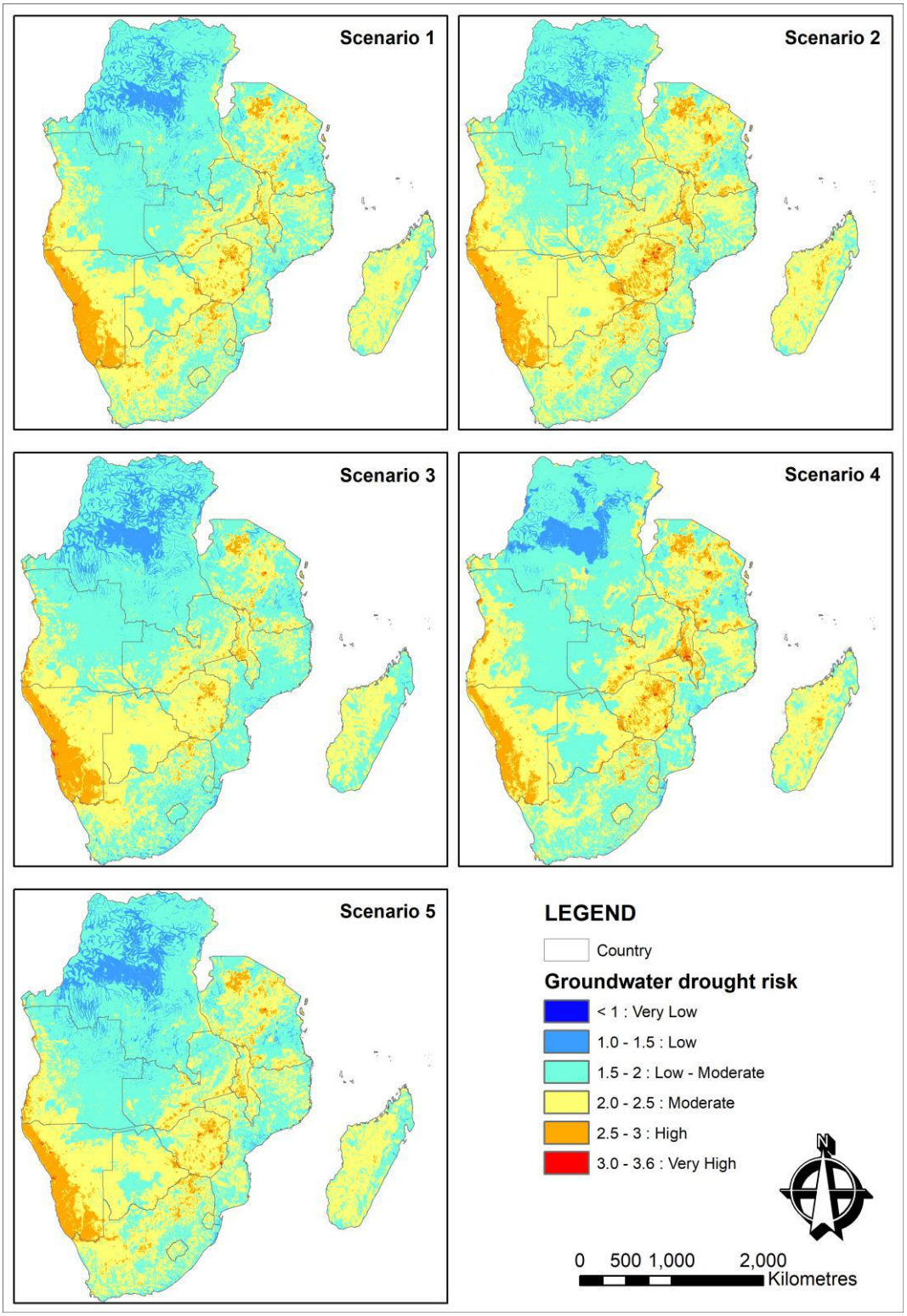

Figure 4-3: **The five scenario maps produced for the five weighting scenarios listed in Table 4-6**

Figure 4-3 shows all the maps from the five scenarios. Visually the maps look similar and correlation analyses show more than 95% correlation between all five maps.

The five scenario maps were further classified according to groundwater drought risk and the results were compared using image differencing. The image differencing approach adopted is when a pair of maps are subtracted from each other and change statistics are derived and these are shown in Figure 4-4 and Figure 4-5. The calculation compares the classified maps pixels in a pair of scenario images and record the proportion of pixels that are in the same class in both images and those that change classes from on map to the next. For example, a value of 100% indicates that all pixels are classified in the same class in both maps and therefore the classified maps are identical. The total class change percentages for all classes and scenarios are presented in the graph in Figure 4-4. Example of the image differencing results for some of the scenarios are presented in Tables 4-7 a, b and c.

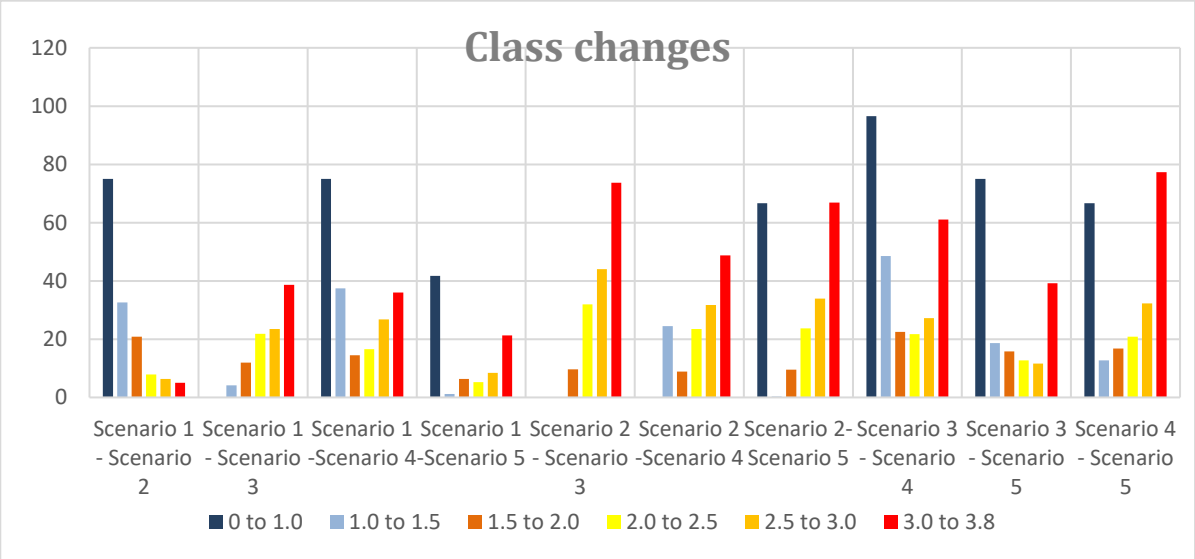

Figure 4-4: The total percentage class changes between the different scenarios

Table 4-7: Image differencing results per class for three scenario differences

A

Scenario 2 – Scenario 3	0 to 1.0	1.0 to 1.5	1.5 to 2.0	2.0 to 2.5	2.5 to 3.0	3.0 to 3.8
0 to 1.0	100	0	0	0	0	0
1.0 to 1.5	0	100	9	0	0	0
1.5 to 2.0	0	0	90	31	0	0
2.0 to 2.5	0	0	1	68	44	0
2.5 to 3.0	0	0	0	1	56	74
3.0 to 3.8	0	0	0	0	0	26
Class changes (%)	**0**	**0**	**10**	**32**	**44**	**74**

B

Scenario 3 – Scenario 4	0 to 1.0	1.0 to 1.5	1.5 to 2.0	2.0 to 2.5	2.5 to 3.0	3.0 to 3.8
0 to 1.0	3	0	0	0	0	0
1.0 to 1.5	97	51	1	0	0	0
1.5 to 2.0	0	49	78	14	0	0
2.0 to 2.5	0	0	21	78	25	0
2.5 to 3.0	0	0	0	8	73	61
3.0 to 3.8	0	0	0	0	3	39
Class changes (%)	**97**	**49**	**22**	**22**	**27**	**61**

C

Scenario 4 – Scenario 5	0 to 1.0	1.0 to 1.5	1.5 to 2.0	2.0 to 2.5	2.5 to 3.0	3.0 to 3.8
0 to 1.0	33	0	0	0	0	0
1.0 to 1.5	67	87	6	0	0	0
1.5 to 2.0	0	13	83	17	0	0
2.0 to 2.5	0	0	10	79	32	0
2.5 to 3.0	0	0	0	3	68	76
3.0 to 3.8	0	0	0	0	0	23
Class changes (%)	**67**	**13**	**17**	**21**	**32**	**77**

The results of image differencing show that although there are differences in the scenario maps, the maximum change in most pixels is by one risk class although a few pixels change by two classes. In order to verify these scenario maps and select the map that best represents the risk class of an area, direct measurements or expert knowledge would be generally used. In this study, there was no information available to make such determinations.

Another useful map to analyse is the coefficient of variation/uncertainty map. It shows areas that are most sensitive to changes in the weightings of the various criteria (Quinn et al., 2015). Figure 4-5 shows the coefficient of variation of the five scenarios in countries with moderate to very-high groundwater drought risk areas. The interpretation of these results is that areas with high coefficient of variation, i.e. the areas most affected by parameter weightings have low groundwater drought risk. Although this map was created using only five scenarios, these initial results show that high groundwater drought risk areas would be classified as such regardless of the weightings used. This needs to be tested using more weighting simulation combinations.

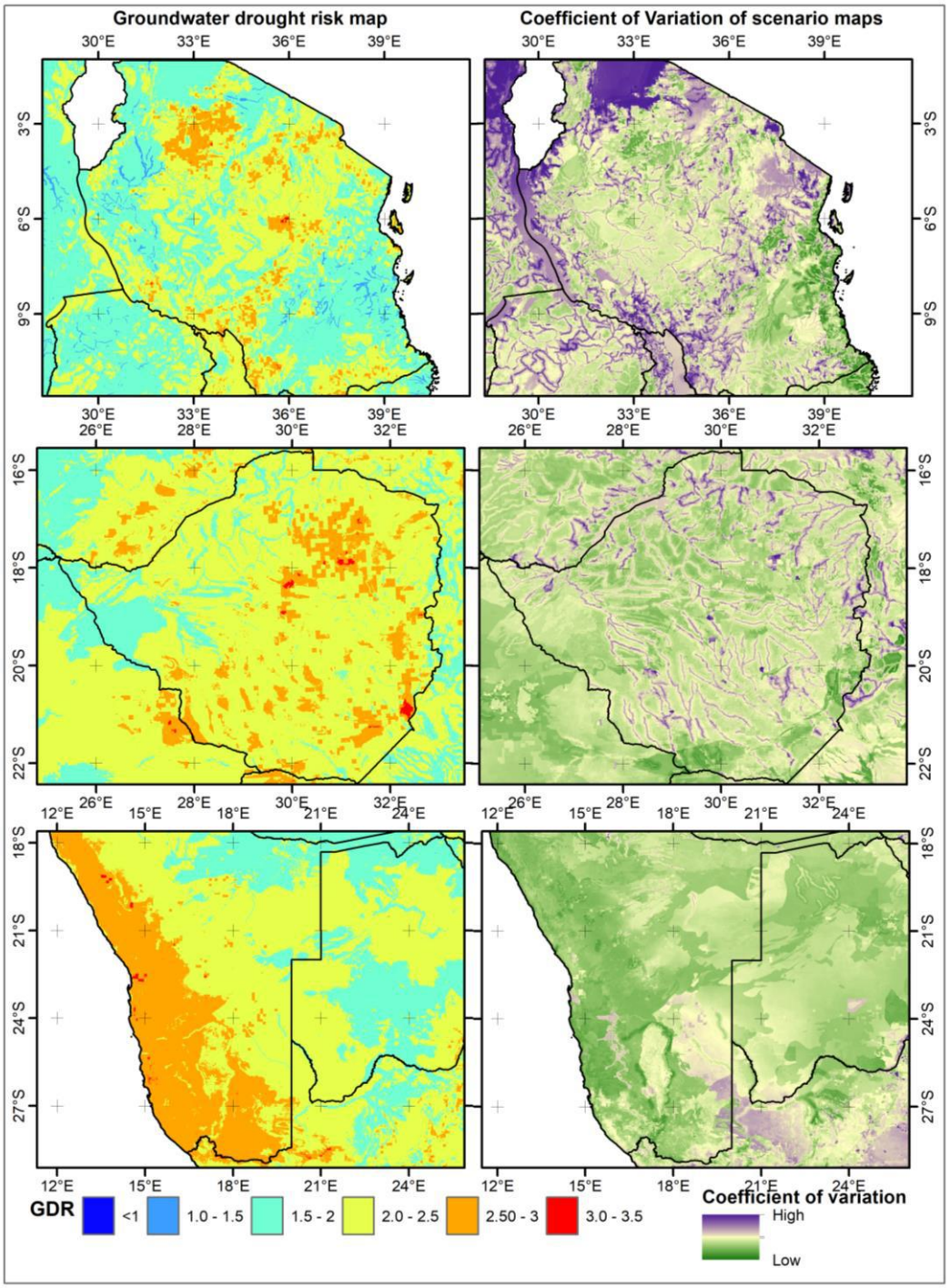

Figure 4-5: Comparison of the GDR map with the coefficient of variation of the five scenario maps

4.3. Scenario analysis using Bayesian Networks

Scenario analysis using Bayesian networks (probabilistic networks) was also be explored. The GRiMMS method does not consider the relations between variables as the structure is vertical or hierarchical and there is no account for the lateral relationships that might exist between the

different parameters. Techniques like Bayesian Networks can be used to evaluate the relationships between the parameters and assess how sensitive the parameters or the groundwater drought risk map is to changes in the other parameters in the network. Bayesian Networks show the relationships between datasets in the specific domain, for example in this assessment the parameters for groundwater drought risk and represent the strength of these relationships as probabilities. They provide a way of handling missing data, allow combination of quantitative and qualitative data, a way of including expert knowledge and provide good predicting accuracy even with small samples. These relationships can be used to perform scenario analysis and also provide a quantitative assessment of the most influential parameters in an assessment.

Bayesian networks are graphical models that allow for the representation and reasoning of any uncertain domain. A Bayesian network is a directed acyclic graph (DAG) made up of a set of random variables from the problem domain, which are represented as nodes. A graph is made up of nodes (or vertices) and edges (or arcs). A DAG is a directed graph with no cycles (a cycle is a path that starts and ends at the same node). The arcs in the Bayesian Network represent the interactions/relationships between the variables.

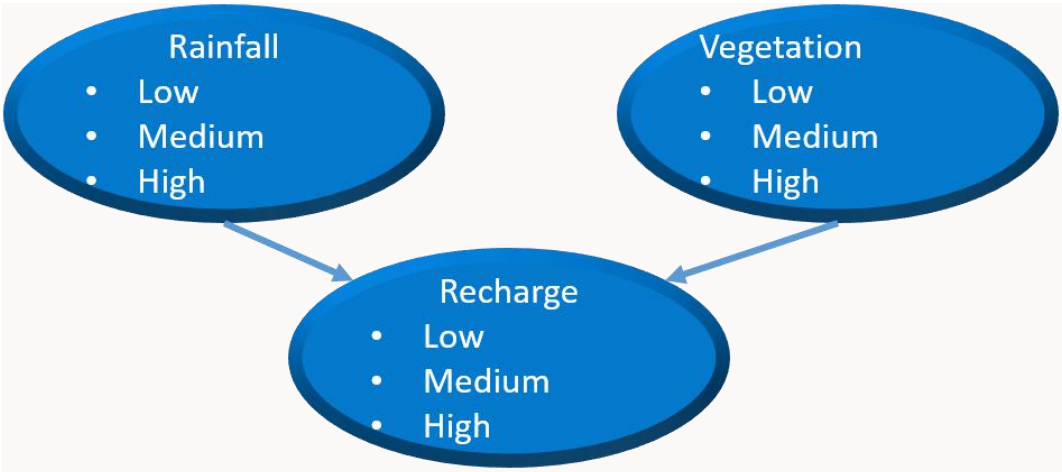

Figure 4-6: A simple network showing three variables, rainfall, vegetation and recharge

Bayesian Networks can handle huge datasets with a lot of parameters and complex relationships and can still process at high speed. Since they are solved analytically, Bayesian Networks provide rapid response during query analysis when the model is updated. This is vital especially when performing scenario analysis and presenting the outcome of these for decision-making. Bayesian Networks do not only go from cause to effect, but analysis can be done from effect to cause in order to perform diagnosis, which assesses the different causes of given scenarios or effects.

The Bayesian Network for the groundwater drought risk map is shown in Figure 4-7. The network is created from data used in the GRiMMS method. Each raster cell on the map is intersected with all the classified layers and the data values are appended to a table; no weighting is applied to the parameters. Each row on the table then constitutes a "case" which is a combination of the different classes for all parameters. In a simplistic approach where all the data is available, probability values are the calculated by counting the number of times a parameter exists in different states. The conditional probabilities are then estimated by the ratio of the corresponding counts (Cowell *et al* 1999).

The Bayesian Network can be used to validate the GRiMMS algorithm, querying different aspects of the parameters and assessing if the results obtained are intuitive or expected according to existing knowledge of the domain. As an example of how to interpret the results, the following are interpretations at some of the nodes:

- Groundwater drought risk: for the whole SADC region, 5% of the area is in the "very low" (values 1-1.5) drought risk and 6% are in the "high" (2.5-3) risk areas and a negligible amount (<0 %) are in the "very high risk"
- Meteorological drought risk: 44% of the SADC region are in the "very low" (0-1) drought risk range

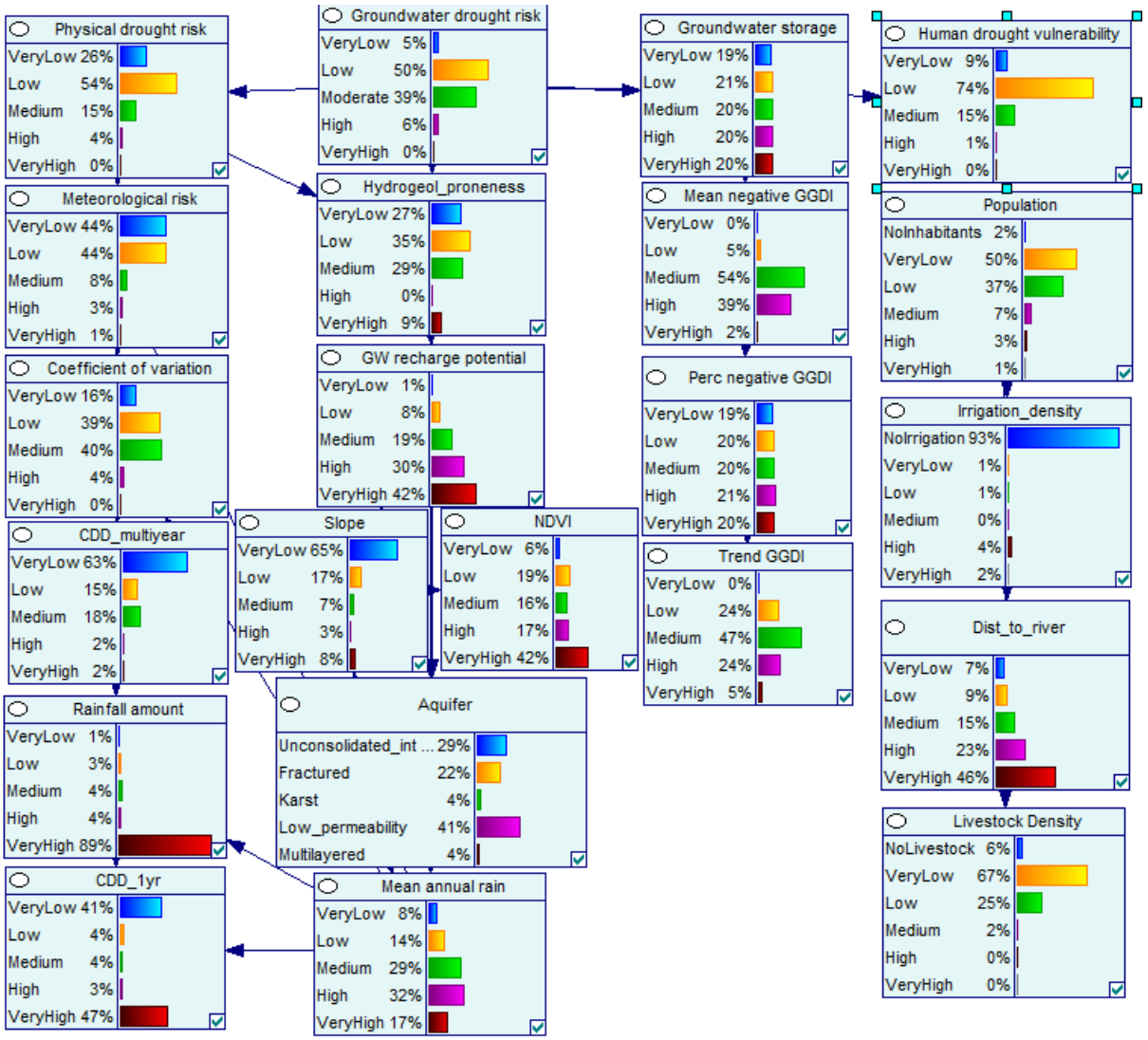

Figure 4-7: **The Bayesian Network showing the base probabilities/proportions for each class of each parameter**

The network can be queried by assessing the characteristics of areas of "very high" mean annual rainfall (Figure 4-8):

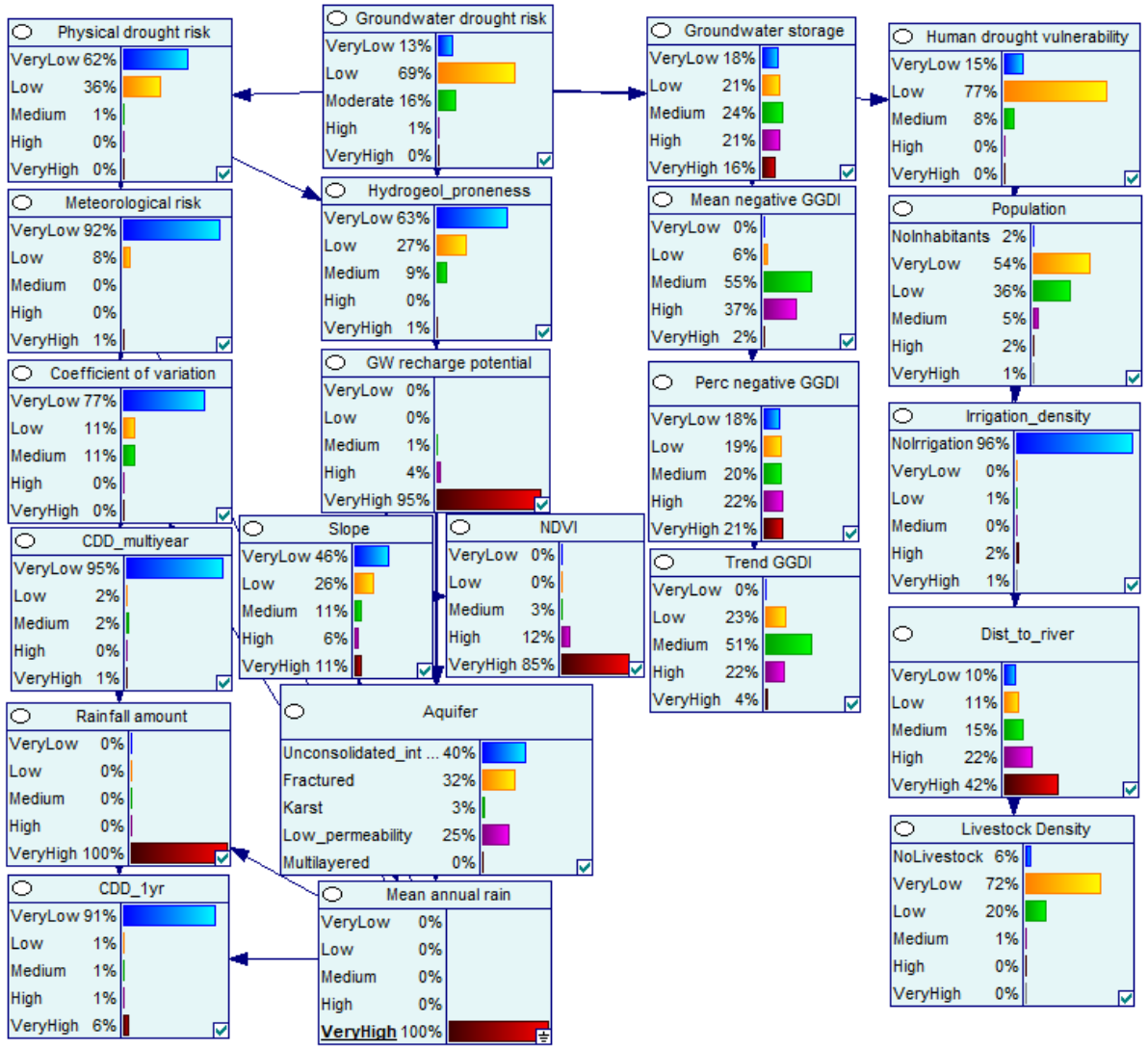

Figure 4-8: **The Bayesian Network showing the base probabilities/proportions for each class of each parameter after query at "very high" mean annual rainfall**

The network can be queried by assessing the characteristics of areas of "very high" human drought vulnerability (Figure 4-9)

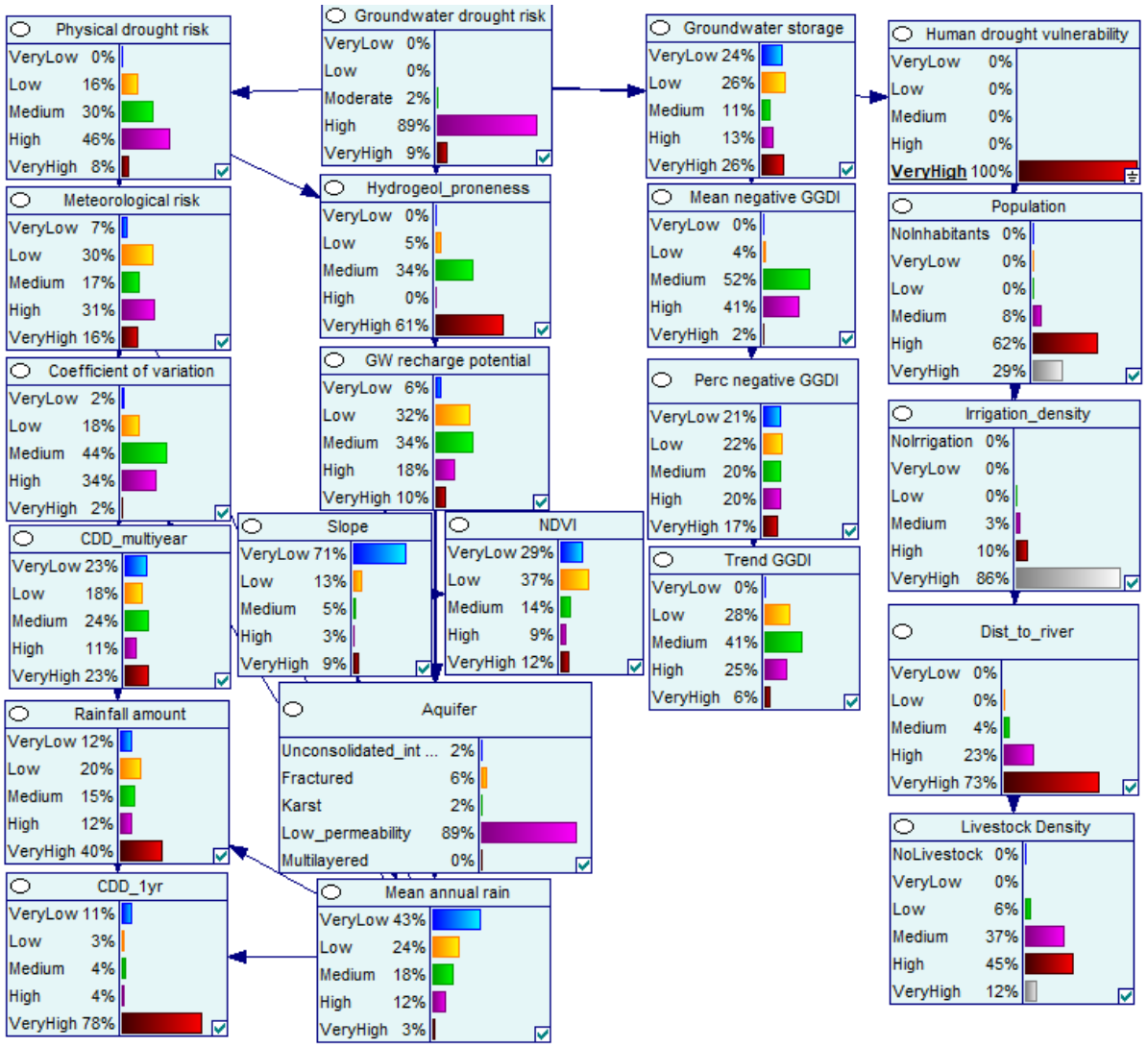

Figure 4-9: **The Bayesian Network showing the base probabilities/proportions for each class of each parameter after query at "very high" human drought vulnerability**

After querying a specific parameter on the map, the probabilities are observed and this change of probabilities can be used to assess the sensitivity of certain aspects of the network. The Bayesian Network provided above is aggregated to the whole SADC region; the same Network can be aggregated at different spatial analysis scales, e.g. country or catchment level.

Assuming that the selected analysis area has uniform characteristics and the cases are general to the entire area, scenarios such as climate change scenarios e.g. increase/decrease in mean annual rainfall can be interrogated by varying the probabilities at the different rainfall classes and assessing quantitatively how they change the groundwater drought risk or other related parameters in the area.

5. VERIFICATION AND VALIDATION OF THE GDR MAP

Verification is meant to assess if the model functions at it is intended to. Model verification should test the robustness of the model to practical insignificant changes in data and the deviations of data and the system from the assumptions made during model development. The model can be checked for consistency against different input datasets (Jakeman *et al* 2006). In this study, the map produced by SADC (2011) can be used to verify our map as it uses the same model but some independent datasets.

The maps are compared in Figure 5-1. The maps compared are the 2011 map, the 2020 map with no GGDI parameters and the final map after the GRACE GGDI parameters are included. The general patterns of groundwater drought risk are similar; the maps highlight the very low to low risk areas and the high to very high-risk areas. This shows that the method is robust and repeatable as it was tested using different datasets at varying spatial and temporal resolutions but still produced similar results. The major differences are in the low to moderate ranges which vary vastly amongst the maps. The GGDI parameters also have the effect of reducing the overall drought risk in the SADC region.

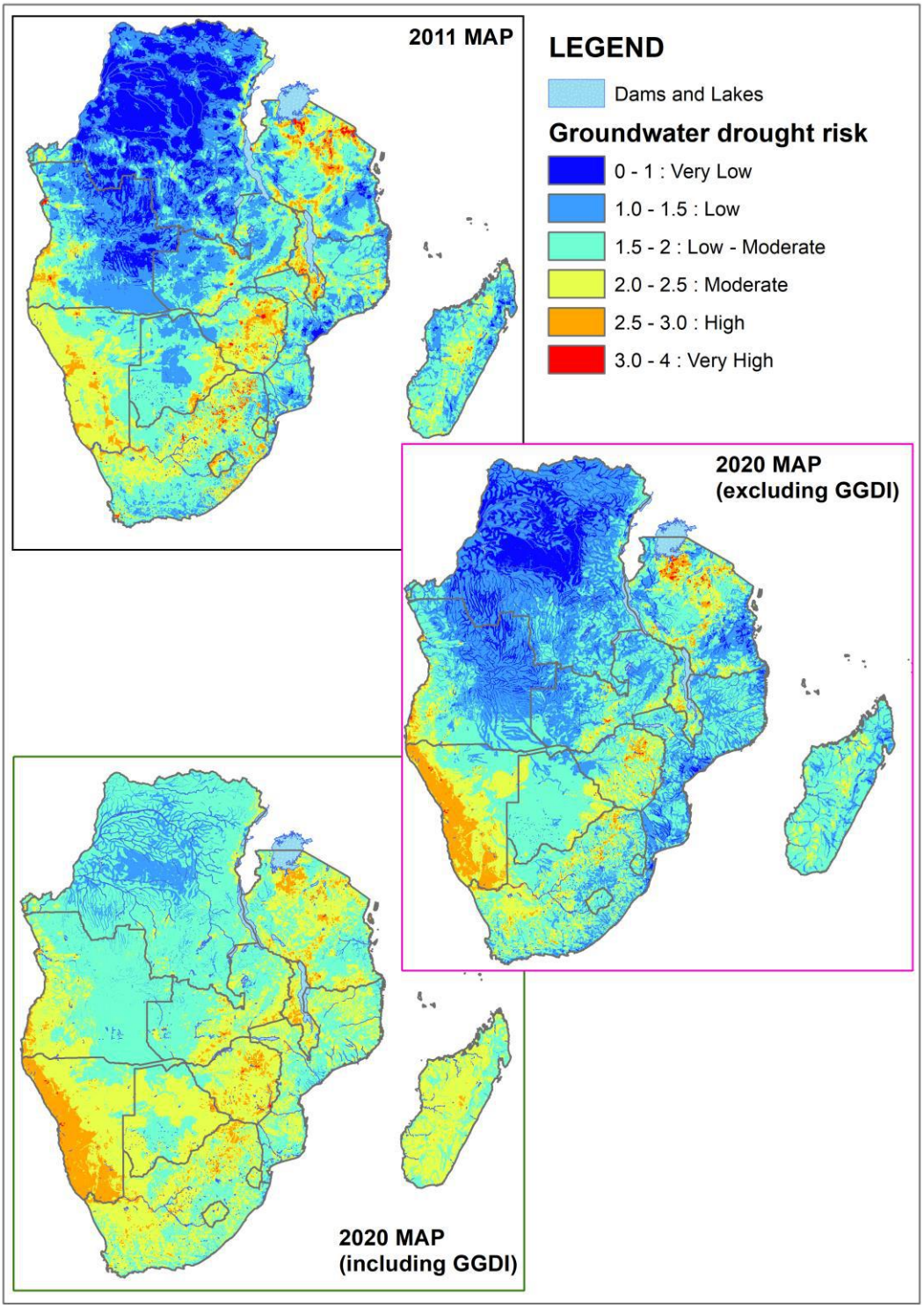

Figure 5-1: Comparison of the different GDR maps after classification according to drought risk values

Validation is an important part of any modelling exercise. A model being a representative/abstraction of the real-world system must be assessed to ascertain if it is a reasonable representation of reality. In this study the aim is to validate the groundwater drought risk map. The most ideal situation is to validate with measurements or ground-truth the data. It

is also acceptable to validate modules are aspects of the model separately from each other using different datasets and results from other models. Often in, practice, it might not be possible to fully validate the model and this is the case in this study. The acceptable approaches for validation include the following:

- Real world measurements (the most reliable and preferred method)
- The use of expert knowledge i.e. independent experts from the modellers
- Validation of the results using outputs from other independent studies (which is not highly recommended as the independent study might not also be a true representation of the system

There is no data per ser on groundwater drought as it is not an observable phenomenon and there are but various approaches that are applicable to our study:

- The comparison of the GDR map with the Africa groundwater datasets created by (MacDonald *et al* 2012) - which used field based datasets from various aquifer studies
- The validation of the GDR map using data and results from independent studies that utilised groundwater levels, rainfall and drought indices like the Standardized Precipitation Index (SPI) for the assessment of groundwater drought (Meyer 2005, Cuthbert *et al* 2019)

Figure 5-2 shows the groundwater storage map and a map showing estimated volumes calculated per country in the SADC region (MacDonald *et al* 2012). These maps are compared to the groundwater drought risk map. The groundwater maps were created using the 1:5 million scale geological map of Africa and quantitative information from the national hydrogeological maps and the georeferenced aquifer studies for aquifer productivity. For each of the aquifer flow/storage types an effective porosity range was assigned based on a series of case studies across Africa and surrogates in other parts of the world. A total of 283 aquifer datasets were compiled from 152 aquifer studies identified from various literature. Good quality hydrogeological maps and studies were available for most of southern Africa. To estimate groundwater storage the saturated aquifer thickness was multiplied by effective porosity. Estimates of the total volume groundwater per country were produced and these were also represented as water depth.

There is some correlation between the groundwater storage map especially countries like Malawi, Madagascar, Zimbabwe, Tanzania Zambia and Namibia have low groundwater volumes and on the groundwater drought risk map the areas most prone to groundwater drought are in these

countries. The DRC has low groundwater drought risk and large groundwater volumes as indicated in data from MacDonald et al. 2012

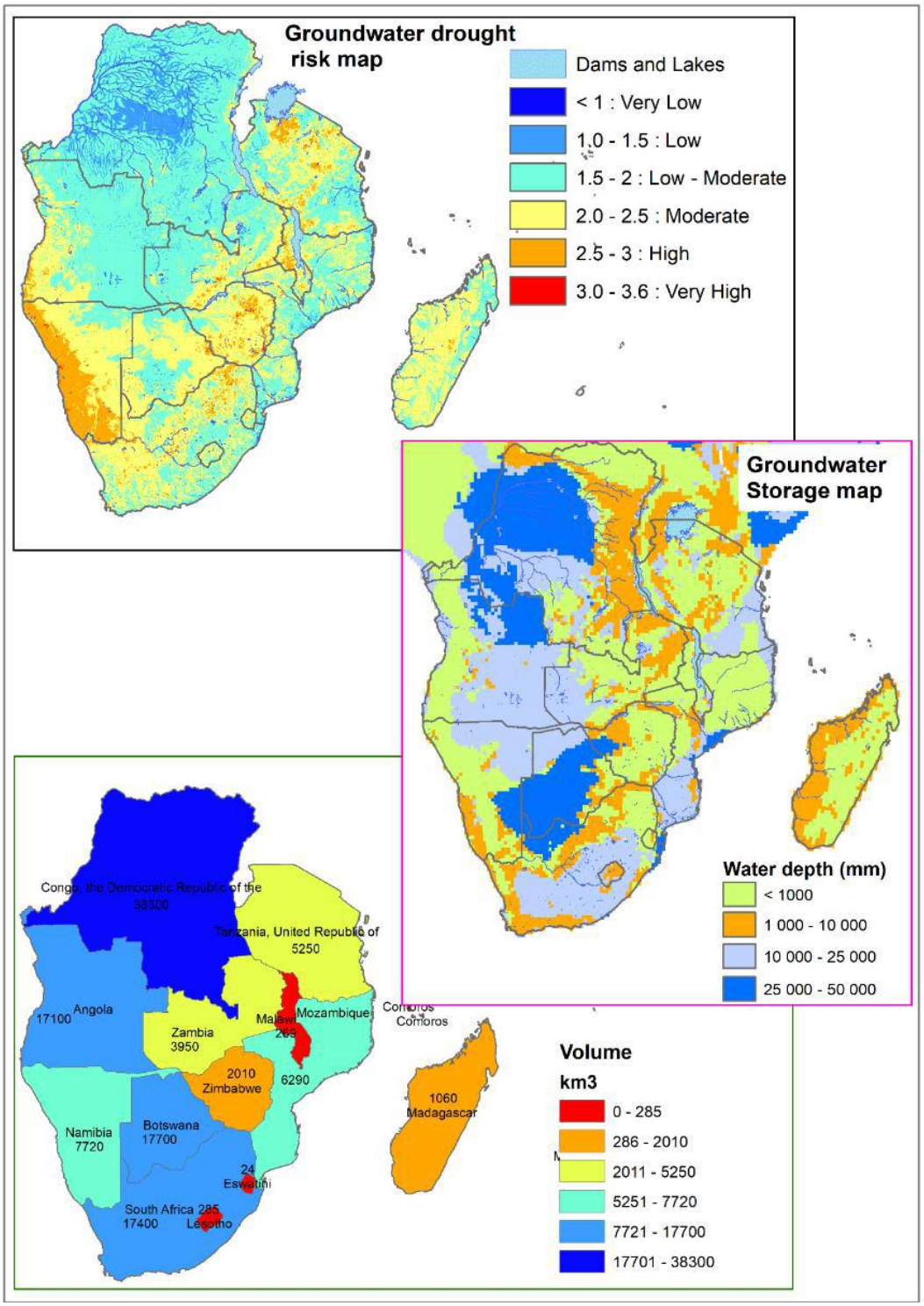

Figure 5-2: **British Geological Survey groundwater storage maps for Africa compared to the groundwater drought risk map (MacDonald et al 2012)**

Indices like the Standardized Precipitation Index (SPI) can be used to assess drought and therefore validate the groundwater drought risk map. The SPI is the most used indicator worldwide, and in 2009, WMO recommended SPI as the main meteorological drought index that countries should use to monitor and follow drought conditions (Hayes *et al* 2011). The SPI indicator, which was developed by Mckee *et al* (1993), and described in detail by Edwards and Mckee (1997), measures precipitation anomalies at a given location, based on a comparison of observed total precipitation amounts for an accumulation period of interest (e.g. 1, 3, 12, 24, up to 72 months), with the long-term historic rainfall record for that period. Statistically Guttman (1994) determined that the SPI from 1-24 months is the best practical range for 50-60 years of data. Beyond 24 months, 80-100 years data is required. If SPI is calculated on less than 30 years of data, the sample size is smaller and the confidence in the result is weaker. For hydrogeological drought analysis, 6 – 24 months SPI should be considered.

The historic record is fitted to a probability distribution (the "gamma" distribution), which is then transformed into a normal distribution such that the mean SPI value for that location and period is zero. For any given region, increasingly severe rainfall deficits (i.e., meteorological droughts) are indicated as SPI decreases below –1.0, while increasingly severe excess rainfall are indicated as SPI increases above 1.0. The advantages of SPI are that it is easy to calculate, can be calculated at multiple timescales and enables comparison of data from different climates (WMO 2012). The standardised classes for SPI are as shown in Table 5-1:

Table 5-1: SPI values and their classification

SPI values	Classification
>=2	Extremely wet
1.50 to 1.99	Severely wet
1.00 to 1.49	Moderately wet
-0.99 to 0.99	Near normal
-1.00 to -1.49	Moderately drought
-1.5 to -1.99	Severely drought
<=-2	Extreme drought

The has been the development of groundwater drought indices for groundwater drought analyses and some examples are:

- The Standard Water-Level Index (SWI), applied by Bhuiyan (n.d.) in India
- The Standard groundwater Index (SGI), similar to SPI but derived from groundwater level data (Bloomfield and Marchant 2013)

The discussion of the derivation and application of these indicators is beyond the scope of this project but can be investigated in follow up work or on site-specific studies.

There are various studies in literature that correlate the SPI to the groundwater level data or SGI and use the relationships to assess and monitor groundwater drought and some examples are listed below:

- Leelaruban *et al* (2017) studied 32 boreholes in the United States and correlated the water levels to various drought indices. The results showed good correlation between groundwater levels and 24 months SPI had the highest correlation with the data with correlation coefficients of - 0.6 (moderate) or higher
- Liu et al 2016 conducted a study in which they correlated the 1 to 12 months SPI and SGI of boreholes in China with varying results in different boreholes and regions in the study area. Moderate correlation values of between 0.5 and 0.6 were obtained and the results showed clear discrepancies between the SGI and the SPI.
- Kubicz (2018), in the study of German and Dutch boreholes, also found low correlation between SGI and 24 months SPI in some boreholes with the correlation coefficients ranging from 0.17-0.3
- Kubicz and Bąk (2019) studied boreholes in Poland and analysed data from 1981-2015 and found low correlation values between monthly average groundwater level and 24 months SPI
- Bloomfield and Marchant (2013) were more successful in establishing relationships between SPI and SGI after analysed wells in the UK with 29 years records of data, high correlations coefficient for 0.7-0.87 were obtained
- Meyer (2005) conducted a study in South Africa in which groundwater levels were compared with SPI calculated from rainfall data. The boreholes used are shown in Figure 5-3. The study revealed good correlation between the time-series SPI and groundwater level data

The overall conclusions from these studies was that the low level of the correlation coefficient did not imply the lack of correlation but rather indicates that other factors besides precipitation influence groundwater drought. Bloomfield and Marchant (2013) and Van Loon (2015), indicated that the lack of a linear relationship between meteorological drought and groundwater drought is usually because both droughts are delayed.

Bloomfield and Marchant (2013); Chamanpira *et al* (2014); Kumar *et al* (2016) acknowledged that groundwater level and SGI time-series data are influenced by local recharge processes and regional to site specific saturated process. Khan *et al* (2008); Whittemore *et al* (2016) suggested

that relationships between SPI and the level of groundwater depend primarily on location in the hydrodynamic system, rainfall shortages, and groundwater exploitation accounting for economic purposes, in this case for irrigation of fields

For validation of the groundwater drought risk map in this study, the idea was correlate the SPI data with long-term groundwater level data and characterise the drought at these locations. The challenge was the availability of long-term time-series groundwater level data covering the whole SADC region. The only data available for validation was the data from Cuthbert *et al* (2019) (see Figure 5-3). Groundwater anomalies were correlated with SPI calculated from CHIRPS version 2 monthly rainfall data for the years 1981-2019. 1-12 months and 18- and 24-months SPI values were calculated using the SPI Generator software (University of Nebraska 2020). The software also output information on identified droughts at various thresholds, drought duration, peak values and frequency of the SPI values. This is a lot of information and an in-depth analysis is beyond the scope of this study. The study will only highlight the aspects pertinent to the validation of the GDR map. The SPI values were correlated with groundwater level anomalies.

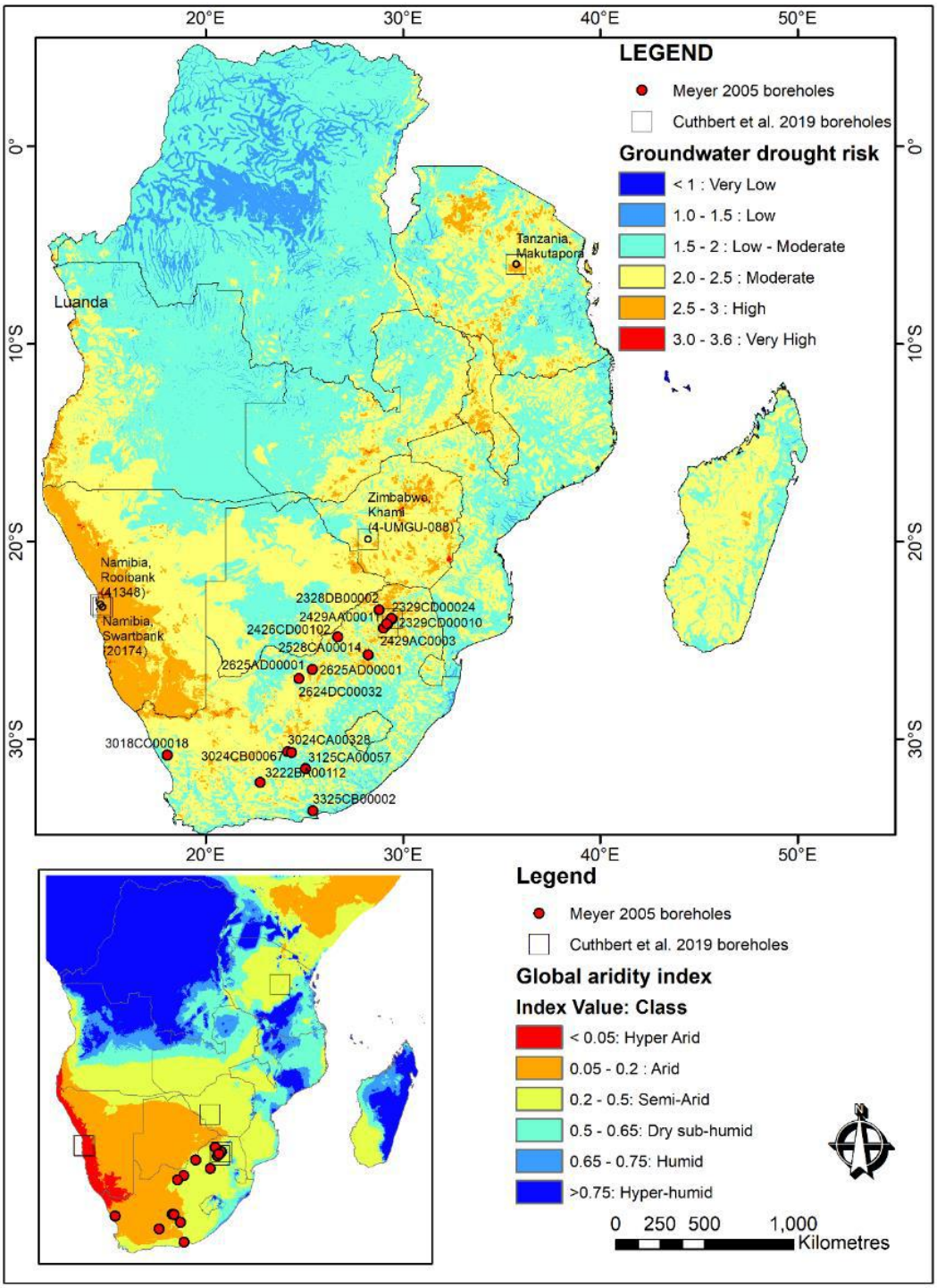

Figure 5-3: **Boreholes from Cuthbert et al. 2019 and Meyer 2005 overlaid on the groundwater drought risk map and the aridity index**

Table 5-2 list the boreholes used in analysis, the dates and number of records assessed and the correlation coefficient values obtained at the 9, 12, 18- and 24-months accumulation level. WMO (2012) recommends 1-2 month SPI for meteorological drought, 1-6 month for agricultural drought

and 6-24 month SPI for hydrological drought analyses (Lloyd-Hughes and Saunders 2002, Leelaruban *et al* 2017, Kubicz and Bąk 2019).

Table 5-2: The boreholes, groundwater level anomaly data statistics and the correlation to various SPI levels

	Namibia (Rooibank)	Namibia (Swartbank)	Zimbabwe (Khami)	South Africa (Sterkloop)	South Africa (Modderfontein)	Tanzania (Makutapora)
GWL anomaly data	1999-2017	1975-2016	1989-2015	1973-2016	1968-2017	1955-2016
GWL anomaly number of records	60	86	211	6090	76414	522
6-month SPI correlation	-0.38	0.04	0.31	0.43	-0.17	-0.09
7-month SPI correlation	-0.41	0.10	0.36	0.47	-0.17	-0.05
8-month SPI correlation	-0.38	0.08	0.43	0.52	-0.17	-0.04
9-month SPI correlation	-0.36	0.10	0.50	0.54	-0.18	-0.03
10-month SPI correlation	-0.36	0.15	0.57	0.56	-0.18	-0.03
11-month SPI correlation	-0.38	0.14	0.60	0.58	-0.16	0
12-month SPI correlation	-0.36	0.16	0.60	0.61	-0.14	0.02
18-month SPI correlation	-0.32	0.28	0.61	0.64	-0.04	0.06
24-month SPI correlation	-0.30	0.33	0.59	0.67	0	0.06

There were low correlation values between the SPI products and the groundwater anomaly data as shown in Table 5-2. There was mixed result obtained with the Zimbabwe (Khama) and the South Africa (Sterkloop) boreholes showing the highest and moderate correlation to SPI. The lowest correlation was obtained for the Tanzania (Makutapora) borehole. Various authors have ascertained that this low correlation does not imply no correlation but rather indicates that other factors besides precipitation influences groundwater drought, e.g. local aquifer characteristics and groundwater abstraction. It could well be that there are not enough rainfall data (39 years of data) and there are a few records for some of the boreholes.

Despite this low correlation, there were some trends that could be identified from the results. Drought periods identified for all boreholes with the 1-month SPI correlated with independent

data on the droughts that have been experienced in the countries (EM-DAT 2009, Masih *et al* 2014) (Figure 5-4 and Table 5-3).

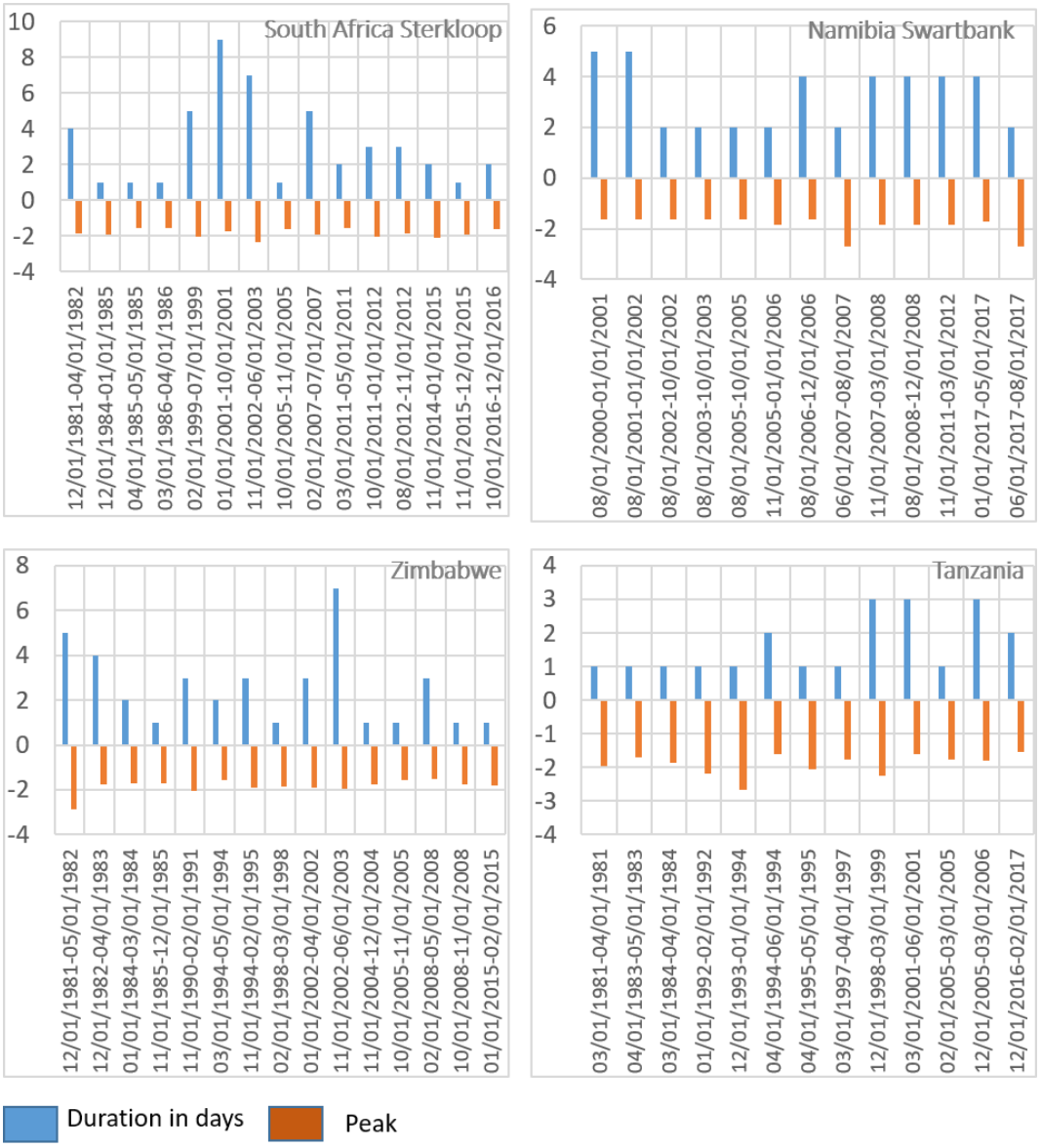

Figure 5-4: **1 month SPI droughts for the boreholes and their durations and peak values**

Table 5-3: Droughts experienced in the different countries

Country	Drought years
Angola	1981, 1985, 1989, 1997, 2001, 2004, 2012
Botswana	1965, 1968, 1970, 1981-1984, 1984-1985, 1987-1988, 1991-1993, 1990, 2005
Democratic Republic of Congo	1978, 1983
Comoros	1981
Lesotho	1968, 1983, 1990, 1991-1993, 2002-2003, 2007, 2011
Madagascar	1981, 1988, 2000, 2002, 2005, 2008
Mozambique	1979, 1981, 1984-1985, 1987, 1990, 1998, 2001, 2003, 2005, 2007, 2008, 2010
Mauritius	1999
Malawi	1987-1988, 1990, 1991-1993, 1992, 2002, 2005-2006, 2007, 2012
Namibia	1981, 1990, 1991-1993, 1995, 1998, 2001, 2002-2003, 2013
Eswatini	1981, 1984, 1990, 2001, 2007
Tanzania	1967, 1977, 1984-1985, 1988, 1990, 1996, 1997-2000, 2002-2003, 2004, 2006, 2011
South Africa	1964, 1980, 1981, 1986, 1988, 1990,1991-1993, 1995, 2004
Zambia	1981, 1983, 1990, 1995, 2005-2006
Zimbabwe	1981, 1984-1985, 1990, 1991-1993, 1998, 2001, 2002-2003, 2007, 2008-2009, 2010

Figures 5-5 to 5-9 show the graphs of SPI and groundwater anomalies at the boreholes analysed. The values of groundwater drought risk at these locations are:

- 2.84 (high) at the Namibia Rooibank site
- 2.75 (high) at South Africa Sterkloop
- 2.71 (high) at Namibia Swartbank
- 2.46 (moderate) at South Africa Modderfontein
- 2.41 (moderate) at Zimbabwe Khama
- 2.31 (moderate) at Tanzania
- 1.66 (low) at 3024CA00328 South Africa

Borehole 3024CA00328 was analysed in a separate study by Meyer (2005), correlating a groundwater water level record of more than 40 years near De Aar with the associated SPI (Figure 5-5). The correlation between the two datasets over the entire record period was good and both the larger and smaller anomalies (amplitude and duration) correlated well.

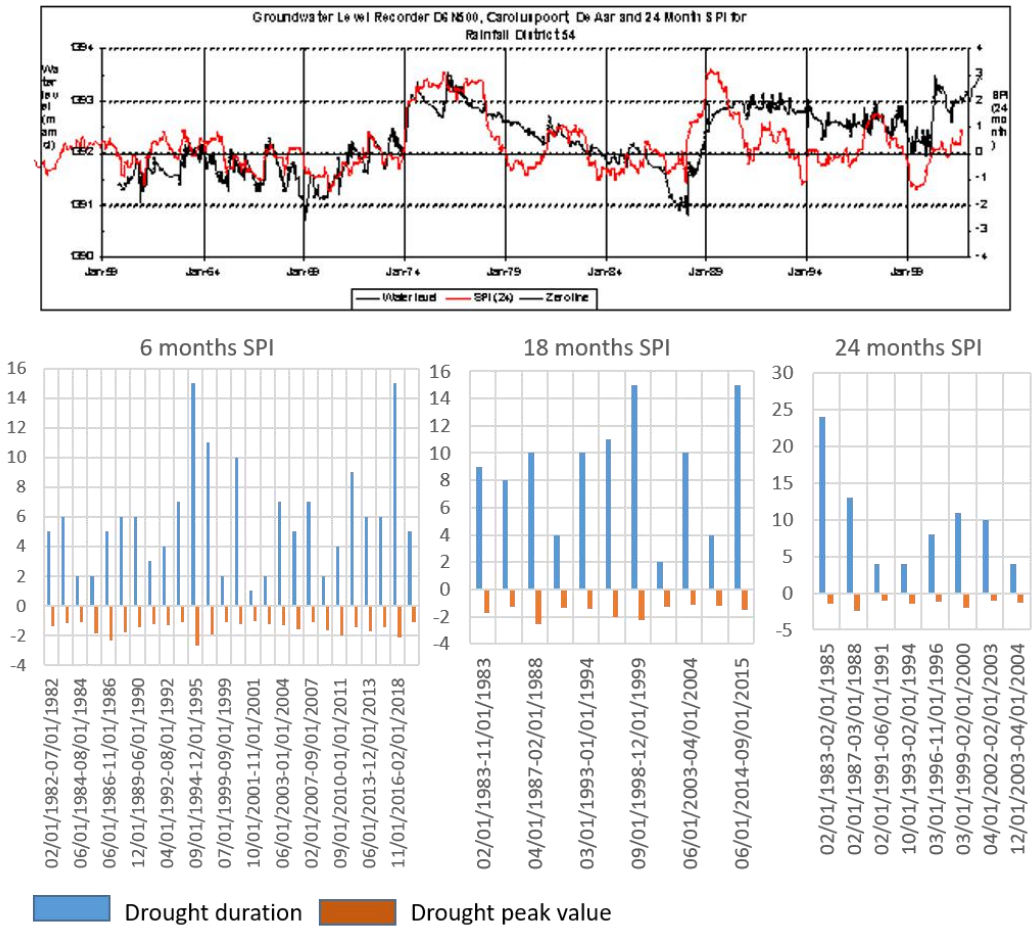

Figure 5-5: **3024CA borehole groundwater level graph and 24 month SPI at the top and the drought graphs at the bottom.**

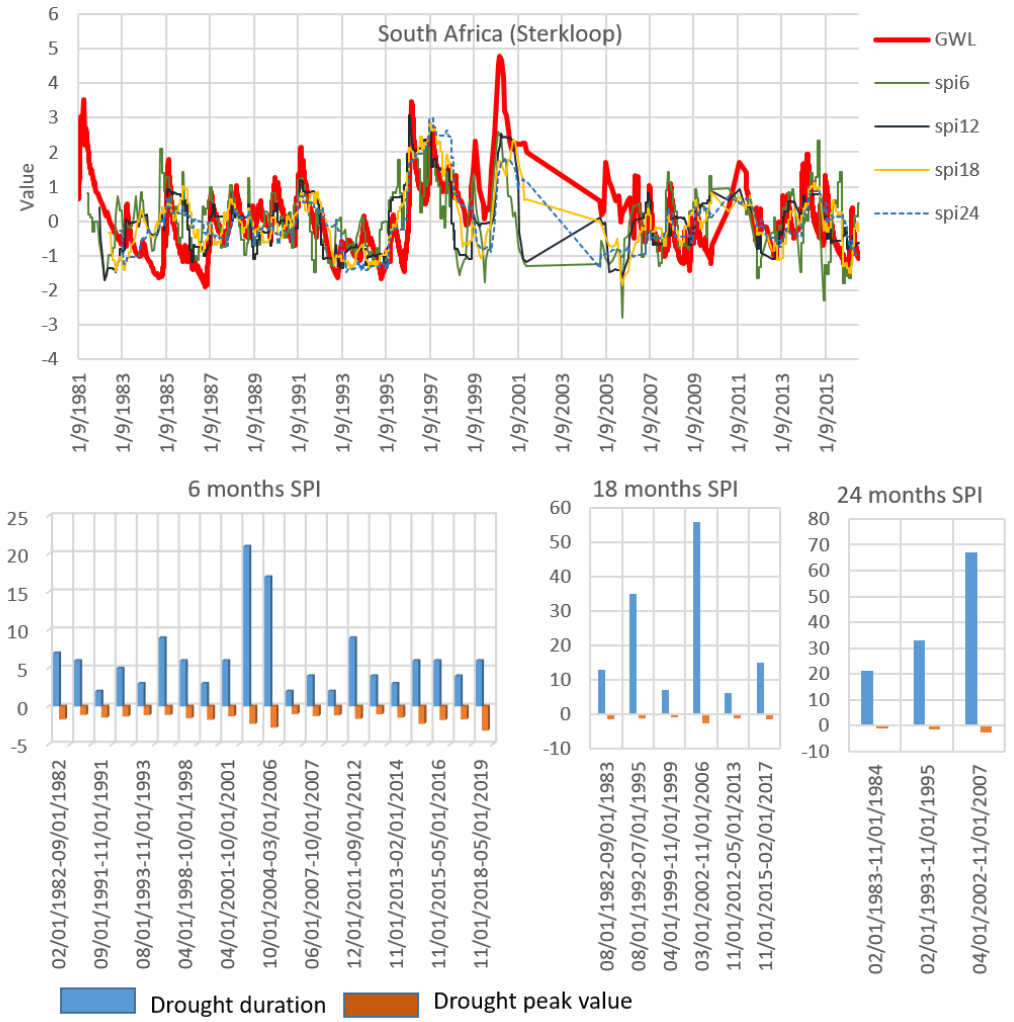

Figure 5-6: **South Africa (Sterkloop) borehole groundwater level anomalies and SPI plots at the top and the SPI drought graphs at the bottom**

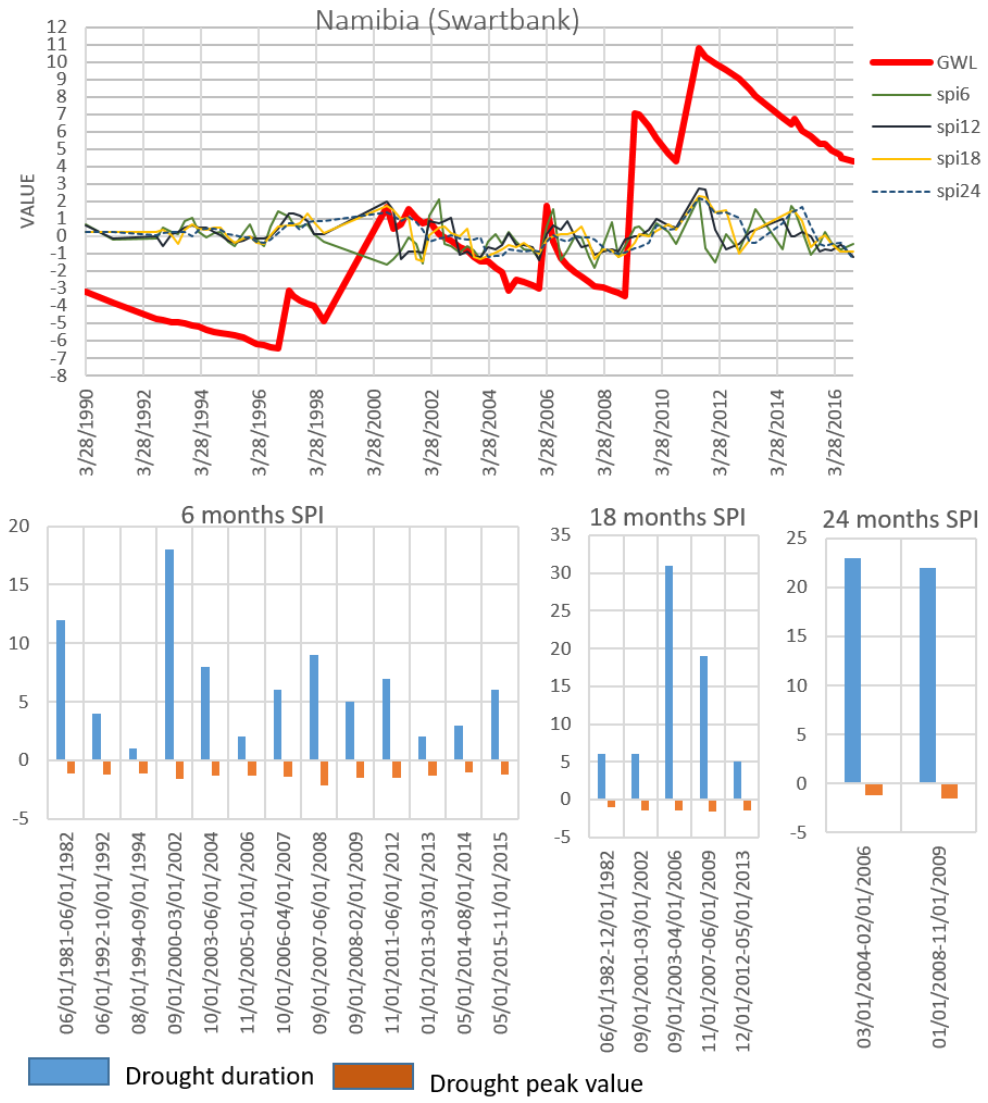

Figure 5-7: **Namibia (Swartbank) borehole groundwater well anomalies and SPI plots at the top and the SPI drought graphs at the bottom.**

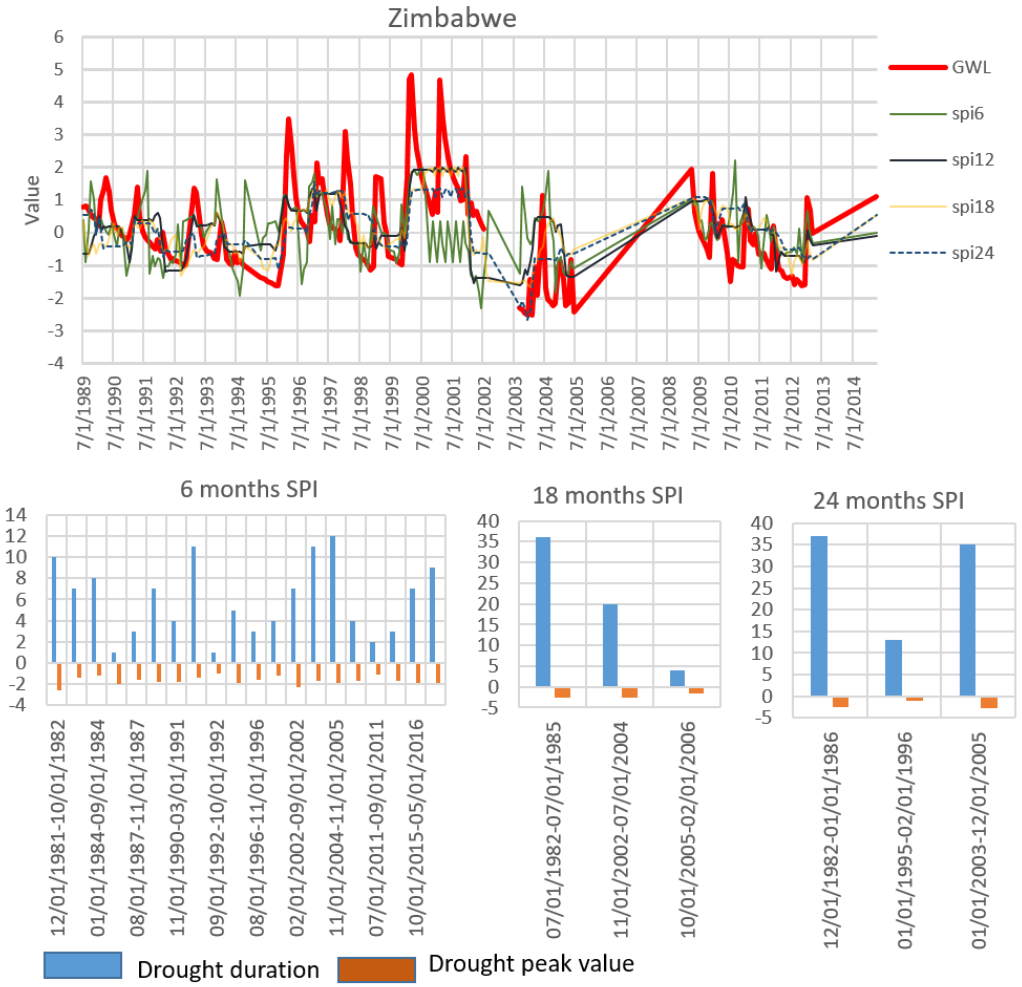

Figure 5-8: **Zimbabwe (Khami) borehole groundwater well anomalies and SPI plots at the top and the SPI drought graphs at the bottom**

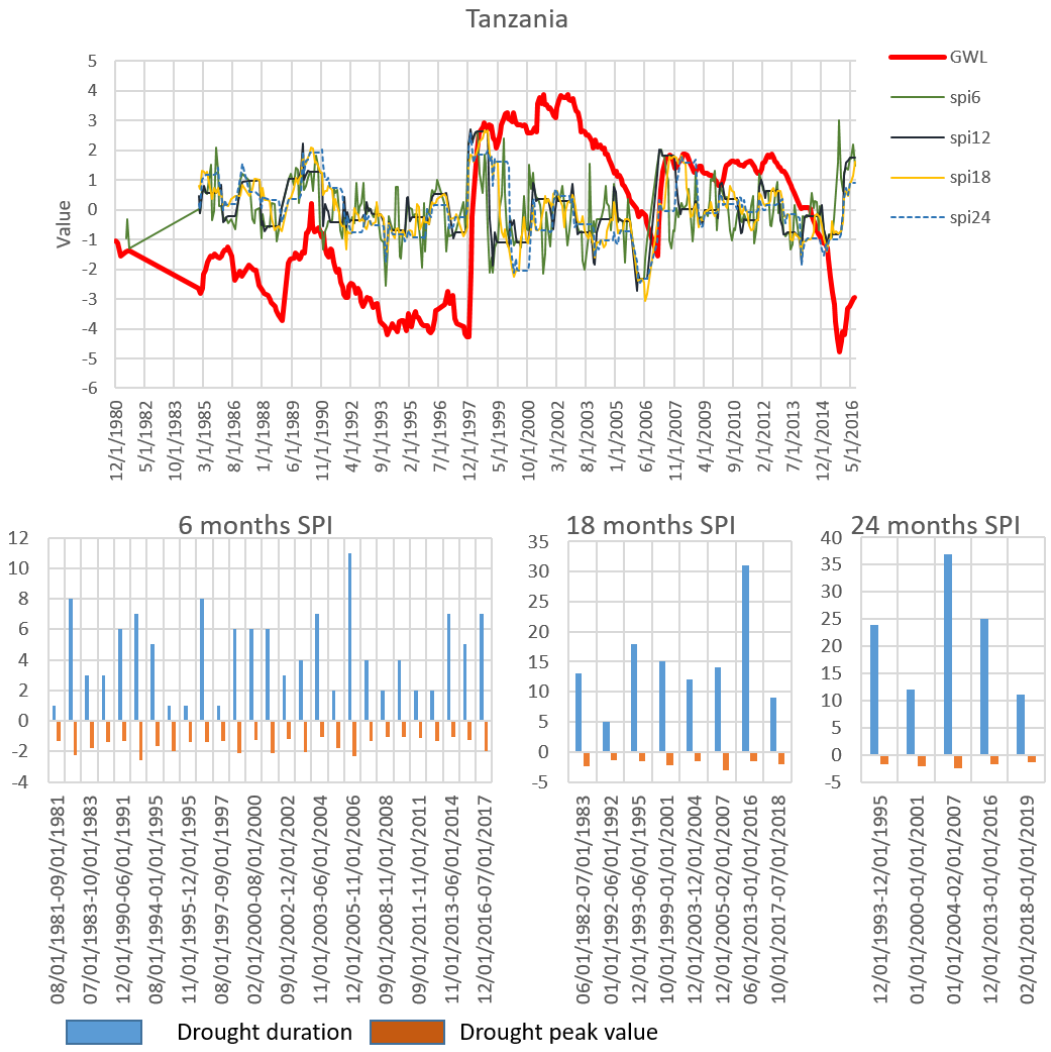

Figure 5-9: **Tanzania (Makutapora) borehole groundwater well anomalies and SPI plots at the top and the drought graphs at the bottom.**

The only aspect of the graphs that can be linked to groundwater drought risk are the fluctuations in the values of both the groundwater level anomalies and the SPI. Meyer (2005) found that in boreholes were groundwater levels follow even the small variations in SPI values, it is an indication that at least some groundwater recharge occurs during almost every year. In borehole 3024CA00328, a low groundwater drought risk location, the graphs follow this trend. In boreholes the high-moderate drought risk areas, especially Namibia, Zimbabwe and Tanzania, the groundwater levels decline for long periods of time before recovery. Meyer (2005) noted this trend in some boreholes, of long declining levels, in some cases up to 25 years and these periods are then terminated by abrupt rises or return of the groundwater levels to the original reference level, or sometimes even higher. Depending on the intensity and duration of the rainfall event or the period over which above average rainfall is recorded, this return of the groundwater level occurs within months after the onset of the rainfall event.

This was confirmed by Cuthbert *et al* (2019), who assessed the relationships between precipitation and recharge across a diverse range of climatic and geological contexts in sub-Saharan Africa, using groundwater-level time series data. Cuthbert *et al* (2019) concluded that in arid areas there are large groundwater response times and this phenomenon is evident in the groundwater level anomaly graphs at the locations in Namibia, Tanzania and Zimbabwe. Episodic or infrequent recharge occurring during a few seasons or years in a decade is prevalent in these environments. The greatest recharge can occur during years of relatively low total precipitation because of intense precipitation occurring over a range of timescales depending on the local conditions of soils, geology and rainfall intensity. Cuthbert *et al* (2019) also noted that groundwater in some currently hyper-arid regions was recharged when a wetter climatic regime prevailed in the past and this was referred to as having 'palaeo' recharge frequency.

6. CONCLUSIONS

The GRiMMS algorithm is a GIS based approach that involves the weighting of parameters and adding them to get a groundwater drought risk map. The GRiMMS algorithm was updated and revised by the inclusion of a groundwater storage sensitivity module, which incorporates GRACE satellite imagery groundwater drought indices. The groundwater drought risk map is generated for regional analysis and it should be used with caution on more site-specific studies. This is due to the low resolutions of the data used at that scale and also the generalisations that do not take into account local conditions as well as the loss of detail, information and generalisations when the data is grouped into classes. The algorithm is also applicable to small scale analysis but more detailed data can be used to refine the results.

GRACE is a novel application of measuring Earth's gravitation field to characterize terrestrial water storage changes on a regional scale. GRACE data provide an opportunity to include regional groundwater storage information into the GRiMMS algorithm. Here the major challenges include defining a set of unique factors representing groundwater storage drought, as well as resolving the resolution mismatch between the GRACE data and the GRiMMS algorithm. To define a set of representative groundwater storage drought factors the GGDI approach is used to define the percentage negative GGDI, the mean negative GGDI, and the linear trend in the GGDI. Together these factors were combined as the groundwater storage risk module. This module describes the sensitivity of groundwater storage to drought conditions. The map derived from groundwater storage risk illustrate spatial distributions of varying groundwater storage risk, with the main high groundwater storage risk area underlain by parts of southern Mozambique, Zimbabwe, Malawi, Northern Angola, and parts of the Namibian coast. The scale mismatch was addressed using linear interpolation approach resampling the GGDI factors from ~25km to 5km. An attempt was made to resolved resolution issues by downscaling of the GRACE data. However, this process yielded inconsistent results. While the scale of GRACE data is better suited for regional scale analysis, an attempt was made to ground truth the GRACE GWS data and the GGDI using groundwater level time-series data. Overall, the GRACE GWS data show a poor correlation with groundwater level anomalies. While the GGDI did show an overall better correlation, it still does not fully mimic trends in the local groundwater level data. It must be noted that resolving the scale mismatch between GRACE data and local scale conditions is an ongoing process in the literature.

The major challenge with this GIS approach is justifying or selecting the weightings assigned to the parameters. Groundwater drought risk is not an observable phenomenon so there is no "measured data" from which to estimate these weights. Sensitivity analysis was used to assess the differences in the groundwater drought risk maps as the weights of the various parameters were varied. Five scenario maps were created and the results were analysed using image

differencing to compare a pair of scenarios at a time and nothing how the pixels change class value from one map to the next. The associated uncertainty due to weighting variations were also presented using a coefficient of variation map generated from the five maps. The results from the coefficient of variation map showed that most areas with high to very high groundwater drought risk are not sensitive to changes in the weighting of parameters. Although a limited number of scenarios were tested, this initial finding shows that these areas will be highlighted as high risk regardless of the weightings applied. This needs to be verified with more detailed data at more localised scales.

Bayesian Networks have been introduced as a tool for doing scenario analysis. The Network learns patterns from the data (or expert knowledge in the absence of measured data) and these are presented graphically as percentage probabilities. Any node on the network can be queried and the effects of the changes are propagated throughout the network and this query computation is done rapidly. Bayesian Networks are applicable at any spatial level of analysis are useful in scenario analysis for example accessing the effect of climate change scenarios on the groundwater drought risk and other related parameters. This tool can be investigated further in follow up work.

Validation of the model is also a crucial aspect to ensure that it is a representative of reality. Validation can be conducted on the entire model or on separate aspects but preferably using measured data. In the absence of measured data, results from independent studies or expert knowledge can be used for validation of the maps. In the report, different aspects of the GRiMMS algorithm were validated using independent datasets. For example, the groundwater recharge potential map was validated using a global recharge data from various aquifer studies compiled by Moeck *et al* (2020) and some moderate correlation was obtained between the datasets. These results should be used with caution due to the distribution of data, which did not cover most parts of the study. More data is needed to verify these results, especially from boreholes in the humid climates; there were no boreholes with long groundwater level time series records.

The groundwater drought risk map was validated using the groundwater storage maps produced by Macdonald et al 2012. There was some agreement between the two maps as the countries of low groundwater volumes identified in Macdonald et al 2012 where the countries with areas with high to very high groundwater drought risk throughout the region.

The drought risk map was also validated using data by comparing groundwater level anomaly data with the SPI products derived from rainfall data for boreholes in South Africa, Namibia, Zimbabwe and Tanzania. There were low correlation values between the SPI products and the groundwater anomaly data. Despite this low correlation, there were some trends that could be identified from

the results drought areas identified using SPI products could be linked to declining groundwater levels. Groundwater drought risk could be associated to the shape of the groundwater level graphs. In high drought risk areas, there are long declining levels, which are then terminated by abrupt rises or return of the groundwater levels to the original reference level, or sometimes even higher, depending on the intensity and duration of the rainfall event. In low drought risk areas, the groundwater level curves tend to follow even small variations in SPI, showing some groundwater recharge occurs during almost every year. This was supported with studies by Meyer (2005) and Cuthbert *et al* (2019) which were conducted on a small dataset. The challenge is finding a lot of boreholes with a long groundwater level record.

Several aspects of the GRiMMS algorithm that were not addressed in this report include the inclusion of human capacity aspect of the human groundwater drought vulnerability and groundwater threats to compute the groundwater insecurity map. These would be addressed in the next phase of the project, where more localised analysis will be conducted. This was done as the datasets that constitute these models, e.g. groundwater intensive use and groundwater quality are only available at a local scale and in certain areas and cannot therefore be applied at a regional scale

7. REFERENCES

Adams S, Titus R and Xu Y 2004 *Groundwater recharge assessment of the basement aquifers of Central Namaqualand* (Pretoria, South Africa) Online: http://www.wrc.org.za/wp-content/uploads/mdocs/1093-1-041.pdf

Aquino C M S and Oliveira J G B 2012 Estudo da dinâmica do Índice de Vegetacão por Diferença Normalizada (NDVI) no núcleo de São Raimundo Nonato-PI *GEOUSP - Espaço e Tempo* **1** 157–68 Online: http://www.revistas.usp.br/geousp/article/view/74261

Aziz A, Umar M, Mansha M, Khan M S, Javed M N, Gao H, Farhan S Bin, Iqbal I and Abdullah S 2018 Assessment of drought conditions using HJ-1A/1B data: a case study of Potohar region, Pakistan *Geomatics, Nat. Hazards Risk* **9** 1019–36 Online: https://www.tandfonline.com/doi/full/10.1080/19475705.2018.1499558

Bhuiyan C *Various Drought Indices For Monitoring Drought Condition In Aravalli Terrain Of India*

Bloomfield J P and Marchant B P 2013 Analysis of groundwater drought building on the standardised precipitation index approach *Hydrol. Earth Syst. Sci.* **17** 4769–87

Chamanpira G, Zehtabian G, Ahmadi H and Malekian A 2014 *Effect of Drought on Groundwater Resources; a Study to Optimize Utilization Management (Case Study: Alashtar Plain)* vol 3

Chen Y, Yu J, Shahbaz K and Xevi E 2009 A GIS-Based Sensitivity Analysis of Multi-Criteria Weights *18 th World IMACS / MODSIM Congress* (Cairns, Australia) pp 13–7 Online: http://citeseerx.ist.psu.edu/viewdoc/download?doi=10.1.1.584.2948&rep=rep1&type=pdf

Cheng M and Tapley B D 2004 Variations in the Earth's oblateness during the past 28 years *J. Geophys. Res. Solid Earth* **109** Online: https://agupubs.onlinelibrary.wiley.com/doi/full/10.1029/2004JB003028

CIESIN 2016 *Gridded Population of the World, Version 4 (GPWv4)* Online: https://sedac.ciesin.columbia.edu/data/collection/gpw-v4/documentation

Cleveland R, Cleveland W, McRae J and Terpenning I 1990 A seasonal-trend decomposition procedure based on Loess *J. Off. Stat.* **6** 3–73 Online: https://www.wessa.net/download/stl.pdf

da Costa A M, de Salis H H C, Viana J H M and Pacheco F A L 2019 Groundwater recharge potential for sustainable water use in urban areas of the Jequitiba River Basin, Brazil *Sustain.* **11**

Cowell R ., Dawid P, Lauritzen S . and Spiegelhalter D . 1999 *Probabilistic Networks and Expert Systems* (Springer-Verlag)

Cuthbert M O, Taylor R G, Favreau G, Todd M C, Shamsudduha M, Villholth K G, MacDonald A M, Scanlon B R, Kotchoni D O V, Vouillamoz J-M, Lawson F M A, Adjomayi P A, Kashaigili J, Seddon D, Sorensen J P R, Ebrahim G Y, Owor M, Nyenje P M, Nazoumou Y, Goni I, Ousmane B I, Sibanda T, Ascott M J, Macdonald D M J, Agyekum W, Koussoubé Y, Wanke H, Kim H, Wada Y, Lo M-H, Oki T and Kukuric N 2019 Observed controls on resilience of groundwater to climate variability in sub-Saharan Africa *Nature* **572** 230–4 Online: http://www.nature.com/articles/s41586-019-1441-7

Didan K, Barreto Munoz A, Solano R and Huete A 2015 *MODIS Vegetation Index User's Guide (MOD13 Series)* Online: https://vip.arizona.edu/documents/MODIS/MODIS_VI_UsersGuide_June_2015_C6.pdf

Edwards D C and Mckee T B 1997 *Characteristics of 20th century drought in the United States at multiple time scales* (Colorado State University. Libraries) Online: https://mountainscholar.org/handle/10217/170176

EM-DAT 2009 The International Disaster Database Online: https://www.emdat.be/staff/debarati-guha-sapir

Van Engelen V W P and Dijkshoorn J A 2012 *Global and National Soils and Terrain Digital Databases (SOTER) Procedures Manual* (Wageningen, 2012) Online: http://www.isric.org

FAO 1989 *Arid zone forestry: A guide for field technicians* (Rome, Italy) Online: http://www.fao.org/3/t0122e/t0122e00.htm#Contents

FAO 1993 *Forest resources assessment 1990: Tropical countries* Online: http://www.fao.org/3/t0830e/T0830E00.htm

Frappart F and Ramillien G 2018 Monitoring groundwater storage changes using the Gravity Recovery and Climate Experiment (GRACE) satellite mission: A review *Remote Sens.* **10**

Funk C C, Peterson P J, Landsfeld M F, Pedreros D H, Verdin J P, Rowland J D, Romero B E, Husak G J, Michaelsen J C and Verdin A P 2014 *A quasi-global precipitation time series for drought monitoring: U.S. Geological Survey Data Series 832* Online: https://pubs.usgs.gov/ds/832/pdf/ds832.pdf%0Ahttps://pubs.er.usgs.gov/publication/ds832

Gilbert M, Nicolas G, Cinardi G, Van Boeckel T P, Vanwambeke S O, Wint G R W and Robinson T P 2018 Global distribution data for cattle, buffaloes, horses, sheep, goats, pigs, chickens and ducks in 2010 *Sci. Data* **5** 1–11 Online: www.nature.com/sdata/

Grandmont K, Cardille J A, Fortier D and Gibryen T 2012 Assessing land suitability for residential development in permafrost regions: A multi-criteria approach to land-use planning in northern Quebec, Canada *J. Environ. Assess. Policy Manag.* **14**

Guttman N B 1994 On the sensitivity of sample L moments to sample size *J. Clim.* **7** 1026–9 Online: http://journals.ametsoc.org/jcli/article-pdf/7/6/1026/4699470/1520-0442

Hagenlocher M, Meza I, Anderson C C, Min A, Renaud F G, Walz Y, Siebert S and Sebesvari Z 2019 Drought vulnerability and risk assessments: state of the art, persistent gaps, and research agenda *Environ. Res. Lett.* **14** Online: https://doi.org/10.1088/1748-9326/ab225d

Hayes M, Svoboda M, Wall N and Widhalm M 2011 The lincoln declaration on drought indices: Universal meteorological drought index recommended *Bulletin of the American Meteorological Society* vol 92 (American Meteorological Society) pp 485–8 Online: http://journals.ametsoc.org/bams/article-pdf/92/4/485/3738361/2010bams3103_1.pdf

Jakeman A J, Letcher R A and Norton J P 2006 Ten iterative steps in development and evaluation of environmental models *Environ. Model. Softw.* **21** 602–14 Online: www.elsevier.com/locate/envsoft

Khan S, Gabriel H F and Rana T 2008 Standard precipitation index to track drought and assess impact of rainfall on watertables in irrigation areas *Irrig. Drain. Syst.* **22** 159–77 Online: https://link.springer.com/article/10.1007/s10795-008-9049-3

Kubicz J 2018 The application of Standardized Precipitation Index (SPI) to monitor drought in surface and groundwaters *E3S Web of Conferences* vol 44 (EDP Sciences) p 00082 Online: https://doi.org/10.1051/e3sconf/20184400082

Kubicz J and Bąk B 2019 The reaction of groundwater to several months' meteorological drought in Poland *Polish J. Environ. Stud.* **28** 187–95

Kumar R, Musuuza J L, Van Loon A F, Teuling A J, Barthel R, Ten Broek J, Mai J, Samaniego L and Attinger S 2016 Multiscale evaluation of the Standardized Precipitation Index as a groundwater drought indicator *Hydrol. Earth Syst. Sci.* **20** 1117–31 Online: https://hess.copernicus.org/articles/20/1117/2016/

Landerer F W and Swenson S C 2012 Accuracy of scaled GRACE terrestrial water storage estimates *Water Resour. Res.* **48** Online: https://agupubs.onlinelibrary.wiley.com/doi/full/10.1029/2011WR011453

Leelaruban N, Padmanabhan G and Oduor P 2017 Examining the relationship between drought indices and groundwater levels *Water (Switzerland)* **9**

Lloyd-Hughes B and Saunders M A 2002 Seasonal prediction of European spring precipitation from El Niño-Southern Oscillation and Local sea-surface temperatures *Int. J. Climatol.* **22** 1–14 Online: http://doi.wiley.com/10.1002/joc.723

Van Loon A F 2015 Hydrological drought explained *Wiley Interdiscip. Rev. Water* **2** 359–92 Online: http://doi.wiley.com/10.1002/wat2.1085

MacDonald A M, Bonsor H C, Dochartaigh B É Ó and Taylor R G 2012 *Quantitative maps of groundwater resources in Africa* vol 7 (Institute of Physics Publishing)

Masih I, Maskey S, Mussá F E F and Trambauer P 2014 A review of droughts on the African continent: a geospatial and long-term perspective *Hydrol. Earth Syst. Sci.* **18** 3635–49 Online: https://hess.copernicus.org/articles/18/3635/2014/

Mckee T B, Doesken N J and Kleist J 1993 *The relationship of drought frequency and duration to time scales*

Meyer R 2005 *Analysis of groundwater level time series and the relation to rainfall and recharge* (Pretoria, South Africa)

Moeck C, Grech-Cumbo N, Podgorski J, Bretzler A, Gurdak J J, Berg M and Schirmer M 2020 A global-scale dataset of direct natural groundwater recharge rates: A review of variables, processes and relationships *Sci. Total Environ.* **717** 137042

Mogaji K A, Lim H S and Abdullah K 2015 Regional prediction of groundwater potential mapping in a multifaceted geology terrain using GIS-based Dempster–Shafer model *Arab. J. Geosci.* **8** 3235–58 Online: https://link.springer.com/article/10.1007/s12517-014-1391-1

Mohan C, Western A W, Wei Y and Saft M 2018 Predicting groundwater recharge for varying land cover and climate conditions-a global meta-study *Hydrol. Earth Syst. Sci* **22** 2689–703 Online: https://doi.org/10.5194/hess-22-2689-2018

National Park Service 2019 Arid and Semi-arid Region Landforms Online: https://www.nps.gov/subjects/geology/arid-landforms.htm

Ó Dochartaigh B, Doce D D, Rutter H K and MacDonald A M 2011 *User Guide: Aquifer Productivity (Scotland) GIS datasets, Version 2* Online: www.bgs.ac.uk/gsni/

Quinn B, Schiel K and Caruso G 2015 Mapping uncertainty from multi-criteria analysis of land development suitability, the case of Howth, Dublin *J. Maps* **11** 487–95 Online: https://www.tandfonline.com/doi/full/10.1080/17445647.2014.978907

Robinson T P, Wint G R W, Conchedda G, Van Boeckel T P, Ercoli V, Palamara E, Cinardi G, D'Aietti L, Hay S I and Gilbert M 2014 Mapping the Global Distribution of Livestock ed M Baylis *PLoS One* **9** e96084 Online: https://dx.plos.org/10.1371/journal.pone.0096084

Rodell M, Chen J, Kato H, Famiglietti J S, Nigro J and Wilson C R 2007 Estimating groundwater storage changes in the Mississippi River basin (USA) using GRACE *Hydrogeol. J.* **15** 159–66 Online: https://escholarship.org/uc/item/1qs6s67c

Rodell M, Famiglietti J S, Wiese D N, Reager J T, Beaudoing H K, Landerer F W and Lo M H 2018 Emerging trends in global freshwater availability *Nature* **557** 651–9 Online: https://pubmed.ncbi.nlm.nih.gov/29769728/

Rodell M, Houser P R, Jambor U, Gottschalck J, Mitchell K, Meng C J, Arsenault K, Cosgrove B, Radakovich J, Bosilovich M, Entin J K, Walker J P, Lohmann D and Toll D 2004 The Global Land Data Assimilation System *Bull. Am. Meteorol. Soc.* **85** 381–94 Online: http://journals.ametsoc.org/bams/article-pdf/85/3/381/3734956/bams-85-3-381.pdf

SADC 2010 *Explanatory Brochure for the South African Development Community (SADC) Hydrogeological Map & Atlas* (Gaborone, Botswana)

SADC 2011 *SADC Regional Groundwater Drought Vulnerability Mapping* (Gaborone, Botswana) Online: https://www.un-igrac.org/sites/default/files/resources/files/SADC Regional Groundwater Drought Risk Mapping.pdf

Sakumura C, Bettadpur S and Bruinsma S 2014 Ensemble prediction and intercomparison analysis of GRACE time-variable gravity field models *Geophys. Res. Lett.* **41** 1389–97 Online: https://agupubs.onlinelibrary.wiley.com/doi/full/10.1002/2013GL058632

Save H, Bettadpur S and Tapley B D 2016 High-resolution CSR GRACE RL05 mascons *J. Geophys. Res. Solid Earth* **121** 7547–69 Online: https://agupubs.onlinelibrary.wiley.com/doi/full/10.1002/2016JB013007

Siebert S, Burke J, Faures J M, Frenken K, Hoogeveen J, Döll P and Portmann F T 2010 Groundwater use for irrigation – a global inventory *Hydrol. Earth Syst. Sci.* **14** 1863–80 Online: https://hess.copernicus.org/articles/14/1863/2010/

Singh L and Saravanan S 2020 Satellite-derived GRACE groundwater storage variation in complex aquifer system in India *Sustain. Water Resour. Manag.* **6** 43 Online: https://doi.org/10.1007/s40899-020-00399-3

Swenson S, Chambers D and Wahr J 2008 Estimating geocenter variations from a combination of GRACE and ocean model output *J. Geophys. Res. Solid Earth* **113** Online: https://agupubs.onlinelibrary.wiley.com/doi/full/10.1029/2007JB005338

Swenson S and Wahr J 2006 Post-processing removal of correlated errors in GRACE data *Geophys. Res. Lett.* **33** Online: https://agupubs.onlinelibrary.wiley.com/doi/full/10.1029/2005GL025285

Thapa R, Gupta S, Guin S and Kaur H 2018 Sensitivity analysis and mapping the potential groundwater vulnerability zones in Birbhum district, India: A comparative approach between vulnerability models *Water Sci.* **32** 44–66

Thomas B F, Famiglietti J S, Landerer F W, Wiese D N, Molotch N P and Argus D F 2017 GRACE Groundwater Drought Index: Evaluation of California Central Valley groundwater drought *Remote Sens. Environ.* **198** 384–92 Online: http://dx.doi.org/10.1016/j.rse.2017.06.026

Trabucco A and Zomer R J 2018 *Global Aridity Index and Potential Evapotranspiration (ET0) Climate Database v2* Online: https://cgiarcsi.community/2019/01/24/global-aridity-index-and-potential-evapotranspiration-climate-database-v2/

UNEP 1997 *World atlas of desertification* Online: https://digitallibrary.un.org/record/245955?ln=en

University of Nebraska 2020 SPI Program Online: https://drought.unl.edu/droughtmonitoring/SPI/SPIProgram.aspx

Villholth K G, Tøttrup C, Stendel M and Maherry A 2013 Integrated mapping of groundwater drought risk in the Southern African Development Community (SADC) region *Hydrogeol. J.* **21** 863–85

Wahr J, Molenaar M and Bryan F 1998 Time variability of the Earth's gravity field: Hydrological and oceanic effects and their possible detection using GRACE *J. Geophys. Res. Solid Earth* **103** 30205–29 Online: https://agupubs.onlinelibrary.wiley.com/doi/full/10.1029/98JB02844

Watkins M M, Wiese D N, Yuan D N, Boening C and Landerer F W 2015 Improved methods for observing Earth's time variable mass distribution with GRACE using spherical cap mascons *J. Geophys. Res. Solid Earth* **120** 2648–71 Online: https://agupubs.onlinelibrary.wiley.com/doi/full/10.1002/2014JB011547

Whittemore D O, Butler J J and Wilson B B 2016 Assessing the major drivers of water-level declines: new insights into the future of heavily stressed aquifers *Hydrol. Sci. J.* **61** 134–45 Online: http://www.tandfonline.com/doi/full/10.1080/02626667.2014.959958

WMO 2015 *Guidelines on the definition and monitoring of extreme weather and climate events* Online: https://www.wmo.int/pages/prog/wcp/ccl/opace/opace2/documents/DraftversionoftheGuidelinesontheDefinitionandMonitoringofExtremeWeatherandClimateEvents.pdf

WMO 2012 *Standardized Precipitation Index User Guide* (Geneva: WMO) Online: https://library.wmo.int/index.php?lvl=notice_display&id=13682#.X0dNPcgzbIU

Xu Y and Beekman H E 2019 Review: Groundwater recharge estimation in arid and semi-arid southern Africa *Hydrogeol. J.* **27** 929–43 Online: https://doi.org/10.1007/s10040-018-1898-8

Yin W, Hu L, Zhang M, Wang J and Han S-C 2018 Statistical Downscaling of GRACE-Derived Groundwater Storage Using ET Data in the North China Plain Journal of Geophysical Research : Atmospheres Statistical Downscaling of GRACE-Derived Groundwater Storage Using ET Data in the North China Plain *J. Geophys. Res. Atmos.* **123** 5973–598